universität wien

DISSERTATION

Titel der Dissertation

„Visualization of thymocyte – dendritic cell interactions during negative selection“

Verfasserin

Mag. rer. nat. Elisabeth Vollmann

angestrebter akademischer Grad

Doktorin der Naturwissenschaften (Dr. rer. nat.)

Wien, 2011

Studienkennzahl lt. Studienblatt:	A 091 441
Dissertationsgebiet lt. Studienblatt:	Doktorstudium der Naturwissenschaften Genetik – Mikrobiologie (Stzw)
Betreuerin / Betreuer:	Prof. Dr. Josef Penninger and Prof. Dr. Ulrich von Andrian

Summary 1

Zusammenfassung 2

Introduction 3
Evolution of the thymus 3
Thymic architecture and thymus development 5
T cell development 9
Thymic antigen presenting cells in positive and negative selection 15
Cortical thymic epithelial cells 15
Medullary thymic epithelial cells 17
Thymic dendritic cells 19
Dendritic cells 22
Methods to study DC migration 25
Traffic molecules in DC migration 28
DC migration from blood to tissues 30
DC traffic to non-lymphoid tissues 31
Dendritic cell traffic to BM 34
Dendritic cell trafficking to the thymus 34
Multi-photon microscopy 37

Aims of the thesis 43
Aim 1: To establish MP IVM for transplanted thymi 44
Aim 2: To analyze the motile behavior of thymic DCs and T cells 45
Aim 3: To analyze homed versus thymus resident DCs 45
Aim 4: To test whether thymus resident DCs acquire blood borne Ag 45

Results 47
Aim 1: To establish MP IVM for transplanted thymi 47
Subaim 1.1: To analyze transplanted thymi 47
Transplanted thymus – anatomy and cellular composition *47*
Dendritic cell trafficking to transplanted thymi *50*
Subaim 1.2: To develop an imaging strategy to perform MP IVM of thymi 53
Aim 2: To analyze the motile behavior of thymic DCs and T cells 57
Subaim: 2.1 To differentiate between cortex and medulla in vivo 57
Subaim 2.2: To analyze DC and thymocyte motility in cortex and medulla 59
Subaim 2.3: To analyze the effect of cognate Ag on thymocyte behavior 62
Aim 3: To analyze homed vs. thymus resident DCs 66
Aim 4: To test whether thymus resident DCs acquire blood borne Ag 70
Subaim 4.1: To test whether thymic DCs can sample the blood 70
Subaim 4.2: To evaluate whether homed and thymus resident DCs can extend transendothelial protrusions 77
Subaim 4.3: To assess the mechanism by which transendothelial DCs gain access to the blood stream 80

Discussion 83
In vivo imaging of the thymus 83
Thymocyte behavior 88
Thymic DCs 92
The role of CX_3CR1 in transendothelial DCs 94
Concluding remarks 96

Materials and methods 97
Mice 97
Reagents 97
BM chimeras 98
DC isolation 98

Thymus transplantation **98**
In vivo labeling of thymic medullas **99**
Multi-photon microscopy **99**
Peptide loading of DCs **100**
Interaction analysis **100**
Immunofluorescence **100**
Homing assays **101**
Intravascular labeling of leukocytes **101**
Statistical analysis **102**

Abbreviations **103**

References **106**

Curriculum vitae **125**

Acknowledgments **127**

Summary

A functional immune system has to protect the body from pathogens while being tolerant to self-antigens (sAg). To achieve this goal, developing thymocytes are subjected to tolerance mechanisms. Central tolerance takes place within the thymus and removes the bulk of auto-reactive thymocytes by either clonal deletion (negative selection) or redirection into a regulatory T cell lineage (Treg). Dendritic cells (DCs) are key players in this process. They acquire and present self-peptide in the context of major histocompatibility complexes (MHC) to thymocytes and can either promote survival or apoptosis of interacting T cells. To induce tolerance, sAgs are either expressed in the thymus or they have to enter the organ from the blood.

Thymic DCs can be distinguished and subdivided into distinct subsets according to their surface markers as well as by their origin. Thymus resident DCs differentiate locally from a progenitor cell, while homed DCs enter the thymus fully differentiated from the blood.

Here, we show by subjecting live, anesthetized mice to multi-photon intravital microscopy (MP IVM) that peptide-pulsed, homed DCs promote stable interactions with antigen specific but not non-specific thymocytes. Our observations also suggest a functional sub-specialization between thymus resident and homed periphery-derived DCs. While the latter can deliver peripheral sAg to the thymus as their cargo, some resident DCs are strategically positioned in the thymus to extend processes across the endothelial barrier of capillaries and thus are exposed to circulating sAg within blood stream.

Zusammenfassung

Ein funktionierendes Immunsystem muss den Körper vor Pathogenen schützen und gleichzeitig tolerant gegenüber Selbstantigen (sAg) sein. Um dieses Ziel zu erreichen, müssen sich entwickelnde Thymozyten Toleranzmechanismen unterziehen. Zentrale Toleranz findet im Thymus statt und entfernt den Großteil der autoreaktiven Thymozyten durch klonale Deletion (negative Selektion) oder durch das Umleiten von autoreaktiven Thymozyten in eine regulierende T Zell Linie. Dentritische Zellen (DZ) sind Schlüsselfiguren in diesem Prozess. Sie verschaffen sich Zugang zu harmlosem Selbstpeptid und präsentieren dieses den Thymozyten auf Haupthistokompatibilitätskomplexmolekülen. Damit fördern sie entweder das Überleben der interagierenden Zellen oder induzieren Apoptosis. Für diesen Vorgang muss Selbstantigen entweder im Thymus exprimiert werden, oder es muss vom Blut in dieses Organ gelangen.

Thymische DZ kann man sowohl anhand der Expression von spezifischen Oberflächenmarkern unterscheiden, wie auch anhand ihres Ursprunges. Thymus residente DZ differenzieren lokal von einer Vorläuferzelle, während eingewanderte Zellen bereits vollständig differenziert vom Blut in den Thymus gelangen.

Mittels Multiphotonenmikroskopie konnten wir erstmals in anästhesierten Mäusen zeigen, daß peptidgeladene, eingewanderte DZ stabile Interaktionen mit antigenspezifischen aber nicht mit unspezifischen Thymozyten fördern. Wir haben herausgefunden, daß es eine Spezialisierung zwischen thymus-ansässigen und eingewanderten DZ gibt. Während die Letztgenannten peripheres Selbstantigen als ihre Fracht in den Thymus liefern, sind ansässige DZ strategisch platziert um die endotheliale Schicht der Blutgefäße zu durchbrechen und Zugang zu zirkulierendem Antigen aus dem Blut zu erlangen.

Introduction

Evolution of the thymus

The immune system is divided into two arms, the innate and the adaptive immune system. The innate immune system equips the body with the ability to react promptly to bacterial, fungal, parasitic and / or viral insults. To do so, innate immune cells express a broad range of germline encoded extracellular and intracellular receptors that are specific for commonly encountered features of bacteria, fungi, parasites and viruses. Because these receptors are germline encoded, innate immunity fails to generate a "tailored" immune response without the help of the adaptive immune system. Cells of the adaptive immune system, such as B and T lymphocytes, carry B/T cell receptor that were generated by somatic diversification of antigen receptor genes during the cells' development. The B and T cell repertoire is polyclonal and each cell expresses a unique antigen receptor, which leads to a broad range of specificities. Natural killer (NK) cells have also been shown to trigger adaptive immune reactions[1,2]. The adaptive immune system provides a customized immune response and has the unique capacity to generate immunological memory. While the innate immune system reacts with the same kinetics to a previously encountered pathogen, the memory formation of the adaptive immune system allows for an expedited immune reaction upon re-encounter of the same pathogen[3].

The innate arm of the immune system is evolutionarily older than the adaptive one as evidenced by the fact that all multi-cellular organisms are equipped with an innate immune system[4] while only jawed vertebrates (gnathostomes) have an adaptive immune system that utilizes T and B cell receptors (TCR, BCR), RAG proteins, MHC-I and MHC-II molecules[5-7]. Interestingly, lamprey and hagfish, the nearest living relatives of the evolutionarily older jawless vertebrates (agnathans), also have an adaptive immune system. However,

the diversification process that leads to a broad lymphocyte repertoire in agnathans is distinct from the one in gnathostomes[8,9].

The genome of jawed vertebrates has undergone two rounds of at least partial duplication, which resulted in the current organization of BCR, TCR and MHC loci. The genes that encode the BCR and TCR are exist in the germline in a non-functional state, with the 5' portion of each gene (which encodes the antigen binding domain) arranged as arrays of variable (V), diversity (D) and joining (J) gene segments[10]. The duplication events presumably occurred after the split of gnathostomes and cyclostomes (which include agnathans) as lampreys only express a single TCR in lymphocyte-like cells due to the lack of additional copies of V- and J-like sequences in their genome[7]. Their adaptive immune system relies instead on the recombination of leucine-rich repeats (LRRs) that form the variable lymphocyte receptors (VLRs) of lymphocyte-like cells[8,11]. Lampreys have T- and B-like lymphocytes, that express type A and type B VLR genes, respectively. In contrast to the adaptive immune system of jawed vertebrates that use RAG protein mediated recombination to generate a diverse B and T cell repertoire, diversification in lamprey is mediated by the cystidine deaminases 1 and 2 (CDA1, CDA2). CDA1 promotes the generation of type A VLRs (TCR-like) while CDA2 promotes VLRB gene segment recombination (BCR-like)[12,13].

Until recently, the evolutionary origin of the thymus remained enigmatic. However, Boehm and colleagues, in two elegant studies, identified thymus like tissue, termed thymoid, in the tips of the gill filament and the neighboring secondary lamellae of the agnathan lamprey[14,15]. Thymoids were identified in lamprey larvae according to the expression of the Foxn1 orthologue Foxn1, as well as VLRA genes, CDA1 and the absence of VLRB genes and CDA2. It is of note that the expression of Foxn1 is indispensable for thymus formation in gnathostomes[16]. Furthermore, non-functional VLRA gene rearrangements could only be detected in lymphocyte-like cells from thymoids but not from blood indicating that this is the place where T-like lymphocytes develop in lampreys[15].

To date it is believed that the evolution of adaptive immune systems in gnathostomes and agnathans occurred independently of each other. However, given the striking similarities such as the dependence on recombination events to generate diverse lymphocyte receptors, and the functional similarity of VLRA and VLRB expressing lymphocytes to T and B cells, respectively, as well as the identification of a thymus like structure, this idea may be called into question.

Thymic architecture and thymus development

In mammals, the thymus is a multilobular organ that is located anatomically in the anterior superior mediastinum, in front of the heart, between the lungs and behind the sternum (**Fig. 1a**). In humans and mice, the thymus consists of two lobes. It can be subdivided into two distinct anatomical regions: the outer cortex and the inner medulla. One can find distinct stromal and hematopoietic cell types in these compartments. The cortex consists of T cell progenitors and cortical thymic epithelial cells (cTEC), while semi-mature and mature T cells as well as the presence of medullary thymic epithelial cells (mTECs) are unique to the medulla. Other cell types, such as macrophages (MΦ) and mesenchymal cells can be found in both compartments. Thymic DCs are enriched in the medulla and the cortico-medullary junction (CMJ), while they are sparse in the cortex. The CMJ is the transitional area between cortex and medulla. Other structures such as blood vessels are present in both anatomical regions, although, their quality differs. For instance, large venules are predominantly found at the CMJ. Lastly, the thymus is a well-innervated organ; like in other organs, neurons “travel” along the vasculature of blood vessels in thymi[17] (**Fig. 1b**).

The cortex can be further subdivided into the subcapsular area (SCA) and bona fide cortex. To date, the specific features of this area remain understudied. However, it is known that TCRß selection takes place in the subcapsular area (SCA, see also section “T cell development”).

One of the specific features of the CMJ is the occurrence of large blood vessels that are sheathed by the perivascular space (PVS). This is also the entry point of progenitor cells that home to the thymus and the point of exit of mature, naïve T cells[18].

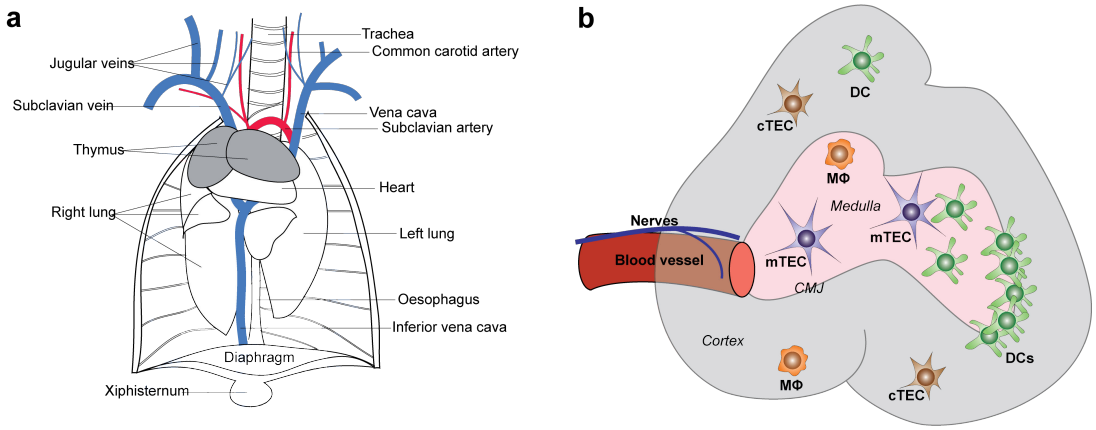

Fig. 1. Anatomy of the murine thymus. (**a**) In mammals, such as mice and humans, the thymus is located within the rib cage, directly contacting the heart and the lungs. (**b**) In general, the thymus is composed of the outer cortex and the inner medulla. These distinct anatomical regions harbor different, functionally specialized cell types.

In mice and humans, the thymus has its origin in the foregut, which develops from the third pharyngeal pouch. This pouch gives also rise to several other organs in the neck and chest, such as the parathyroid glands and the thymus[19].

It was believed for a long time that the two different anatomical regions of the thymus, the cortex and the medulla, develop from the ectoderm and endoderm, respectively. This concept has been revised by two convincing studies that have utilized single cell transplantation and cell lineage tracking strategies to identify medullary and cortical thymic epithelial cell (TEC) progenitors. Indeed, one single progenitor cell can give rise to a small, albeit complete, thymus consisting of both cortex and medulla. This finding led to the conclusion that cortical and medullary TECs can develop from a single bi-potent progenitor cell[20,21].

The earliest indication of thymus development in mice can be detected at gestation day E10.5 by the appearance of epithelial cells in the endodermal layer of the third pouch that express the tight junction molecules claudin-3

(Cld3) and Cld4[22]. Forkhead box N1 (*Foxn1*) is expressed in the fetal thymus anlage one day later on E11.5. Foxn1 is indispensable for thymus development and Foxn1$^+$ cells are committed to become TECs[16,23,24]. Furthermore, specification between thymus and parathyroid glands is achieved by the mutually exclusive expression of Foxn1 (for thymus) and Gcm2 (for parathyroid)[23].

The early E11.5 thymus anlage consists of homogenous TEC progenitors and is encapsulated by neural crest (NC) derived mesenchymal cells. At the beginning of vascularization of the thymus at E14.5, NC derived cells can also be found sheathing the vasculature as they eventually differentiate into perivascular cells or pericytes. NC derived cells are crucial during early thymopoeisis, which is highlighted by delayed and impaired thymus function in their absence[25-28]. Recently, perivascular cells have been identified as an important source of sphingosine-1-phosphate (S1P) and have therefore been implied in the S1P dependent emigration of naïve, mature T cells from the post-natal mouse thymus into the blood stream[18].

It is noteworthy that seeding of the thymus anlage occurs before vascularization. Fetal liver derived lymphoid progenitor cells are recruited to the adjacent primodorum as early as E11.5 and can be found in the fetal thymus on E12.5[29]. The presence of hematopoietic cells in the thymus coincides with the onset of cortex / medulla differentiation. This is not surprising given the reciprocal interplay between thymocytes and thymic stroma, also termed thymic crosstalk. Lymphopenic thymi fail to develop and / or maintain normal cortical and medullary structures further highlighting the importance of hematopoietic cells in the thymus. Positively selected thymocytes play an essential role in the formation and maintenance of medullas and Aire expressing mTECs via RANK/RANKL signaling[30,31]. Other candidates for thymic crosstalk are Notch1 and its ligands Delta-like 1 (Dll1) and Dll4 that are expressed by TECs. While the role for Notch1-Dll1 and Notch1-Dll4 signaling in T cell development has been well established (see also section “T cell development”), potential effects on TEC development remain unclear.

It has been shown that a single TEC precursor can give rise to mTECs and cTECs. Experiments involving reaggregated fetal thymic organ cultures (RTOCs) that were grafted into T cell sufficient recipient mice further provided important insights in cortex and medulla formation. Briefly, the generation of RTOCs relies on the reaggregation of previously enzymatically generated single cell suspensions of thymic stroma cells. Using this technique, it was shown that medullas arise clonally while the cortex appears to be polyclonal[32]. Furthermore, it was shown that mTECs in the adult thymus are actively proliferating and develop from the EpCAM^{+} Cld3^{low}4^{low} UEA-1^{-} mTEC precursor that gives rise to semi-mature EpCAM^{+} Cytokeratin5^{+} MTS10^{+} UEA-1^{+} CD80^{low}86^{low} Aire^{-} mTECs that eventually mature to EpCAM^{+} Cytokeratin5^{+} MTS10^{+} UEA-1^{+} Cld3^{+}4^{+} CD80^{high}86^{high} Aire^{+} mTECs[22,33,34]. This discovery demonstrated that mTECs develop via a progressive maturation rather than a parallel development of several mTEC lineages.

With the initiation of the development of the thymus, its journey from the third pharyngeal pouch to its final location within the ribcage begins. On E12.5, the thymus anlage and the parathyroid grow into two distinct domains and finally separate from the third pouch and from each other by E13.5. Although physically separated, they still migrate together to their final destination within the body. Thus, the thymus “detours” by taking the parathyroid route[19]. Interestingly, the location of so-called cervical thymi coincides with this route, suggesting these ectopic thymi may result from TEC progenitors that have dissociated from the thymus anlage on route. The number and location of cervical thymi in mice and humans is not conserved, indicating that their generation is not strictly regulated[35,36].

With its arrival in the rib cage, directly above the heart, the thymus has found its final destination (**Fig. 1a**). The murine thymus reaches its peak cellularity at about four to six weeks of age. After that, it starts to involute and thymic T cell output gradually decreases. In humans, thymus involution starts at birth[37]. Thymic involution is accompanied by an overall decline in cell numbers. cTEC numbers are especially reduced in involuting thymi, leading to a relative enrichment of mTECs and medullary regions and the fusion of monoclonal medullas. Furthermore, thymic involution is accompanied by the

accumulation of fatty tissue in the perivascular space and thus expands this region within the thymus. Even though thymic output is reduced, thymopoeisis still persists in the elderly[38].

T cell development

T cell precursors in the thymus do not have long term self-renewing capacity under physiological conditions[39] and consequently T cell output relies on the replenishment of T cell precursors[40]. This is achieved by the periodic recruitment of common lymphoid precursors (CLPs) from the BM via the blood. Thus, T cell development starts with the entry of these cells into the thymus at the CMJ. There are different subsets of CLPs that can home to the thymus and give rise to T cells. Interestingly, CLP-2 but not CLP-1 cells are equipped with the appropriate homing molecules to access the thymus.[41] Homing of CLP-2 cells follows a classical multi-step adhesion cascade that consists of tethering, rolling, integrin activation followed by sticking / firm arrest and finally diapedesis. Rolling is mediated by PSGL-1 – P-selectin and VLA4 ($\alpha_4\beta_1$) – VCAM-1 interactions. $G\alpha_i$ mediated activation of VLA4 and LFA-1 ($\alpha_L\beta_2$) leads to firm interaction with VCAM-1 and ICAM-1, respectively, and arrest. This activation is dependent on the CCR9 – CCL25 (TECK) receptor – ligand pair[41] (**Fig. 2**). The last step of the homing cascade, the extravasation from the venules into the thymus has not yet been described.

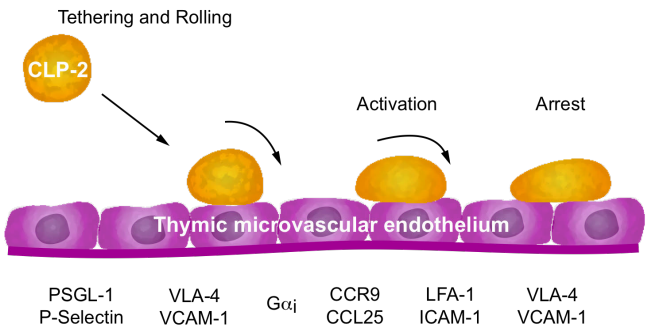

Fig. 2. CLP-2 cells home to the thymus by employing a multi-step adhesion cascade. Rolling is mediated by PSGL-1 – P-selectin and VLA4 – VCAM-1 interactions. Signaling of the receptor – ligand pair CCR9 – CCL25 through $G\alpha_i$ triggers activation of LFA-1 and VLA-4 integrins and thus promote firm arrest[41].

The most immature T cell precursors in the thymus express low levels of CD4 and lack surface expression of CD8[42]. They are generally referred to as double negative thymocytes (DN). They can be further subdivided into DN1-3 and DN4 / pre-double positive (DP) cells. The most immature DN1 cell is characterized by the expression of the stem cell factor receptor c-Kit (CD117) and CD44. They can be found in the cortex, in proximity to venules at the CMJ, from which they presumably have entered the thymus. Upon entering the organ in periodic waves, DN1 cells proliferate and are released asynchronously to replenish continuously the intrathymic T cell pool and to advance to DN2 cells[40].

DN2 cells upregulate CD25 but lose the low expression of CD4 and thus are $CD4^{-}8^{-}25^{+}44^{+}117^{+}$. They migrate towards the capsule and are found deep within the cortex. This migration has been shown to be mediated by the expression of CXCL12 by scattered cortical stromal cells and the corresponding chemokine receptor CXCR4 on the thymocytes as well as the CCR9 – CCL25 receptor – ligand-pair. DN2, as well as more committed DN3 cells, anchor to thymic epithelial cells during migration by utilizing the homotypic adhesion molecule E-cadherin as well as VLA4 – VCAM-1 interactions. DN2 cells express Notch1, which causes their T lineage specification, although they still maintain the potential to give rise to other cells types such as DCs and NK cells. During the migration through the cortex towards the capsule, Notch1-expressing DN2 and DN3 cells are in close contact with epithelial cells, which express the Notch ligands Dll1 and Dll4. Constant signaling through Notch is essential to maintain T cell lineage commitment and deletion of Notch converts pro-T cells to intrathymic B cells and DCs[43]. DN2 cells also up-regulate *Rag* genes and rearrange TCRγ and TCRδ but not TCRβ or TCRα gene segments.

DN cells that have reached the capsule have down-regulated CD44 and thus are characterized as $CD4^{-}8^{-}25^{+}44^{-}117^{-}$ DN3 cells. DN3 cells proliferate actively and expand approximately fourfold. They continue to express Notch and have greatly diminished potential to differentiate into cell types other than

T cells. Furthermore, RAG proteins are expressed and the TCRβ locus is accessible for RAG mediated gene recombination. Almost all DN3 cells carry at least one fully rearranged TCRβ allele. In-frame rearrangements promote survival and allow the cells to advance to the β-selection checkpoint. This process requires the surface expression and association of the TCRβ chain with an invariant TCRα chain to form the pre-TCR[44,45]. Only if the pre-TCR allows for signaling, DN3 cells receive a survival signal and undergo a proliferative boost that goes in hand with the advance to DN4 / pre $CD4^+8^+$ double positive (DP)[46,47].

Post β-selection DN4 / pre-DP cells are characterized by the downregulation of CD25 and the partial up-regulation of CD4, CD8 and CD27. They can be identified by the following surface marker profile: $CD4^{low}8^{low}25^-27^+44^-117^-$. Pre-DP and $CD4^+8^+$ DP cells leave the sub-capsular area and migrate randomly in the cortex[48]. The cues that promote the migration away from the capsule are poorly understood. Cortical DP cells express RAG proteins and rearrange the TCRα locus. The rearranged TCRα chain is paired with the TCRβ chain and subjected to positive selection. During this process TCR specificities are selected that can interact with self-peptide presented on MHC-I or MHC-II of cTECs. Interaction promotes survival, while failure to do so leads to “death by neglect”. Positive selection enriches for a self-restricted T cell pool. However, by doing so, it also enriches for autoreactive T cells. Hence, further quality control steps are required to remove potentially dangerous, autoreactive thymocytes. It is noteworthy that positive selection is very wasteful as it removes over 90% of the generated T cells.

Positive selection does not only select for thymocytes that can interact with self-MHC, it also determines CD4 versus CD8 lineage commitment. Several studies have focused on the identification of factors that contribute to either lineage decision. Work to date supports a “duration-of-signal” instructional model, in which persistent TCR signaling leads to the expression of the transcription factors GATA3 and ThPOK and the development of CD4 SP cells, while intermittent TCR signaling in combination with IL-7 activates Runx3, a ThPOK silencer that further promotes CD8 lineage commitment[49-52].

Therefore cells that have passed positive selection are committed to either $CD4^+$ or $CD8^+$ T cells and downregulate CD8 or CD4 respectively, resulting in a $CD4^+8^-$ or $CD4^-8^+$ semi-mature single positive T cell (SP). Semi-mature SP cells also co-express CD24 (HSA, heat stable antigen), CD69 and low levels of L-selectin (CD62L) as well as CCR7. The CCR7 ligands CCL21 and CCL19 are present in the thymic medulla and responsible for the migration of positively selected thymocytes from the cortex to the CMJ and medulla[48,53]. It is noteworthy that positively selected T cells can also undergo negative selection in the cortex with no involvement of the medulla under the premise that they already express a fully functional TCR and that the selecting peptide is presented in this anatomical region of the thymus (e.g. to ubiquitously expressed antigens (Ag))[54]. However, because of the limited availability of self-peptide that is required for the induction of tolerance to a wide spectrum of sAgs in the cortex, failure of polyclonal thymocytes to migrate into the medulla results in incomplete tolerance induction and autoimmunity[18,55]. It is also of note that the available peptide repertoire for positive and negative selection differs (see also section “Thymic antigen presenting cells in positive and negative selection”).

Semi-mature SP T cells in the CMJ and the medulla are subjected to central tolerance. This process either removes auto-reactive T cells (negative selection) or redirects them into a regulatory T cell lineage. To do so, the affinity of the TCR of developing thymocytes with self-peptide that is present on MHC-I and MHC-II molecules is tested. In contrast to positive selection, weak interactions promote survival while high affinity interactions induce apoptosis. Interactions with intermediate affinity drive SP T cells, especially $CD4^+$ SP cells, into a regulatory T cell lineage and induce expression of the IL-2Rα chain (CD25) and Foxp3[56]. Post-selection thymocytes mature into $CD4^+$ or $CD8^+$ SP $S1P_1^+$ $CD62L^+69^-$ mature, naïve thymocytes that no longer can be subjected to negative selection. Instead, the engagement of the TCR on these cells triggers clonal proliferation[57]. Mature thymocytes also express KLF2 (Kruppel like factor 2), a transactivator of the sphingosine-1-phosphate receptor 1 ($S1P_1$) promoter, the expression of which is critical for thymocyte egress into the blood[58]. Emigrating T cells first enter the perivascular space

and then reverse transmigrate into the blood[18]. Administration of IL-7 has been shown to promote thymocyte egress as well[59]. However, because thymocytes in IL-7R deficient mice did not show an egress defect[60], the role of IL-7 and its receptor in egress from the thymus remains puzzling. αβ T cells leave the thymus four – five days after becoming SP thymocytes[61] (see **Table 1** and **Fig. 3** for a schematic overview of T cell development in the thymus).

Table 1. T cell development

T cell precursor	Phenotype	Migration direction (* denotes predominant localization)	Developmental events
CLP-2	lin$^-$ CD127$^+$ Thy-1$^-$ Sca-1^{low} c-Kit$^-$ B220$^+$ CD19$^-$	Blood ↓ CMJ* ↓ Thymic stroma / cortex	• Homing from the circulation to the thymus in waves
DN1	CD4^{low} CD8$^-$ CD25$^-$ CD44$^+$ CD117$^+$	CMJ ↓ Cortex* ↓ SCA	• Proliferation • Desynchronization of T cell development
DN2	CD4$^-$ CD8$^-$ CD25$^+$ CD44$^+$ CD117$^+$ CCR9$^+$ CXCR4$^+$	CMJ ↓ Cortex* ↓ SCA	• T lineage specification • TCR αβ versus γδ lineage commitment • TCRγ and TCRδ rearrangement • Proliferation
DN3	CD4$^-$ CD8$^-$ CD25$^+$ CD44$^-$ CD117$^-$ CCR9$^+$ CXCR4$^+$	Cortex ↓ SCA* ↓ Cortex	• T lineage specification • TCR αβ versus γδ lineage commitment • TCRβ rearrangement • β selection • Proliferation
DN4 / pre-DP	CD4^{low} CD8^{low} CD25$^-$ CD27$^+$ CD44$^-$ CD117$^-$	SCA ↓ Cortex* ↓ CMJ	• Proliferation • TCRα rearrangement • Positive selection • CD4 / CD8 lineage commitment
DP	CD4$^+$ CD8$^+$ CD25$^-$ CD27$^+$ CD44$^-$ CD117$^-$	Cortex ↓ CMJ*	• Negative selection / Treg induction
Semi-mature SP	CD4$^+$ CD8$^-$ **or** CD4$^-$ CD8$^+$ CD24$^+$ CD62L^{low} CD69$^+$ CCR7$^+$	Medulla*	• Negative selection / Treg induction
Mature SP	CD4$^+$ CD8$^-$ **or** CD4$^-$ CD8$^+$ CD24$^-$ CD62L$^+$ CD69$^-$ S1P$_1^+$ KLF2$^+$	Medulla* ↓ PVS* ↓ Circulation*	• Maturation • Thymic egress

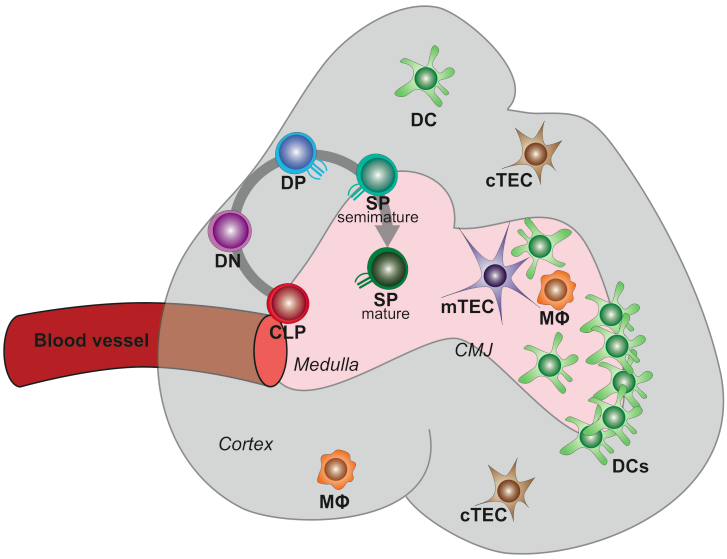

Fig. 3. Schematic overview of T cell development in the thymus. T cell development starts with the homing of CLPs to the thymus at the CMJ. Next, they migrate towards the capsule and differentiate into DN thymocytes and rearrange the TCRβ chain. After passing β-selection, the migration direction is reversed and the now DP thymocytes migrate towards the medulla. On route, they rearrange their TCRα chain and are subjected to positive selection in the cortex. Positively selected DP cells maturate into SP semi-mature T cells and enter the medulla, where negative selection takes place. Cells that have passed negative selection advance to mature, naïve T cells and finally emigrate from the thymus into the blood at the CMJ.

Thymic antigen presenting cells in positive and negative selection

The thymic microenvironment is geared to support T cell development and selection. T cell selection is a process that requires the presentation of self-peptide in the context of MHC molecules to developing thymocytes. During positive selection, this process promotes survival while during negative selection the outcome is reversed. The profound differences in the consequences of TCR engagement have been attributed to several factors. Positive and negative selection take place in different anatomical regions of the thymus, the cortex and the medulla, respectively. The cortex provides a more nourishing environment than the medulla, which is at least partially attributed to the higher density of IL-7 expressing cells[60,62]. The T cells that are subjected to positive versus negative selection also differ in their developmental stage. Thymocytes that are undergoing positive selection are more immature than T cells that are facing negative selection. Depending on their developmental stage, TCR signaling is translated differentially. Because of the spatial separation, the microenvironment and consequently the type of interacting antigen presenting cells (APCs) vary as well. For instance, positive selection relies on presentation of Ag by cTECs while negative selection is mediated by mTECs and medullary DCs as APCs. Each of these cell types employ a unique mechanism to acquire a broad range of sAg for presentation on MHC complexes and T cell selection. In light of these differences, the previously dismissed idea that positive and negative selection rely on different peptide pools has recently regained its popularity[63,64].

Cortical thymic epithelial cells

cTEC are indispensable for positive selection and are exclusively found in the cortex. They have unique antigen processing properties as evidenced by their expression of the ß5t subunit as part of the proteasome. The proteasome is the major catalytic force generating peptides from

cytoplasmatic proteins for presentation on MHC-I molecules. The expression of the ß5t subunit in cTECs is evolutionarily conserved among jawed vertebrates that have a thymus that supports T cell development[65]. It has been shown that expression of this subunit in the thymus imprints its specific cleavage site signature on the generated peptide repertoire and that the ß5t subunit is indispensable for proper positive selection of cells that eventually will give rise to CD8 SP T cells. Positively selected thymocytes migrate into the medulla where they encounter mTECs and DCs as the main APCs involved in negative selection. mTECs and DCs express the ß5i but not ß5t subunit of the proteasome. Thus the proteasome-derived self-peptides in cortex and medulla carry the distinct signatures of the ß5t and ß5i subunit, respectively, and the peptide repertoire presented is thus likely to be different. Deletion of the cortex specific ß5t subunit leads to the expression of the ß5i subunit in the cortex, resulting in a similar proteasome-derived self-peptide repertoire in cortex and medulla. In this case, the very same peptides that promote survival upon interaction in the cortex during positive selection are also generated and presented during negative selection in the medulla. However, the outcome is here markedly different and TCR engagement during negative selection results in clonal deletion or Treg induction. Thus, positively selected TCR specificities are more likely to be removed during negative selection when the peptide pools in medulla and cortex overlap. In consequence the deletion of the ß5t subunit leads to a less diverse CD8 T cell pool[64].

Cathepsin L has a similar expression pattern to that of the ß5t subunit. Cathepsins are lysosomal proteases that play a role in the degradation of the invariant chain (Ii) which otherwise protects MHC-II from premature peptide loading. Cathepsins also proteolytically cleave substrates in the lysosome and generate self-peptides for loading and presentation on MHC-II. Therefore, cathepsins play an important role in the selection of MHC-II restricted CD4 T cells. Cathepsin L is preferentially expressed on cTECs while cathepsin S is abundantly found on mTECs and DCs. Similar to deletion of ß5t, deletion of cathepsin L leads to a greatly reduced T cell

repertoire, which in this case is manifested by a reduced number and diversity of CD4 T cells[66].

Lastly, cTECs are also distinct from medullary APCs in that they show constitutively high levels of macroautophagy. Macroautophagy is a cellular process by which long-lived cellular structures, such as mitochondria and parts of the nucleus, are engulfed into autophagosomes that eventually fuse with lysosomes and lead to degradation of the contents. In most tissues, such as muscle, macroautophagy is induced upon food depreviation and acts as a rapid starvation response. Notably, it is constitutively low / off in brain and constitutively on in cTECs in the thymus. As autophagosomes fuse with lysosomes they intersect with the MHC-II loading pathway. Indeed, it was shown that macroautophagy contributes to the generation of self-peptides for presentation by cTECs in the course of positive selection[67,68].

Medullary thymic epithelial cells

The key players for negative selection are mTECs and DCs. mTECs have gained particular attention in the last decade as they have been shown to ectopically express genes that were previously believed to be strictly restricted to other tissues. This process has been termed promiscuous gene expression (PGE) and has been shown to at least partially rely on the transcriptional regulator Aire[69,70]. Aire expression is highest in mature, MHC-II^{high} CD80^{high} CD86^{high} mTECs, although it can also be detected in immature MHC-II^{low} CD80^{low} CD86^{low} mTECs and thymic DCs, albeit at low levels. Even though DCs express Aire, PGE has not been detected in these cells. Failure to express Aire in mTECs or mutations in the Aire gene locus lead to abrogated PGE, which is manifested in severe autoimmunity such as autoimmune polyendocrinopthy-candidiases-ectodermaldystrophy (APECED) in humans and mice[71]. The current belief is that PGE provides an important Ag source to induce tolerance of reactive T cells in the course of negative selection. In order to generate peptides for presentation on MHC-I, the proteasome, using the ß5i subunit, and cathepsin S degrade gene products. How exactly PGE intersects with MHC-II loading pathways is still not entirely

understood. Macroautophagy is less pronounced in mTECs as compared to cTECs; however, it is constitutively on in mTECs, in particular in mature mTECs, albeit at low levels. Indeed it has been suggested that mTECs also employ macroautophagy to process self-Ag to make it available for loading on MHC-II[67].

mTECs, especially mature mTECs, like DCs express the necessary molecules for peptide presentation and promotion of negative selection and central tolerance. However, the role of this cell type in central tolerance is somewhat puzzling. For instance, it was suggested that mTECs are specialized in inducing regulatory T cells rather than promoting apoptosis in T cells upon TCR triggering[72]. This finding was challenged by an in vitro study that has shown that other cell types can also induce Treg development of thymocytes. These data are indicative that the sum of quality of signal one (TCR affinity) and signal two (co-stimulation) of mTECs is lesser as compared to professional APCs, such as DCs. In this case, the same T cell would be directed into a Treg lineage upon interacting with peptide presented on MHC-II by mTECs, while it would undergo apoptosis upon interacting with the same peptide presented by DCs[73]. Given that Ag presentation by mTECs appears to be inefficient, one wonders whether the main purpose of mTECs is the generation and distribution of Ag rather than presenting promiscuously expressed genes per se. Indeed, it was shown that there is a uni-directional flow of Ag and MHC molecules from mTECs to thymic DCs[74,75]. Furthermore, both, mTECs and DCs express connexin34 (Cnx43), a protein that is usually found in gap junctions. Connexins assemble into hemichannels (or connexons) at the surface of a cell. If connexons of two neighboring cells line up and interact, they can form a small channel, referred to as a gap junction. Ag transfer between DCs is mediated at least in part by gap junctions and DCs can access intracellular Ag from apoptotic cells via gap junctions as well[76,77]. Although formal proof is lacking, it is tempting to speculate that DCs can take advantage of the same mechanism to acquire promiscuously expressed Ag from mTECs. Thus, it has been suggested that one of the main functions of mTECs is to generate a broad range of self-Ag and to make it available to DCs for presentation in order to induce central tolerance[78].

Thymic dendritic cells

Thymic DCs have been identified early on as being indispensable for negative selection[79]. Phenotypically they have been characterized by the expression of CD11c and MHC-II. cDCs in the thymus can be further subdivided into $CD8\alpha^{+}CD11b^{-}$ and $CD8\alpha^{-}11b^{+}$ DC subsets. Interestingly, the majority of thymic DCs are pDCs which represent 30-50% of the thymic DC population. The bulk of thymic DCs is believed to develop in situ from progenitor cells[80]. It has been shown that up to 30% of pDCs and $CD8\alpha^{+}$ DCs carry IgH rearrangements of the TCRα chain, indicating that they have developed from DN2/DN3 cells[81] (**Fig. 4**). Indeed, CLP as well DN1-3 cells can give rise to thymic DCs, though with decreasing efficiency[43]. The accumulation of thymic DCs in the medulla, especially of $CD11c^{+}11b^{-}$ DCs is at least in part regulated by the expression of XCL1 by mature MHC-II^{high} mTECs and XCR1 by the DCs[82]. It has also been shown that fully differentiated, yet immature DCs have the capacity to home to the thymus (see also section “Dendritic cell trafficking to the thymus”). Upon entering the thymus, they upregulate maturation associated markers such as MHC-II and CD80[80]. They localize almost exclusively in the medulla with a slight enrichment at the CMJ[83]. Homing of DCs to the thymus has been shown to be an important tool to deliver peripheral Ag to the thymus and to make it available for negative selection[83,84] (see also section “Thymic antigen presenting cells in positive and negative selection”). Thymic DCs still maintain the capacity do proliferate and may undergo one or two cell divisions upon entering the organ[80]. It is possible that this is a mechanism to prolong the persistence of Ag similarly to cycling splenic DCs whose daughter cells continue to present captured Ag[85].

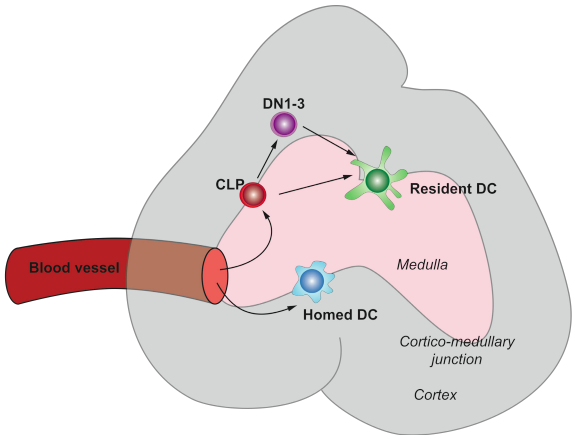

Fig. 4. Schematic of thymic DCs and their precursors. Thymus resident DCs can arise locally form CLP that home to the thymus, DN1, DN2 and DN3 cells. In contrast, homed DCs enter fully differentiated into the organ from the blood.

Lastly, small peptide-like antigenic material can also enter the thymus directly from the blood and get presented by thymic DCs. Elegant pioneer work from Raviola et al. has helped describing the so-called blood-thymus barrier. The authors established the size cut-off for the thymus-blood barrier to be around 12 kDa by intravenous injection of proteins with molecular weights ranging from 12 – 462 kDa in combination with electron microscopy. Proteins that are larger than 12 kDa, such as horseradish peroxidase (MW 45 kDa), have been found to be trapped in the vasculature. At the CMJ, horseradish peroxidase was also detected between endothelial cells. As this region is also the "hot spot" where trafficking of cells to and from the thymus takes place, the extravascular appearance of horseradish peroxidase could be a bystander effect, rather than the result of active shuttling. This hypothesis was supported by the fact that the protein remained extracellular. Only in the cortex, a minute amount of cells showed peroxidase activity in vacuoles, however, given the natural presence of lipid peroxidases in vacuoles, it remains open whether the detected signal comes from the injected protein or the expression of endogenous peroxidases[86]. More recently, the potential uptake of antigenic material from the blood has been revisited. Intravenous injection of cognate protein Ag into TCR tg animals and the consequent deletion of thymocytes pointed towards "leakiness" of the blood-thymus barrier. However, given the time scale between i.v. injection and assessment of cell death as a read-out for negative selection, alternative explanations appear more likely. For instance, i.v. injection of cognate protein into animals with a peripheral protein specific TCR repertoire leads to peripheral T cell

activation and causes a cytokine storm that induces massive apoptosis of thymocytes[87]. Furthermore, it has been shown that DCs deliver peripheral Ag as their cargo to the thymus. Therefore blocking of DCs migration into the thymus is an indispensable pre-requisite for these experiments[88,89].

Dendritic cells

This following section is based on the review "Mechanisms and consequences of dendritic cell migration" by Alvarez et. al[90].

DCs are specialized antigen presenting cells that play a dual role in inducing adaptive immune responses to foreign Ags and in maintaining T cell tolerance to self[90,91]. DCs consist of several distinct subsets distinguishable by surface and intracellular phenotypic markers, immunological function and anatomic distribution (**Table 2**). In mice, all DCs express (to varying amounts) the CD11c integrin and MHC-II molecules, and are further phenotypically distinguished by their differential expression of CD8α, CD4, CD11b, Langerin, PDCA-1 as well as a growing list of other markers[92]. These markers have been used in various combinations to define several subpopulations, some of which are highly restricted to specific organs whereas others occur at characteristic frequencies among a mixture of DC subsets, especially in secondary lymphoid organs (SLOs). Arguably the clearest phenotypic and functional distinction can be made between the bulk of $CD11c^{high}$ $MHC\text{-}II^{+}$ cDCs and the type I interferon producing pDCs, which are $CD11c^{low}$ $MHC\text{-}II^{+/low}$ and express unique differentiation markers in both mice and humans. Irrespective of their phenotypic idiosyncracies or immunological role, DCs exert their activity in discrete locations often remote from their place of origin, which implies that DCs possess advanced migratory skills to navigate through the body.

All DCs ultimately derive from hematopoietic stem and progenitor cells (HSPCs) in the bone marrow (BM), which give rise to several distinct progenitors that can differentiate into one or more DC subsets[93-95]. Facultative DC progenitors are not restricted to the BM (although some fully differentiated DCs are generated there) but can be found in multiple locations, including blood, lymph, spleen and most visceral organs[85,95,96]. These progenitors can differentiate into DCs upon challenge in peripheral tissues[96].

Substantial numbers of DCs are also physiologically generated in the thymus[90,97].

Table 2. Traffic molecule profiles of mouse dendritic cells[90]

DC subset and phenotype	Migratory route	Chemokine receptor expression (ligand)	Other traffic molecules	References
Precursor DCs				
• Hematopoietic stem and progenitor Cell (HSPC) $CD45^+$ Lin^- $c\text{-}Kit^+$ $Sca\text{-}1^+$	BM ↓ Blood ↰*(via TD)* Tissue ↵ ↳ SLO ↳ Afferent lymphatics ↴	CXCR4 (CXCL12)	VLA-4, LFA-1, CD44, PSGL-1, $S1P_{1\text{-}4}$, α4-integrin, α5-integrin	98 96
• Macrophage DC precursor (MDP) $CD34^+$ Lin^- $c\text{-}Kit^{int}$ $CD11b^-$	BM ↓ Blood Tissue ↵ ↳ Spleen	CX_3CR1 (fractalkine)	n.d.	93
• Common dendritic progenitor (CDP) or clonal DC precursor (pro-DC) $CD34^+$ Lin^- $c\text{-}Kit^{int}$ $Flt\text{-}3^+$	BM ↓ Blood Tissue ↵ ↳ SLO	n.d.	CD44 L-selectin	95 94
• Monocyte subsets $CD115^+$ $CD11b^+$ $Ly6C^{low/int/high}$ $F4/80^{lo}$ $CD62L^{+/-}$	BM ↓ Blood Tissue ↵ ↳ SLO	CX_3CR1 (fractalkine), CXCR4 (CXCL12), CCR2 (MCPs), CCR8(CCL1), CCR5 (MIP/RANTES)	CD99, VLA-4, PSGL-1	99 100
Differentiated DCs				
• Langerhans cell $Langerin^+$ MHC II^+ $Dectin\text{-}1^+$ $CD11b^{++}$ $CD11c^+$ $CD24a^+$ $CD205^+$ $CD45^{lo}$ $CD8\alpha^{+/-}$ $CD103^-$	Epidermis↺ ↓ Dermis ↓ Afferent lymphatics ↓ LN	*Immature* CCR2 (MCPs), CCR6 (CCL20), CX_3CR1(fractalkine) *Mature* CCR7 (CCL19/21), CXCR4 (CXCL12)	$S1P/S1P_R$, LFA-1, VLA-4,	101 102 103
• Dermal DC: langerin+ subset $Langerin^+$ $MHCII^+$ $CD103^+$ $CD11b^{lo}$ $CD11c^{int}$ $CD45^{hi}$ $CD8\alpha^-$	Dermis ↓ Afferent lymphatics ↓ LN	*Immature* CCR2 (MCPs), CX_3CR1(fractalkine) *Mature* CCR7 (CCL19/21)	P/E selectin ligands	101 104 103
• Dermal DC: langerin- subset $Langerin^-$ $MHCII^+$ $CD11c^+$ $DEC205^+$ $CD24a^-$	Dermis ↓ Afferent lymphatics ↓ LN	*Immature* CCR2(MCPs), *Mature* CCR7 (CCL19/21), CXCR4 (CXCL12)	$S1P/S1P_R$, LFA-1, VLA-4	102
• $CD8\alpha^+$ DC $CD8\alpha^+$ $MHCII^+$ $CD11c^+$ $CD4^-$ $CD205^+$ $SIRP\text{-}\alpha^-$	Blood SLO ↵ ↓ ↳ BM Thymus	*Immature* CX_3CR1 (fractalkine) *Mature* CCR7 (CCL19/21)	LFA-1, VLA-4	83 105,106
• $CD8\alpha^-$ DC $CD8\alpha^-$ $MHCII^+$ $CD11c^+$ $CD11b^+$ $CD4^-$ $SIRP\text{-}\alpha^+$ $DCIR2^+$	Blood SLO ↵ ↓ ↳ BM Thymus	*Immature* CX_3CR1 (fractalkine) *Mature* CCR7(CCL19/21)	LFA-1, VLA-4	106 83 105
• $CD8\alpha^-$ $CD4^+$ DC $CD8\alpha^-$ $CD4^+$ $CD11b^+$ $MHCII^+$ $DCIR2^+$	Blood ↓ Spleen	*Immature* CX_3CR1 (fractalkine) *Mature* CCR7 (CCL19/21), CCR5 (CXCL13)	LFA-1, VLA-4	107

Table 2 continued. Traffic molecule profiles of mouse dendritic cells[90]

DC subset and phenotype	Migratory route	Chemokine receptor expression (ligand)	Other traffic molecules	References
Differentiated DCs continued				
• pDCs $B220^+$ $CD11c^{lo}$ $Ly6C^+$ $MHCII^{lo}$ $CD4^{-/+}$ $CD8\alpha^{-/+}$ $PDCA\text{-}1^+$ (human: $CD123^+$ $BCDA\text{-}2^+$, $\text{-}4^+$)	Blood ↙ ↙ ↘ ↘ Tissue Thymus SLO BM	*Immature* CCR2 (MCPs), CXCR3 (CCL9/10/11), CXCR4 (SDF-1), CCR5 (MIP/RANTES), CCR9 (CCL25) *Mature* CCR7(CCL19/21)	L-selectin, ChemR23	108 109 110 111 112
• Lung DCs (2 subsets) (conducting airways) 1. $CD11b^{hi}$ $CD11c^+$ CD103- (lung interstitium) 2. $CD11b^{low}$ $CD11c^+$ $CD103^+$	Lung ↓ Afferent Lymphatics ↓ LN	*Immature* $CCR7^{lo}$ (CCL19/21) *Mature* $CCR7^{hi}$ (CCL19/21), CCR8 (CCL1)	$S1P/S1P_R$, CD38	113
• Lamina propria DCs (4 subsets) 1. $CD11c^{high}$ $CD11b^-$ $CD205^+$ $CD103^+$ 2. $CD11c^{high}$ $CD11b^+$ $CD205^+$ $CD103^+$ 3. $CD11c^{int}$ $CD11b^{int}$ $CD205^-$ $CD103^-$ 4. $CD11c^{int}$ $CD11b^+$ $CD205^-$ $CD103^-$	Lamina Propria ↓ Afferent Lymphatics ↓ LN	*Immature* CCR6 (CCL20), CX_3CR1 (fractalkine) *Mature* CCR7(CCL19/21), CCR8(CCL1)	n.d.	114
• Peyer's Patch DCs (3 subsets) 1. $CD11c^+$ $CD8\alpha^+$ $CD11b^-$ 2. $CD11c^+$ $CD8\alpha^-$ $CD11b^+$ 3. $CD11c^+$ $CD8\alpha^-$ $CD11b^-$	Peyer's Patches	*Immature* CCR6(CCL20), CCR1(CCL9), CX_3CR1 (fractalkine) *Mature* CCR7 (CCL19/21)	n.d.	114

Fully differentiated DCs are found in healthy tissues as immunologically immature cells, i.e. they are equipped with highly active endocytic machinery for the sampling of Ags but have not acquired the capacity for full-fledged priming of naive T cells[115]. Some tissues are notably enriched for DCs, such as the skin and mucosal surfaces, the most common sites of entry for microbial pathogens, and the SLOs where adaptive immune responses to such pathogens are initiated. Indeed, a central function of DCs in non-lymphoid tissues is the transport and presentation of antigenic cargo into and within SLOs. This is owed to the DCs' ability to enter small lymph vessels in peripheral tissues and migrate to local draining lymph nodes (LNs). Somewhere en route to the LN these Ag-bearing DCs mature, i.e. they assume an immunostimulatory phenotype concurrent with increased expression of MHC complexes and upregulation of the co-stimulatory molecules and cytokines needed for efficient T cell priming. A small fraction of DCs that enter lymphatics are not retained in LNs, but travel along the lymphatic tree to the venous circulation. These blood-borne DCs can deliver their antigenic cargo to the spleen[85,116] and to primary lymphoid tissues, i.e. the BM[84,105] and thymus[80,83,117-119].

Given this complex life cycle, the ability of DCs and their progenitors to migrate throughout the body is a critical aspect of their immunological function. The term “migration”, as discussed here, encompasses several discrete events that occur in different environments under different biophysical conditions, and invoke numerous context-specific cellular and molecular mechanisms (**Fig. 5**). Specifically, DC migration entails: (1) the ability of newly formed DCs or their progenitors to exit their place of origin (i.e. the BM, spleen and thymus) and enter the blood; (2) the recruitment of the circulating cells into target tissues; (3) the extravascular lodging and interstitial motility needed to sample Ags; (4) the capacity to access lymph vessels to travel either to LNs or back to the blood; and (5) the ability to interact with migrating lymphocytes and other immune cells in a manner that allows the exchange of critical information regarding the nature and context of presented Ags. For the purpose of this thesis we will specifically discuss DC migration from the blood to primary lymphoid tissues.

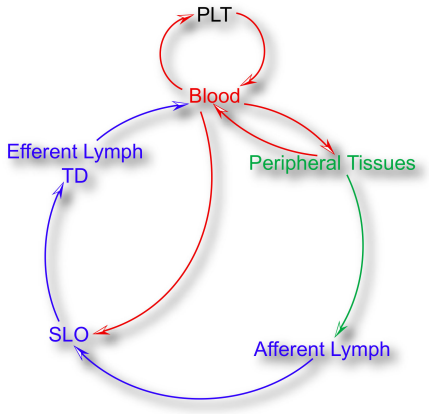

Fig. 5. Programmatic outline of DC and DC precursor trafficking routes. DCs develop from precursors that originate from primary lymphoid tissues (PLT) such as the BM and the thymus. Precursors and committed DCs enter the circulation and seed peripheral tissues and SLOs. From peripheral tissues, they can access afferent lymph upon receiving a mobilization signal and travel to the draining LN. Leukocytes leave LNs via the efferent lymph and are collected in the TD, which eventually guides DCs and their precursors back into the circulation[90].

Methods to study DC migration

Many DCs begin their journey with their release from the BM into the blood and subsequent traffic into peripheral lymphoid and non-lymphoid tissues. In non-lymphoid tissues, DCs eventually proceed into LNs through afferent lymphatics and, in some instances, return back to the blood via the thoracic duct (TD). Throughout this journey migrating DCs must apply specialized skills to reach their target destination, including the capacity to: traverse vessel walls and other anatomic barriers; recognize and adhere to specific

microvascular endothelial cells in the presence of shear stress in the blood-stream; sense and follow soluble and surface-bound chemoattractant cues through the interstitium; and scan and interact productively with a vast number of lymphocytes in primary and secondary lymphoid organs. Although no single method in the immunologist's toolbox sufficiently covers all the diverse steps that constitute a DC's longwinded journey, the combined application of the techniques discussed below has been instrumental to carve out an ever more detailed picture of how DC migration impacts physiological and pathological immune responses.

A number of techniques has been particularly useful in studying DC trafficking from blood into peripheral tissues or SLOs, such as intravital videomicroscopy (IVM)[105,120] and flow cytometric or histology-based DC homing assays[121], which provide useful information at the single-cell and population level, respectively. A detailed analysis of DC interactions with endothelial ligands under precisely controlled biophysical conditions is also afforded by the use of flow chamber devices[122]. Profound insights into DC traffic signals involved in transvascular diapedesis and interstitial navigation have been achieved using in vitro chemotaxis assays[123].

Trafficking of DCs from tissues to SLOs via the lymph has been exhaustively studied, in particular, by classic assays that mobilize DCs from peripheral tissues with fluorescent tracers, followed by enumerating the emigration and immigration of fluorescent DCs from the periphery and into the draining LN, respectively[124]. This approach relies on the assumption that the number and phenotype of fluorescent DCs recovered from a LN are indicative of their migration and not due to acquisition of fluorescent tracer by LN-resident cells. A more recent approach involves genetic manipulations that permanently or conditionally label DCs through fluorescent proteins driven, for example, by promoters for langerin[125], CD11c[126] and CX_3CR1[106]. This offers the advantage that unperturbed endogenous DCs can be studied in situ, but has the potential drawback that reporter expression levels may change during maturation or differentiation. The development of a photoconvertible fluorescent protein, Kaede, which upon exposure to UV light shifts its excitation and emission spectrum, has emerged as another useful system to

monitor the cellular trafficking patterns, including those of DCs, in transgenic mice[127]. Similarly, the emergence of a photoactivatable GFP (PA-GFP) has offered new possibilities to tag cells and has proven useful to gain a better understanding of the migratory properties of leukocytes, especially during germinal center formation[128,129]. Purified or in vitro differentiated DCs have also been genetically or chemically labeled and injected into tissues to study their trafficking to and function within draining LNs[121,130]. This allows for more quantitative and time-resolved analyses of the molecular mechanisms, kinetics, and immunological sequelae of DC migration. However, several caveats of these approaches must be kept in mind, including the large, non-physiological numbers of DCs that must be transferred, the need for ex vivo manipulation, and that transferred DCs are often not native to the tissue being studied. In this regard, parabiotic or competitive BM chimeric mouse models offer advantages for studying physiological recruitment and turnover of DCs and, in conjunction with adoptive transfer strategies, have been useful in addressing the migration and differentiation of rare DC precursors[80,83,85,94-96].

Technological advances in IVM and multi-photon (MP) imaging have recently enabled researchers to directly visualize DC migration and DC interactions in their native environment[131-133]. Conventional IVM uses brightfield transillumination or epifluorescence microscopy that permits two-dimensional imaging of intravascular adhesion events in surgically exposed tissues in real time[134]. This approach has helped to pinpoint the precise role of trafficking molecules during DC-endothelium interactions as part of the intravascular multistep adhesion cascade. MP IVM uses infrared-pulsed laser excitation to generate high-resolution optical sections of living tissue containing fluorescently-labeled cells, such as DCs, migrating and engaging in various cell-cell interactions[135] (see also section “Multi-photon microscopy”). Additional novel imaging modalities have recently been introduced such as bioluminescence imaging, magnetic resonance imaging, and positron emission tomography which provide non-invasive tracking of leukocyte populations, including DCs, throughout the entire body, although with considerable less spatial and/or temporal resolution to visualize single-cell dynamics[136].

Traffic molecules in DC migration

Circulating DCs and their precursors exit the blood in response to tissue-specific recruitment signals that are displayed on the vascular wall. These include signals that emanate from sites of inflammation (like the pro-inflammatory chemokines (chemotactic cytokines)) or from normal tissues that recruit DC precursors during the initial seeding and subsequent physiological turnover of tissue-resident DCs[137]. Circulating leukocytes can only follow these recruitment signals by engaging adhesion molecules, which allow them to withstand the shear stress exerted by microvascular blood flow and to commence transvascular movement into the target tissue. DCs express specific adhesion molecules and maturation-dependent chemoattractant receptors that allow them to respond to a variety of ligands[138,139], which control their trafficking. For example, to access non-lymphoid peripheral tissues and navigate within them, immature DCs (and some of their precursors, particularly monocytes) utilize specific chemokine receptor-ligand pathways, such as CCR2 – CCL2 (MCP-1)[99,140], CCR5 – CCL5[141,142], and CCR6 – CCL20[143]. When DCs become mature they downregulate their responsiveness to these inflammatory chemokine pathways and traffic to the draining LNs by upregulating CCR7, which responds to two ligands, CCL19 and CCL21[144-146]. These chemokines are expressed by peripheral lymphatic endothelial cells as well as LN stroma cells and guide DCs to downstream LNs[147-149].

DCs and their precursors are recruited from blood into tissues (except the spleen) following a cascade of sequential molecular and cellular interactions, analogous to what has been shown for the extravasation of other circulating leukocytes. According to this paradigm, leukocyte extravasation occurs in a series of distinct steps including tethering, rolling, activation by a chemoattractant, firm adhesion, and diapedesis[150].

On most leukocytes, including circulating DCs, tethering and rolling are primarily mediated by one or more of the three members of the selectin family and occasionally by α_4 integrins. Two selectins, P- and E-selectin, are

expressed on activated endothelium, whereas L-selectin is found on leukocytes. Selectins bind sialyl-Lewis X-like carbohydrates presented by sialomucins, such as P-selectin glycoprotein ligand 1 (PSGL-1)[151].

Rolling cells must next encounter a chemoattractant stimulus, often (but not always) in the form of a chemokine presented on venular endothelial cells[152]. Most chemoattractants signal through pertussis toxin (PTX)-sensitive G protein-coupled receptors (GPCRs), causing clustering and conformational activation of integrins. Activated integrins, in particular LFA-1 ($\alpha_L\beta_2$), VLA-4 ($\alpha_4\beta_1$), Mac-1 ($\alpha_M\beta_2$) and $\alpha_4\beta_7$ mediate firm arrest of the rolling cells by binding to members of the immunoglobulin superfamily (IgSF), including ICAM-1 (ligand for LFA-1 and Mac-1), ICAM-2 (ligand for LFA-1), VCAM-1 (ligand for VLA-4 and weakly for $\alpha_4\beta_7$) and MAdCAM-1 (ligand for $\alpha_4\beta_7$)[153].

Upon firm arrest, leukocytes respond to localized chemoattractant and/or adhesion molecule gradients, which provide guidance cues for diapedesis and directed leukocyte migration. The essential molecular determinants involved in tethering, rolling, firm adhesion and diapedesis are expressed by both circulating DCs and precursors that can give rise to DCs, such as monocytes[154] and HSPCs[155]. Indeed, IVM experiments have determined that both cDCs and pDCs tether and roll efficiently along venular endothelium in an E- and P-selectin dependent fashion and, like other inflammatory cells, can be recruited from the blood to sites of inflammation[109,120].

The combinatorial use of selectins, chemoattractant receptors, integrins and their respective ligands provides for a great deal of diversity and selectivity in regulating leukocyte migration to distinct tissues[156]. Individual leukocyte subsets, including DCs, express only a small selection of the broad palette of traffic molecules and, therefore, can only successfully participate in one or a few specific multi-step cascades. Conversely, many specialized microvascular endothelial cells present a highly tissue-specific assortment of adhesion molecules and chemoattractants, thus providing a unique tissue- and situation-specific molecular “area code”. In the subsequent section, we highlight specific examples of how multi-step adhesion cascades control the

movement of intravascular DCs and their precursors into different target organs.

DC migration from blood to tissues

Blood contains both DC precursors and differentiated DC subsets, including pDCs and cDCs, which are a mixture of newly generated cells from the BM and of experienced DCs that have re-entered the circulation from peripheral tissues[124]. There are also pluripotent HSPCs, which recirculate continuously between the blood, peripheral organs and draining lymphatics and can give rise to DCs upon TLR ligation[96]. Blood contains also lineage-committed BM-derived DC precursors that can differentiate into any DC subset found in SLOs[93-95]. An additional source of DCs are circulating monocytes[157]. Two monocyte subsets have been identified in mice and humans that are distinguished by the differential expression of Ly-6C (in mice) and three traffic molecules, CX_3CR1, CCR2 and L-selectin[99,158]. Ly-$6C^{high}CX_3CR1^{low}CCR2^{high}$ ("inflammatory") monocytes are preferentially recruited to distressed tissues in a CCR2 – CCL2 dependent manner. They can give rise to a variety of conventional DCs under both inflammatory and steady-state conditions. The second subset, Ly-$6C^{-}CX_3CR1^{high}CCR2^{-/low}$ ("resident") monocytes, interacts with fractalkine (CX_3CL1), a transmembrane chemokine on resting endothelium. These cells patrol along the luminal surface of microvessels, enter tissues upon inflammation and differentiate into macrophages[99,159].

An abrupt increase in circulating DC numbers occurs when DCs are injected intravenously (i.v.). Although non-physiological, such events are clinically relevant because antigen-pulsed autologous DCs have been given to patients by various routes as anti-cancer vaccines[91,160]. This clinical context highlights the importance of understanding the target organs of circulating DCs and the molecular mechanisms that govern their migration to those sites. Irrespective of their origin and differentiation state, circulating DCs and their precursors gain access to lymphoid and non-lymphoid tissues through multi-step adhesion cascades. The molecules involved in discrete adhesion steps vary

depending on the DC subset and the target tissue, thus providing specificity and selectivity in recruitment (**Fig. 6**).

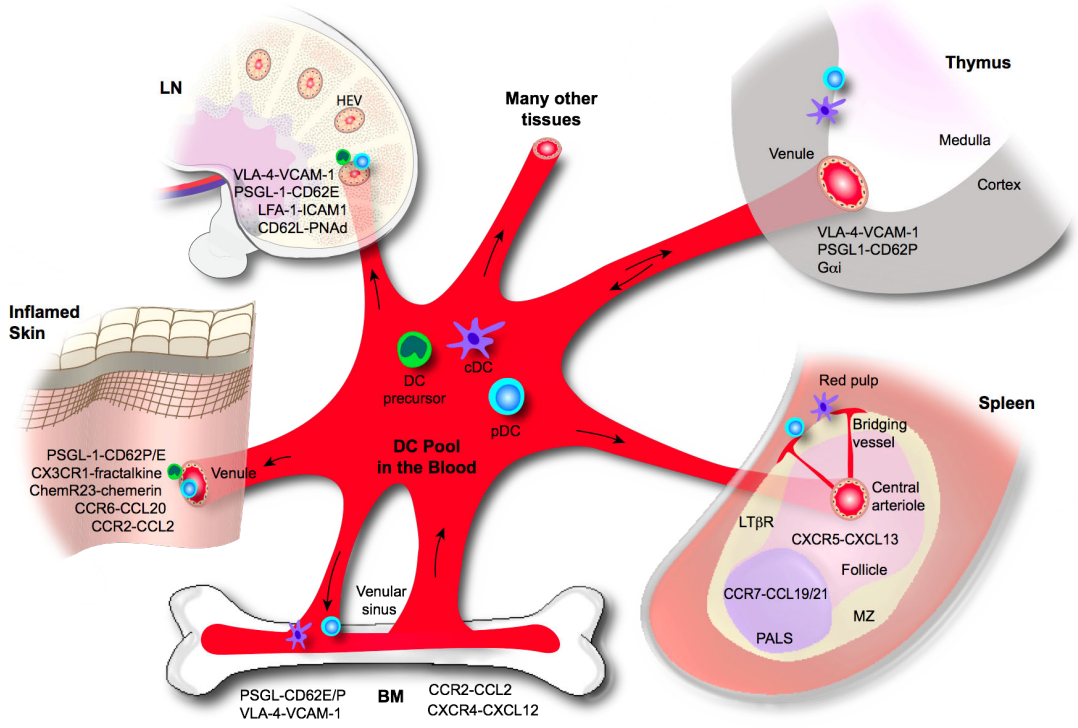

Fig. 6. Hematogenous DC routes[90]. This schematic outline illustrates various routes that DCs can take to and from the blood into various lymphoid and non-lymphoid tissues. DC precursors are released from the BM and enter the blood pool, which consists of: conventional DCs (or cDC), pDCs, and DC precursors (encompassing monocytes, HSPCs, and other committed DC precursors). Potential destinations of blood-borne DCs as well as the major trafficking molecules implicated in their migration are highlighted, including *(from left to right)* the skin, LN, thymus, and spleen, as well as their re-entry into the BM.

DC traffic to non-lymphoid tissues

The recruitment mechanisms that guide fully-committed immature or mature DCs from blood into non-lymphoid tissues are only partly characterized. Our current knowledge is mainly based on adoptive transfers of labeled DCs by i.v. injection. A major fraction of injected mature and immature DCs accumulate in the liver and lungs in mice and humans[105,161,162]. Though the underlying mechanisms governing this distribution are poorly understood, the retention of DCs in the lungs is probably due, at least in part, to mechanical trapping in pulmonary capillaries, rather than active adhesion[105].

IVM experiments have shown that cDCs can efficiently tether and roll in normal murine skin venules, which constitutively express E- and P-selectin[120]. Because sLeX-decorated PSGL-1, the principal ligand for the vascular selectins, is not only highly expressed on DCs[120], but also on monocytes and HSCs[155,163], it is likely that all DCs and DC precursors can engage in rolling interactions in microvascular beds that express P- and/or E-selectin either constitutively (e.g. in skin, BM and thymus) or in response to inflammation. Interestingly, DC extravasation into inflamed skin depends on selectins but not on PSGL-1, suggesting a contribution by other selectin ligands on DCs[164].

Although selectins are clearly important, they mediate only the first step in the multistep adhesion cascade and do not by themselves support DC arrest or accumulation in normal skin. Additional signals are required to trigger integrin activation, arrest and subsequent diapedesis[120,164]. However, little is known about the inflammation-induced or constitutive chemoattractants that trigger these steps. Direct experimental observations of steady-state DC recruitment to normal tissues are particularly challenging, because these are very rare events that may only become prominent after long-term adoptive transfers or in parabiosis settings. Some information may be gleaned from in vitro experiments. For example, a recent study found a role for the IgSF molecule ICAM-2 in the transmigration of immature DCs across endothelial monolayers[165].

Lineage-committed DC precursors (other than monocytes) have not been examined so far for their capacity to home to normal tissues other than SLOs. Reconstitution experiments in irradiated mice with wildtype (wt) and mutant BM have shown that circulating langerhans cells (LC) precursors repopulate severely inflamed skin in a CCR2- and CCR6-dependent manner, but these pathways are apparently not operational in normal skin[140,143]. Accordingly, the CCR2 ligands, CCL2 and CCL7, and the CCR6 ligand, CCL20, are poorly expressed in resting tissues, but markedly increased in inflamed skin[140,143,166].

The so-called inflammatory $CX_3CR1^{low}CCR2^{+}Ly6C^{high}$ monocytes can enter diverse inflamed tissues, including the skin, lung, and intestinal lamina propria, where they give rise to various DC subsets[167-169]. The CX_3CR1^{high}

CCR2^{-} Ly6C^{low} monocytes can also give rise to DCs (or at least CD11c^{+} cells) in the lung[169] and atherosclerotic plaques[170]. However, the role of specific traffic molecules in each case is largely unclear. Arguably the best evidence exists for CCR2, since Ly6C^{high} monocytes fail to accumulate at sites of inflammation in *Ccr2*$^{-/-}$ mice[140]. However, it must be noted that CCR2 controls the inflammation-induced release of monocytes from the BM[171]. Thus, the observed migration defect could either reflect poor monocyte mobilization or defective peripheral recruitment, or both.

Circulating pDCs can also access inflamed tissues, but their homing properties are thought to differ substantially from those of conventional DCs. Compared to the latter, human pDCs exhibit only a weak capacity in vitro to migrate towards pro-inflammatory chemokines (e.g. CCL2, CCL5, and CCL20) despite expressing a similar chemokine receptor profile (e.g. CCR2, CCR5, CXCR3, CXCR4, and CCR7)[110]. On the other hand, pDCs migrate effectively towards CCL19 and CCL21, two homeostatic chemokines that act on CCR7 and are constitutively expressed in SLOs[110]. Indeed, substantial numbers of pDCs are found in SLOs but they are relatively infrequent in most non-lymphoid tissues. In humans, pDCs are enriched in certain inflamed non-lymphoid tissues, such as lupus erythematosus lesions[172], psoriatic skin[173] and the nasal mucosa of allergic rhinitis patients[174], but it has not been determined if their presence at those sites reflects recruitment of differentiated circulating pDCs or local differentiation from progenitors. Direct recruitment of blood-borne pDCs have been documented in normal and inflamed small intestine in mice; pDCs require CCR9 to access the intestinal wall, which physiologically generates CCL25, the ligand for CCR9[175]. Another chemoattractant for circulating pDCs is chemerin[111,112]. This non-chemokine molecule is generated by serine proteases that are activated during coagulation, fibrinolysis, and inflammation. Chemerin is absent from normal skin but is markedly upregulated during cutaneous inflammation and recruits pDCs via the serpentine chemokine-like receptor 1 (CMKLR1 or ChemR23).

Dendritic cell traffic to BM

Some fully committed DCs recirculate from peripheral tissues via the draining lymphatics and blood into primary lymphoid tissues. Through this tortuous route, DCs can deliver Ag from all over the body to both the BM and the thymus. However, immunological consequences in each tissue are markedly different. The BM shares a number of features with bona fide SLOs and serves as a major reservoir for memory T cells[176]. Ag-laden circulating DCs that home to the BM evoke a vigorous memory response that leads to rapid proliferation and peripheralization of responsive T cells[105]. Immature and mature DCs enter the BM equally well by employing a multi-step adhesion cascade. IVM in mouse skull BM has shown that rolling is mediated by interactions of PSGL-1 with P- and E-selectin in BM venules and sinusoids, whereas VLA-4–VCAM-1 is required for sticking. Although DCs express β_2 integrins, homing to the BM is independent of these molecules. DC homing to BM is also not affected by PTX treatment, suggesting that DCs may use an as yet unidentified chemoattractant receptor(s) that does not signal through the conventional $G\alpha_i$ pathway to activate VLA-4[105].

Dendritic cell trafficking to the thymus

Thymic DCs play a key role in generating a self-tolerant T cell repertoire by presenting harmless sAgs to developing T cells during negative selection[79]. According to the expression of their surface markers, thymic $CD11c^+$ $MHC\text{-}II^+$ DCs can be further subdivided into $CD8\alpha^+CD11b^-$ and $CD8\alpha^-11b^+$ cDC and pDCs. Up to 30% of pDCs and $CD8\alpha^+$ DCs carry IgH rearrangements of the TCRα chain, indicating that the have developed from DN2/DN3 cells[81]. In line with this, CLP as well DN1-3 cells can give rise to thymic DCs, though with decreasing efficiency[43]. T lineage commitment of T cell progenitors is achieved by expression of Notch and likewise deletion of Notch1 drives DCs rather than T cell development of precursor cells in the thymus[43]. The accumulation of thymic DCs in the medulla, especially of $CD11c^+11b^-$ DCs is at least in part regulated by the expression of XCL1 by mature $MHC\text{-}II^{high}$ mTECs and XCR1 by the DCs[82].

It has also been shown that fully differentiated, yet immature DCs have the capacity to home to the thymus. Thus, the thymus harbors two distinct populations of DCs; one is derived from intrathymic lymphoid progenitors, whereas the second population originates from the periphery[68,119,177]. Monocytes or DC precursors have not been observed to home to the thymus[94,99]. By contrast, parabiosis and adoptive transfer experiments have established that small numbers of fully differentiated DCs constantly enter the thymus from the blood[80,83,117,119]. It is not clear whether or not all immature DC subsets share the same ability to home to the thymus. Adoptive transfer experiments of splenic Flt3L-expanded DCs led to the conclusion that all DCs subsets home to the thymus equally well[83], however, this finding has been challenged recently. It was shown in parabiotic mice that $CD8\alpha^{+}11b^{-}$ cDCs arise locally in the thymus while pDCs and $CD8\alpha^{-}11b^{+}$ cDCs can enter the organ from the periphery[80,119]. Inflammation-induced maturation selectively blocks the capacity of DCs to home to the thymus, but does not compromise DC trafficking to other organs[83]. This suggests a mechanism to safeguard against inadvertent deletion of T cells that recognize pathogen-associated Ags, which are much more likely to be presented by mature than immature DCs. The differential capacity of immature DCs to access the thymus is probably regulated by an organ-specific multistep adhesion cascade, whereby rolling and sticking are mediated by PSGL-1–P-selectin and VLA-4–VCAM-1, respectively. Unlike in the BM, DC entry into the thymus is PTX sensitive, but the specific $G\alpha_i$-coupled chemoattractant receptor(s) remain(s) to be identified[83] (**Fig. 7**).

Upon entering the thymus, homed DCs upregulate maturation associated markers such as MHC-II and CD80[80]. They localize almost exclusively in the medulla with a slight enrichment at the CMJ. Homing of DCs to the thymus has been shown to be an important tool to deliver peripheral Ag to the thymus and to make it available for negative selection[83,84]. Thymic DCs still maintain the capacity do proliferate and may undergo one or two cell divisions upon entering the organ[80]. It is possible that this is a mechanism to prolong the persistence of Ag similarly to cycling splenic DCs whose daughter cells continue to present captured Ag[85].

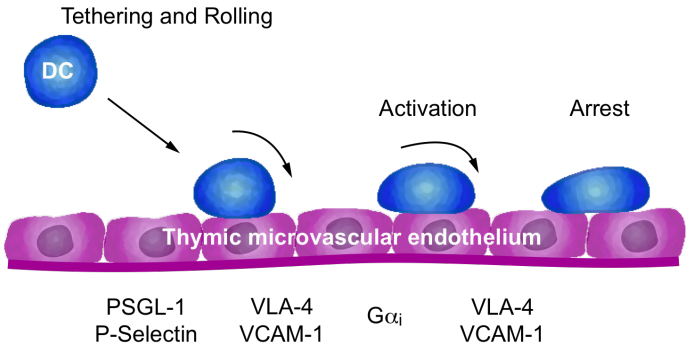

Fig. 7. DCs home to the thymus by employing a multi-step adhesion cascade. Rolling is mediated by PSGL-1 – P-selectin and VLA4 – VCAM-1 interactions. Integrin activation relies on at least one, yet unidentified GPCR and firm arrest is promoted by VLA-4 – VCAM-1.

Multi-photon microscopy

Multi-photon microscopy (MPM) has itself proven to be a particularly useful tool to visualize fluorescently tagged structures deep within tissues. Unlike conventional fluorescent microscopy, which utilizes one-photon excitation, MPM operates at lower laser powers and longer wavelengths. With a penetration depth of up to 500 µm as compared to ~100 µm for conventional confocal microscopy, MPM appears to be far superior. The enhanced penetration depth is mainly owed to the infrared excitation. MPM relies on the principle that the energy of two photons has to add up in order to excite fluorescent molecules. For instance, GFP has an excitation maximum of about 488 nm for one-photon excitation. As MPM relies on the additive effect of two photons, the excitation optimum of GFP for MPM is ~970 nm (**Fig. 8a**). Enough energy is only provided at the focal point where two photons meet to excited fluorescent molecules. As the focal point is very small and confined, excitation of surrounding tissue is efficiently prevented which results in dramatically reduced photo-bleaching and photo-toxicity (**Fig. 8b**). However, one has to keep in mind that infrared excitation produces heat, and thus actual overheating of the tissue sample is a bigger hazard for MPM as compared to conventional fluorescent microscopy[134,135,178,179].

The combination of MPM with time-lapse IVM has greatly advanced our current understanding of leukocyte motility and the interplay of different immune cells, especially in LN. We will here discuss considerations for performing time-lapse MP IVM and parameters that can be extracted from MP IVM to describe fluorescently tagged immune cell “behavior”[90,134,180].

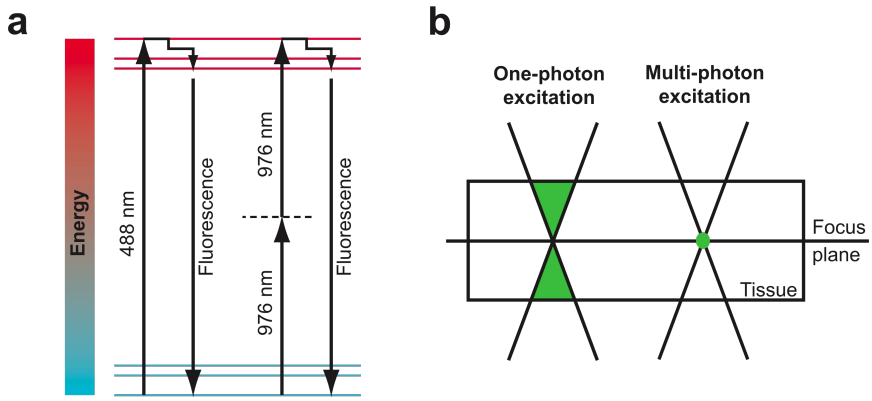

Fig. 8. Comparison of one-photon and multi-photon excitation. (**a**) For one-photon microscopy, one photon provides enough energy to elevate the energy status of a fluorescent molecule from the ground state to the excited state, while in multi-photon activation the additive energy of at least two photons is required. After non-radiative relaxation, the fluorescent molecule returns to the ground state by emitting light. (**b**) One-photon excitation occurs along the laser beam, while multi-photon excitation can only occur at the focal point where two or more photons meet.

MP IVM relies on the acquisition of an imaging volume at given time points over a predetermined time period. In order to gain information about three dimensional (3D) cell behavior, optical section along the *z*-axis are being acquired. Without a doubt, operating at minimal gap sizes between the optical sections and covering large, high resolution imaging volumes provides the highest possible optical and spatial resolution. High-resolution images tend to facilitate post acquisition image processing. Despite this, the large amount of data may make computation analysis time consuming as it causes imaging programs to run less stably. One also has to keep in mind that acquiring large amounts of data will prolong the minimal cycle time between the acquisitions of the imaging volumes. Consequently, the temporal resolution of cellular processes will be compromised. High-resolution *z*-stacks also require a relatively long exposure time as compared to lower resolution *z*-stacks, which greatly increases the probability to cause tissue damage and photo-bleaching. To avoid this, one can work with minimal resolution *z*-stacks that cover smaller volumes, the gap size between optical sections is bigger and the optical sections per se are of lower resolution. The advantage of this clearly lies in the opportunity to acquire *z*-stacks at shorter time intervals and thus, gaining better temporal resolution. Also photo-toxicity is markedly reduced when using minimal resolution *z*-stacks. However, the spatial and

optical resolution is compromised, meaning post-acquisition image processing may prove challenging due to the lower optical resolution. Taken together, clearly the question one seeks to answer with a given experiment dictates the priorities and the compromises that have to be made between spatial and temporal resolution[134,181].

After acquisition, the individual optical sections of each recorded fluorescent channel of the time-lapse recording are compiled into a four dimensional (4D) movie (consisting of *x, y, z* and time parameters) using image processing software. The movie is further analyzed by identifying and tracking of single cells. Basically, a cell's track consists of a sequence of *x, y* and *z* positions that are linked to their corresponding time points within the movie. Using this information, one can extract a variety of parameters to describe the cells motile behavior (**Table 3**).

Table 3. Measurement parameters used for MP IVM[134,179]

Parameter	Description	Unit
3D instantaneous velocity (3DIV)	Velocity measured during a defined time interval (t), e.g., $v_{0\rightarrow1} = d_{0\rightarrow1}/t_{0\rightarrow1}$	µm/min
Mean velocity per track (V)	Mean velocity of a cells track, e.g., $V_{0\rightarrow n} = (v_{0\rightarrow1} + v_{1\rightarrow2} + v_{2\rightarrow3} + \ldots) / n$	µm/min
Displacement (d)	Distance between first and last imaging point, e.g., $d_{0\rightarrow n} = \sqrt{(\Delta x_{0\rightarrow n}^2 + y_{0\rightarrow n}^2 + \Delta z_{0\rightarrow n}^2)}$	µm
Mean displacement (MD)	Average distance migrated from arbitrary points of origin over a selected time (t) representing a multiple of the scan interval (si), e.g., $MD_{(t=1si)} = (d_{0\rightarrow1} + d_{1\rightarrow2} + d_{2\rightarrow3} + d_{3\rightarrow4} + \ldots d_{n-1\rightarrow n})/n$; $MD_{(t=2si)} = (d_{0\rightarrow2} + d_{1\rightarrow3} + \ldots d_{n-2\rightarrow n}) / (n-1)$	µm
Motility coefficient (M)	A measure for a cell's propensity to move away from its point of origin, analogous to the diffusion coefficient of Brownian motion, e.g., $M = d^2/6t$	μm^2/min
Meandering index (MI)	A measure for the directionality of cell migration. Represents the ratio of the displacement (d) over the total path length e.g., $MI = d_{0\rightarrow n} / (d_{0\rightarrow1} + d_{1\rightarrow2} + d_{2\rightarrow3} + \ldots d_{n-1\rightarrow n})$	N/A
Turning angle	The angles at which a cell deviates from a straight line between subsequent measurement intervals.	degrees
Shape index	Measure for a cells polarization, long axis / short axis	N/A

One of the most commonly used motility parameters is velocity. Velocity is the displacement of a cell over time. Given that most cells do not migrate in a strictly straight line, the mean velocity per track is calculated as the velocity between frames (instantaneous velocity) of each track and then averaged with the track. As mentioned before, a cell's migration path rarely follows a

straight line and consequently instantaneous velocity is a parameter that is influenced by the cycle time at which the time-lapse recording was acquired. For instance, shorter time intervals (e.g. 15 sec) will reveal twists and turns in the cells' migratory path that cannot be detected using longer cycle times (e.g. 60 sec). Consequently, the path length of a cell may appear shorter and more directional meaning that the same cell appears to migrate at lower velocities. As to date it is not possible to acquire 4D MPM movies at real-time, one has to assume that the calculated instantaneous velocities are biased towards underestimating the real migration speed to varying degrees depending on the cycle time.

A potential pitfall that is specific to all parameters that are expressed per track, such as mean velocity per track, lies in the accuracy of the cell tracking software. In the simplest setting, automated cell tracking software identifies objects in a predetermined size range whose fluorescence intensities significantly deviate from the background noise. These parameters are set by the individual operating the software and are customized for each fluorescent channel and recording separately. The tracking software then identifies the objects, reduces them to their geometrical center and applies mathematical models to identify the same cell in different frames of the movie that ultimately make up one track. The most commonly used models are the Brownian motion algorithm and autoregressive motion algorithm. The Brownian motion algorithm identifies the most likely path connection between two geometrical centers in any direction with a distance constraint. In contrast the autoregressive algorithm utilizes the displacement (position, speed and direction) of a cell's geometrical center between the previous and the current frame to extrapolate a model and predict the location of the geometrical center in the next frame and then identify the geometrical center that comes closest to this prediction. This cell is then incorporated into the track and the process repeats. Because it is easier to predict the movement of slow moving cells than fast moving cells (with either algorithm), tracks of fast moving cells are prone to errors. Specifically, there is a small tendency towards identifying the "wrong" cell as a part of the track, which results in the fusion of two separate tracks into one. At times, these tracks can be relatively far apart and

consequently, a bias towards higher velocities per track is introduced. Another pitfall is that tracks of fast moving cells have a tendency towards being split up in several tracks, thus resulting in an over-representation of the number of fast moving cell tracks as compared to slow moving cell tracks, and further exacerbating the bias toward high velocities. To summarize, the instantaneous velocity tends to be an underestimate owing to the non-real time data acquisition. Conversely, the mean velocity per track can be biased towards fast moving tracks and may thus overestimate the actual velocity. As instantaneous velocity is less affected by manually / post acquisition introduced errors, it is generally believed that this parameter reflects a cell's real velocity more accurately as compared to mean velocity per track.

Another commonly used motility parameter is the motility coefficient. Similarly to the Brownian diffusion coefficient, it describes the propensity of a cell population to move away from an arbitrary point of origin, or to put in other words, it measures how fast cells "diffuse" from their point of origin. This parameter can be derived by graphing the mean displacement of a cell population versus the square root of time. The mean displacement is calculated for each cell for all frames of a track. It is the mean of displacement between the location at the origin of the track (at t_0) and the cells' location at subsequent time points (at $t_{1\rightarrow n}$, **Fig. 9a**). Plotting the mean displacement versus the square root of time results in a graph that provides information about the quality of the migration on the population level. The resulting graph typically consists of an initial, non linear segment, followed by linear relation of displacement and the square root of time. A persistent linear relation indicates random migration. A plateau is characteristic for confined migration while branching off from the linear regression to the other side is a hallmark for directed migration (**Fig.9b**). Furthermore, the regression line of the graph that fits the linear segment can be used to calculate the motility coefficient[134,181] (**Table 3**).

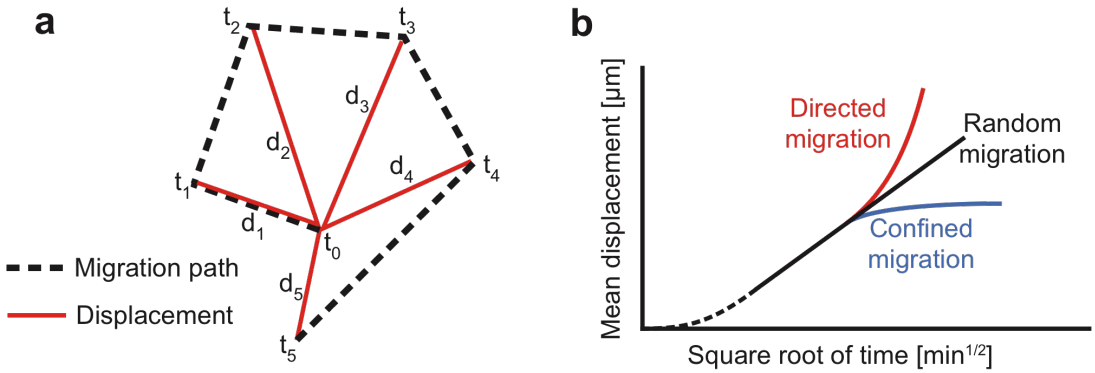

Fig. 9. Scheme of a displacement and mean displacement plot. (**a**) Schematic of the migration path (dashed line) and displacement (d, red line) of a cell at given time points (t). (**b**) Random migration is indicated by a linear relation between mean displacement and the square root of time (black line), faster displacement indicates a directed migration pattern (red line), slower displacement represents confined migration (blue line). Over short periods of time, cells tend to displace faster than random (dashed line, persistent motion).

The meandering index is a popular parameter to further describe the mirgratory path of the cells. It is widely used and known under several different names, such as chemotactic index, confinement ratio or straightness index. Despite the different names, it is always calculated by dividing the tracks displacement by the path length. If the track is a straight line, the meandering index is 1, if the cell's first and last location is the same, e.g. if it didn't move at all or moved in a perfect circle, the meandering index is 0[134,181].

A less commonly used parameter is the turning angle, which measures the deviation of the migration path in subsequent frames. This measure also provides information about the directionality of the migration[134].

Lastly, by measuring the surface of a cell rather than its geometrical center, one can gain information about its shape and the change in shape over time. A cell's roundness is usually measured by the shape index, which is calculated by dividing the short axis by the long axis. A perfect sphere has a shape index of 1, while a perfect line has a shape index of 0. Notably, this index does not give any information about the volume of the cell[179].

Aims of the thesis

A functional immune system has to protect the body from pathogens while being tolerant to self-antigens. To achieve this goal, developing thymocytes are subject to tolerance mechanisms. Central tolerance takes place within the thymus and removes the bulk of auto-reactive thymocytes by either clonal deletion (negative selection) or redirection of auto-reactive thymocytes into a regulatory T cell lineage. DCs are key players in this process. They acquire and present self-peptide in the context of MHC molecules to thymocytes and can either promote survival or apoptosis of interacting T cells.

Thymic DCs consist of two major subsets that can be distinguished according to their surface markers: cDCs and pDCs. They can also be differentiated according to their place of origin. Thymus resident DCs differentiate locally from a progenitor cell, while homed DCs enter the thymus fully differentiated from the blood.

Until recently, the analysis of the crosstalk of different cell types within the thymus has been limited to conventional histological approaches[182] and thus cannot provide any data about the dynamics of interactions. Recently, this limitation has been overcome by employing MP IVM.

Bousso et al. used reaggregated thymic organ cultures (RTOCs) in combination with MP IVM to visualize encounters between thymocytes and stromal cells[183]. Though this in vitro system provides all cell types present in a native thymus, the thymic architecture is disrupted. It can be concluded from recent studies about thymic organization, that intact cortical and medullary regions are indispensable for central tolerance[184]. Additionally, this system cannot provide important factors such as a constant blood flow or innervation that may influence cellular dynamics within the thymus.

Other studies took advantage of so called acute thymic slice preparation to visualize thymocyte – APC interaction during positive selection[185,186]. This approach enables one to follow developing T cells within the cortex and

medulla. However, the disadvantage of this set up is that the preparation of the thymus requires a broad range of different temperatures ranging from 4°-37°C that may influence cellular behavior. Also, factors like blood flow or innervation cannot be provided in this in vitro system. On the other hand, the thymus' normal anatomic localization within the thorax makes intravital imaging strategies extremely challenging. In particular, to observe individual migrating intra-thymic cells and their interactions with other thymic constituents, it is necessary to generate 3D recordings of cells of interest over time intervals ranging from minutes to hours. Even subtle tissue movements would result in motion artifacts that render imaging data uninterpretable. Since the thymus is in direct contact with both the heart and the lungs, it would be extremely difficult to obtain useful imaging information from orthotopic thymi in living animals.

We aimed to circumvent these shortcomings by transplanting embryonic thymus lobes under the kidney capsule of recipient mice. Using this system we were able to visualize T cell behavior in the thymus under selecting and non-selecting conditions. We also specifically focused on DCs as to date, it is poorly understood whether thymus resident versus homed DCs exhibit specialized functions in T cell selection. We employed MP IVM combined with a broad range of other experimental strategies to address whether resident versus homed DCs differed in the mechanisms they used to acquire peripheral Ag for presentation to T cells.

Specifically, we have addressed the following four specific aims:

Aim 1: To establish MP IVM for transplanted thymi

This aim focused on the establishment and optimization of the first model of MP IVM of intact murine thymus lobes. The endogenous thymus in mice is inaccessible to IVM due to motion artifacts, a result of its anatomical location. To circumvent this, we took advantage of a transplantation model. This aim covers the transplantation of embryonic thymi, the analysis of the grafts

(subaim 1.1) and development of the imaging strategy for MP IVM (subaim 1.2).

Aim 2: To analyze the motile behavior of thymic DCs and T cells

We asked whether we could identify cortex and medulla in transplanted animals in vivo (subaim 2.1), describe the motile behavior of thymocytes and DCs in cortex and medulla (subaim 2.2) and address how thymocyte migration is altered when they encounter homed DCs that present cognate Ag (subaim 2.3). These experiments revealed important insights in T cell development and the dynamic interaction of thymocytes with DCs and refined our understanding of negative selection.

Aim 3: To analyze homed versus thymus resident DCs

This aim tested the hypothesis that homed and thymus resident DCs display a different motility behavior. We addressed this by visualizing homed and thymus resident DCs in the same imaging volume using MP IVM. This aim highlighted differences of thymic DCs according to their origin and provided important clues as to whether these subsets exhibit specialized functions.

Aim 4: To test whether thymus resident DCs acquire blood borne Ag

We aimed to test whether thymic DCs that are closely associated with vascular structures could breach the endothelial layer and thus, gain access to blood borne components, such as antigenic material. To test this, we investigated whether thymic DCs could be stained in vivo by an intravenously administered mAb (subaim 4.1). We addressed the possibility of a specialization of thymus resident versus homed DCs in the formation and

extension of transendothelial protrusions into the blood stream by intravenous mAb labeling (subaim 4.2). Furthermore, we administered blocking mAb to a variety of candidate molecules to assess the mechanism by which thymic DCs gain access to the blood (subaim 4.3). The proposed experiments in this aim helped us gain a better understanding of whether and how circulating proteins can be picked up by thymic DCs.

Results

Aim 1: To establish MP IVM for transplanted thymi

Subaim 1.1: To analyze transplanted thymi

Transplanted thymus – anatomy and cellular composition

The thoracic thymus is inaccessible to perform MP IVM as it is located within the rib cage and directly contacts the heart and the lungs. We attempted several transplantation models to circumvent this shortcoming. Grafting embryonic thymi on the skull of recipient mice did not yield good results due to the poor engraftment and extensive formation of scar tissue (not shown). We eventually succeeded by transplanting embryonic thymi under the kidney capsule of recipient mice. The best results were achieved when single thymus lobes from gestation day E14.5-18.5 embryos were grafted under the left kidney capsule of four-week old male recipient mice. Transplanting into female mice led to the formation of extensive connective tissue between the graft and the ovaries, thus, rendering consequent exposure of the graft for MP IVM difficult and inefficient. Thymi were grafted under the left kidney capsule of recipient mice, which is anatomically more distal to the respiratory tract than the right one. Additionally, the spleen is located between the left kidney and the liver, functioning as an important spacer that prevents the formation of highly vascularized adhesions between liver and kidney, which were often observed when grafts were transplanted under the right kidney capsule (**Fig. 10**). We chose four-week old mice as recipients, an age at which the animals were old enough to endure the surgery, yet young enough at the time of imaging four weeks after transplantation to observe the thymus at its peak cellular output.

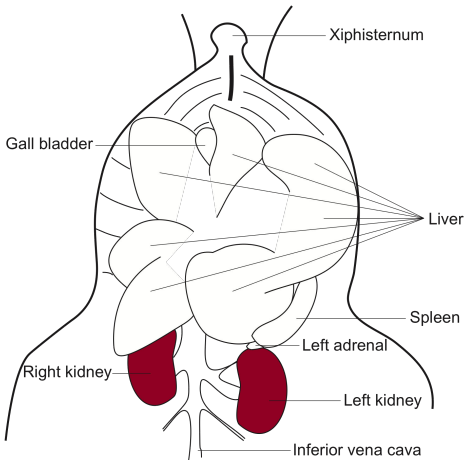

Fig. 10. Mouse anatomy – kidneys. Unlike in humans, in mice the left kidney is anatomically more distal to the thorax and the vascular stem that is feeding the organ with blood (vena and arteria renalis) is longer as compared to the right kidney.

In agreement with previous publications, we obtained good thymus engraftment, revascularization and T cell development by four weeks post-transplantation[187]. At that time, grafted thymi closely resembled their endogenous counterparts. They had developed cortical and medullary regions and the distribution of $CD11c^+$ DCs and PECAM-1^+ vessels was also normal. In transplanted and endogenous thymi, $CD11c^+$ DCs were most abundantly present in the medulla, followed by CMJ and the cortex. In contrast, PECAM-1^+ vessels were evenly distributed throughout the thymus (**Fig. 11a-d**). Furthermore, the same DC subsets could be identified in endogenous and transplanted thymi. Thymic cDCs and pDCs were present at the same ratios. Thymic DCs are composed of a large fraction of pDCs (~50%), followed by $CD11c^+CD8\alpha^+CD11b^-$ and $CD11c^+CD8\alpha^-CD11b^+$ cDCs in twelve-week-old male mice. In contrast, splenic DCs mainly consist of $CD11c^+CD8\alpha^+CD11b^-$ and $CD11c^+CD8\alpha^-CD11b^+$ cDCs, with only a small fraction being pDCs (~10%). Other DC subsets such as $CD11c^+CD4^+CD8^-$ and $CD11c^+CD4^-CD8^-$ DCs can also be found at low frequencies in spleen and thymus and have been combined here as “other DCs” (**Fig. 11e**). It is noteworthy that similar to the cortex-to-medulla ratio, which decreases with time as the thymus involutes, the subset contribution of DCs was also subjected to change with advancing age of the animals. With age, the percentage of pDCs increased at the expense of $CD11c^+CD8\alpha^-CD11b^+$ cDCs (unpublished observation). Transplanted thymi supported T cell development

(**Fig. 11f**) and restored the T cell pool of athymic nude mice that are otherwise devoid of T cells[188].

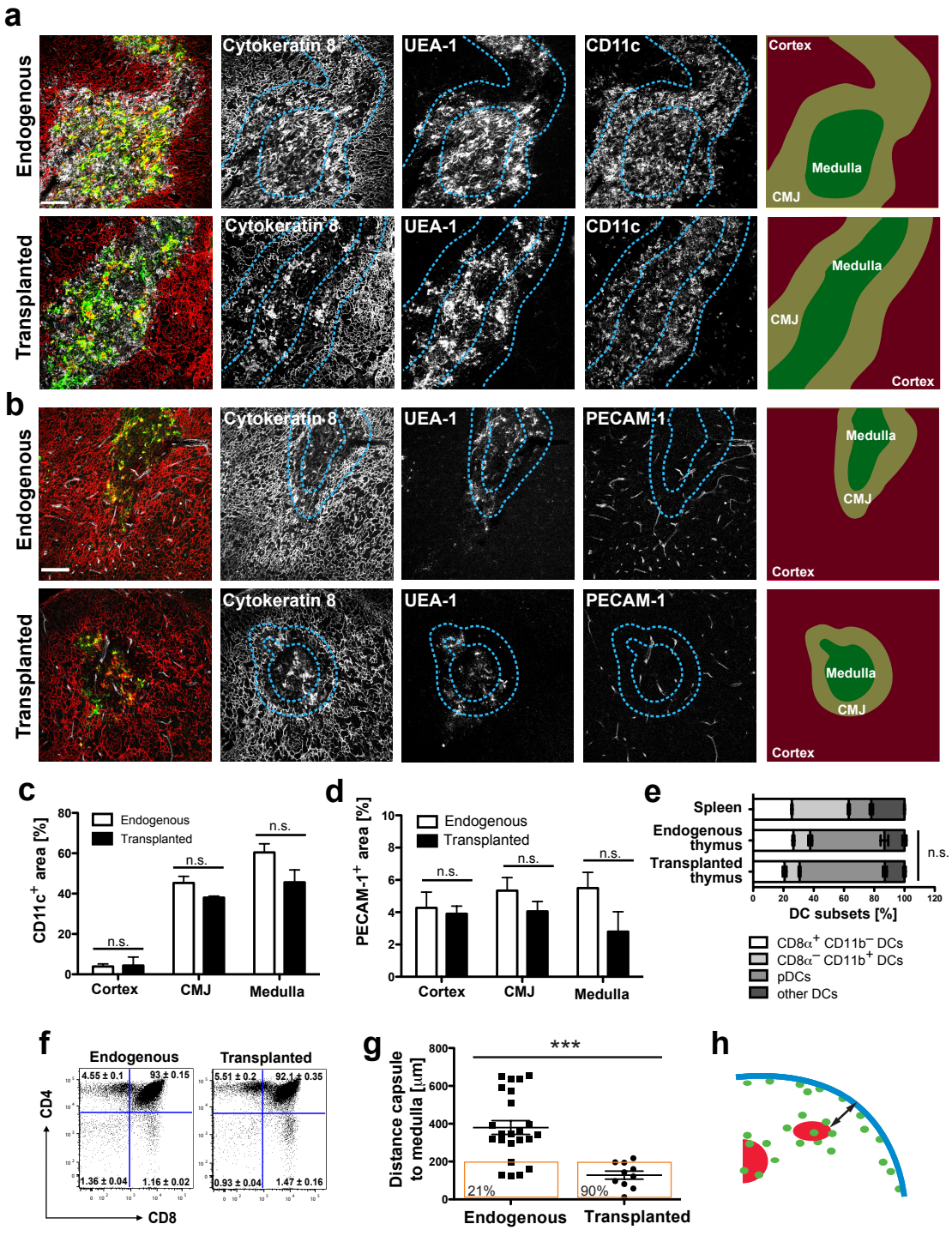

Fig. 11. Transplanted thymi closely mirror their endogenous counterparts. Embryonic thymi were transplanted under the kidney capsule of recipient mice and endogenous and transplanted thymi were analyzed four weeks later. (**a, b**) For immunofluorescence, cryosections were stained with mAbs against cytokeratin 8 (red, **a, b**), CD11c (white, **a**) or PECAM-1 (white, **b**) and the lectin UEA-1, that specifically binds to mTECs (green, **a, b**). Cortex, medulla and CMJ were identified according to the cytokeratin 8 staining. Shown are representative confocal images of endogenous (upper panel) and transplanted thymi

(lower panel, **a, b**). (**c, d**) The percentage of CD11c and PECAM-1 signal above background of the representative anatomic region of transplanted and endogenous thymi was evaluated. (**e**) Flow cytometric analysis of the DC subset composition in spleen, endogenous and transplanted thymus. (**f**) CD4/CD8 profile of thymocytes in endogenous (left panel) and transplanted (right panel) thymi. Representative FACS plots were gated on live, non-doublet cells. (**g**) The shortest distance between the capsule and medullas of transplanted and endogenous thymi was measured as depicted in (**h**, arrow). Each symbol presents an individual animal. Highlighted boxes and corresponding numbers indicate the animals and percentage of animals in which medullas were located within 200 µm below the capsule. Each symbol represents one independent experiment. (**h**) Schematic image of a thymus. Shown are medullas (red), DCs (green) and the capsule (blue). The arrow illustrates the shortest distance between medulla and capsule that was measured and graphed in (**g**). n=3-27 mice per group, *P* values were calculated using one-way ANOVA (**c-e**) or two-tailed, unpaired Student's *t*-test (**g**), ***$P < 0.0001$, n.s. non significant, shown are mean ± s.e.m., scale bar = 50 µm

The thymus is a relatively opaque tissue when exposed to visible light or infrared excitation, thus, structures that are further than 200 µm below the surface are not visible by MPM. The medulla of endogenous six- to twelve-week old mice was located 380 ± 37 µm below the surface and thus cannot be visualized by MPM (**Fig. 11g**). Only 21% of endogenous thymi had medullas that are within 200 µm of the capsule. We found that medullas of transplanted thymi are on average more superficial and only 128 ± 21 µm below the surface and that 90% of the transplanted thymi had medullas that are within range that is readily accessible to MPM (**Fig. 11g, h**). This was most likely due to the overall smaller size of the transplanted thymus.

Dendritic cell trafficking to transplanted thymi

It has been shown previously that fully differentiated immature circulating DCs can gain access to the thymus from the blood by employing a multi-step adhesion cascade[83]. Rolling is mediated by PSGL-1 –P-selectin and VLA4 – VCAM-1 interactions, and at least one yet unidentified chemoattractant that signals through $G\alpha_i$-coupled receptors are required for firm arrest. Maturation of DCs greatly reduces their ability to home to the thymus[83]. Here, we asked whether the same mechanism that grants circulating DCs access to endogenous thymi also allows them to enter transplanted thymi. To address

whether mature DCs home less efficiently to the transplanted thymus, splenic DCs, left untreated or matured overnight with LPS, were differentially labeled and injected intravenously. Analysis of spleen, endogenous and transplanted thymi two hours later revealed that immature DCs readily accessed transplanted and endogenous thymi, while the homing capacity of mature DCs was impaired. It is noteworthy that both mature and immature DCs could enter the spleen (**Fig. 12a**). Pretreatment of immature DCs with *Bordetella pertussis* toxin (PTX) or treatment with non-depleting anti α_4 mAb significantly and equivalently reduced the homing efficiency of DCs to endogenous and transplanted thymi but not spleen (**Fig. 12b, c**). Likewise, pretreatment of mice with blocking mAbs to P-selectin and VCAM-1 interfered with the ability of DCs to accumulate in endogenous and transplanted thymi, but not spleen (**Fig. 12d, e**).

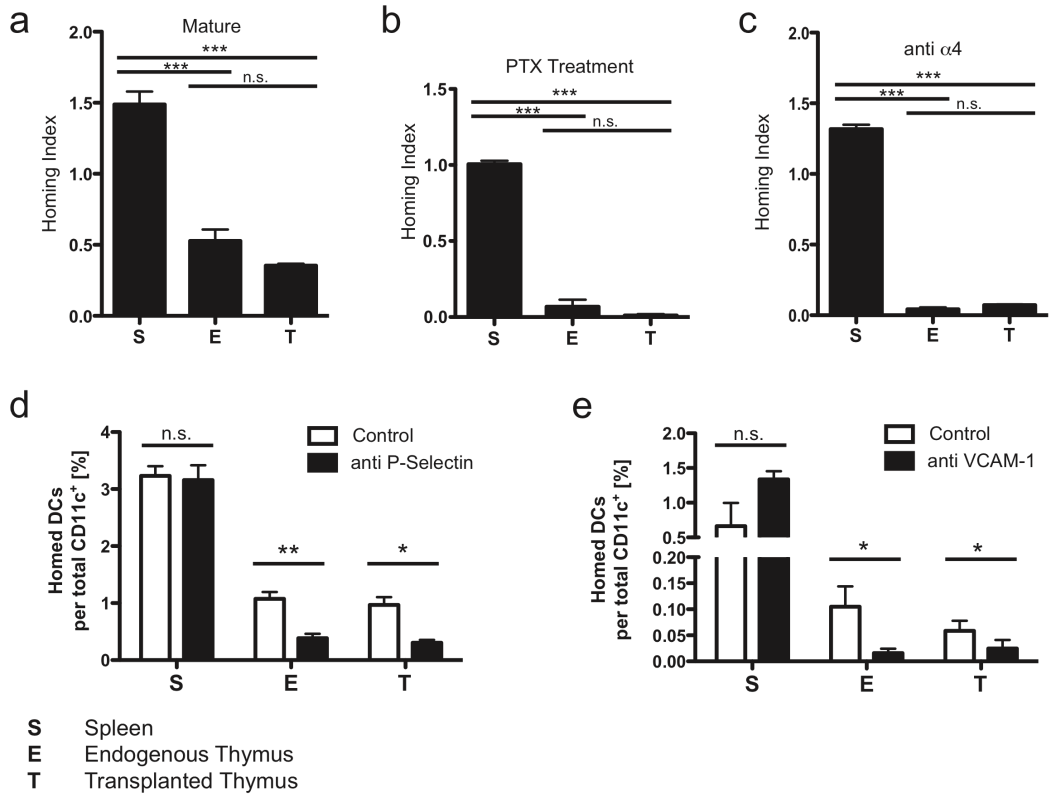

Fig. 12. Adoptively transferred immature DCs employ the same multi-step adhesion cascade to home to transplanted and endogenous thymi. (**a-c**) For competitive homing assays, immature and either LPS maturated (**a**), PTX (**b**) or anti-α4 mAb (**c**) treated DCs, respectively, were differentially labeled and transferred intravenously into recipient mice. 18 hrs later, mice were sacrificed and homing indices were determined by dividing the percentage of homed, pretreated DCs by the percentage of non-treated DCs for spleen, endogenous and

transplanted thymi. (**d, e**) To test the role of P-selectin and VCAM-1 in DC homing to the thymus, mice were treated with blocking mAbs or left untreated before DC transfer and homing was evaluated two hours later. Pooled data from up to five independent experiments, n = 3-7 mice per group. Shown are mean ± s.e.m.; n.s. non significant, ***P < 0.0001, **P < 0.01, *P < 0.05; data were analyzed using one way ANOVA

Taken together, our results demonstrate that immature, but not mature DCs readily access both transplanted and endogenous thymi via the same tissue specific multi-step adhesion cascade: Rolling is mediated by endothelial P-selectin interacting with glycosylated DC-expressed ligands, most likely PSGL-1[83]. At least one yet unidentified chemoattractant that signals through $G\alpha_i$-coupled receptors is required for firm arrest, which is mediated by integrins, including DC expressed VLA-4 binding to VCAM-1, an IgSF member that is constitutively expressed in thymic microvessels.

It has been reported previously that all DC subsets that can be isolated from spleens of donor animals enter the thymus with similar efficiencies[83]. The subset composition of thymic DCs differs from that of splenic DCs that were transferred in homing experiments (**Fig. 11e**) and the finding that all DCs home equally well to the thymus has been challenged recently by a study that suggested that $CD8\alpha^-$ and pDCs but not $CD8\alpha^+$ DCs readily home to the thymus in the steady state[80]. We found that the composition of transferred DCs that can be recovered from thymi varies with the time interval that passes after adoptive transfer. All splenic DC subsets from Flt3L-treated mice homed equally well to the thymus at two hours after adoptive transfer, consistent with earlier studies[83]. However, the homed DC subsets were differentially retained in the organ or had different survival, especially pDCs and $CD8\alpha^+11b^-$ DCs, which were enriched at 18 hours compared to the input population. At this time the subset composition began to resemble the endogenous thymic DC pool (**Fig. 13**). These observation reconcile the apparent differences between previous studies, which are most likely due to differential retention or survival of homed DCs rather than preferential homing of specific DC subsets per se.

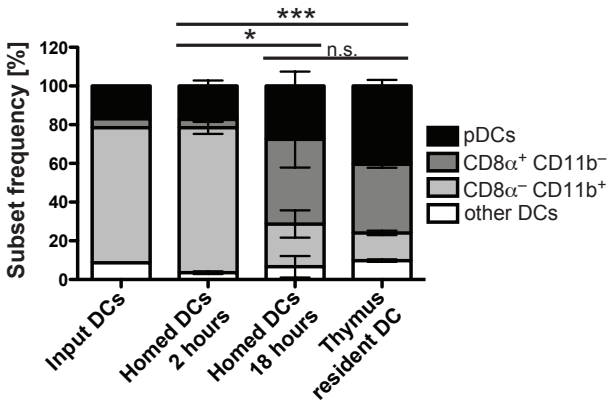

Fig. 13. Phenotype of thymus homing DCs. Splenic DCs were fluorescently labeled and injected intravenously into recipient mice. At two and 18 hours post inject, thymi were harvested and DCs subset composition was evaluated. n = five-ten animals, P values were calculated by two-way ANOVA. ****P* < 0.001, ***P** < 0.05, n.s. non significant, shown are mean ± s.e.m.

Subaim 1.2: To develop an imaging strategy to perform MP IVM of thymi

In order to subject the transplanted thymi to MP IVM, the organs need to be surgically exposed and sufficiently immobilized as motion artifacts may render obtained imaging data uninterpretable. In contrast to conventional IVM, which allows for real time recording, MPM relies on the acquisition at given time intervals (see also section “Multi-photon microscopy”). A series of individual optical sections along the z-axis are taken at a given time interval. The acquired z-stacks are then rendered into 3D volumes and played 250–300x accelerated over real time as a time-lapse movie (**Fig. 14c**). Therefore, even subtle motion artifacts are exacerbated as the image stacks are recorded at time intervals rather than continuous real time acquisition and consequently, any motion artifacts will render the imaging data uninterpretable.

The transplanted thymus was prepared as follows for MP IVM. Transplanted animals were anesthetized by intraperitoneal (i.p.) injection of 150 – 200 µl of a combination of Ketamine HCl (100 mg/kg), Xylazine (10 mg/kg) and Acepromazine (3 mg/kg). The mice were shaved and residual hair was removed by application of nair. The dorsal skin was be prepared for surgery by three applications of Betadine® and 70% alcohol. After verification of

adequate depth of anesthesia for surgery by checking the hind leg withdrawal and palpebral reflex, the thymus-bearing kidney of the anesthetized mouse was gently exposed as follows: The skin was be opened with lateral with a 1 – 1.5 cm dorsal incision. The retro-peritoneum was bluntly dissected from the skin and opened with a small 1 cm incision. The kidney was gently exteriorized and fixed on a small styrofoam platform with two 27G1/2 needles that were placed above and below the transplant, as distal as possible. The exposed organ was then embedded in ring vacuum grease that was filled with PBS to prevent drying out of the organ and a temperature probe was placed in physical contact with the kidney/thymus to constantly measure the temperature. Next, a glass cover slip that was attached to an *x-y-z*–positioner was placed on top of the thymus to avoid potential drifts along the z-axis. To keep the temperature at physiological range (37-39°C), a heating coil was placed on top of the cover slip (**Fig. 14a, b**). This system allowed us to successfully subject the thymus to MP IVM, however, it is sensitive to motion artifacts that may originate from respiration and heart beat (through the renal artery). Furthermore, the immobilization of the organ may cause hypoxia and stasis due to mechanical stress on the kidney's vascular stem causing poor blood circulation. The thymus is also a relatively opaque and densely packed tissue. Hence it requires high laser powers to obtain images of regions that are deep within the tissue such as the medulla, which can cause photo bleaching and tissue damage.

MPM was performed on a Prairie system at an excitation wavelength of 850 nm, from a tunable MaiTai Ti:sapphire laser (Spectra-Physics, see also "Materials and methods"). In order to collect 4D time-lapse recordings, stacks of optical sections of a region of interest were acquired at a pre-determined time interval. To acquire z-stacks, optical sections were taken at vertical step intervals of 3 µm, using a 20x water immerse lens (20/×0.95 numerical aperture water-immersion objective lens, Olympus). The collected data was then rendered into a 4D movie by converting individual z-stacks into 3D volumes using the imaging processing programs such as Volocity (Perkin Elmer) and Imaris (Bitplane). The individual 3D volumes were then converted into a QuickTime movie and typically played at a 250–300x accelerated speed

for presentation purposes. Image processing software was also used to identify single cells and track the movement of their centroids. The data was then exported and analyzed with programs such as MatLab, Excel and Prism (**Fig. 14c**).

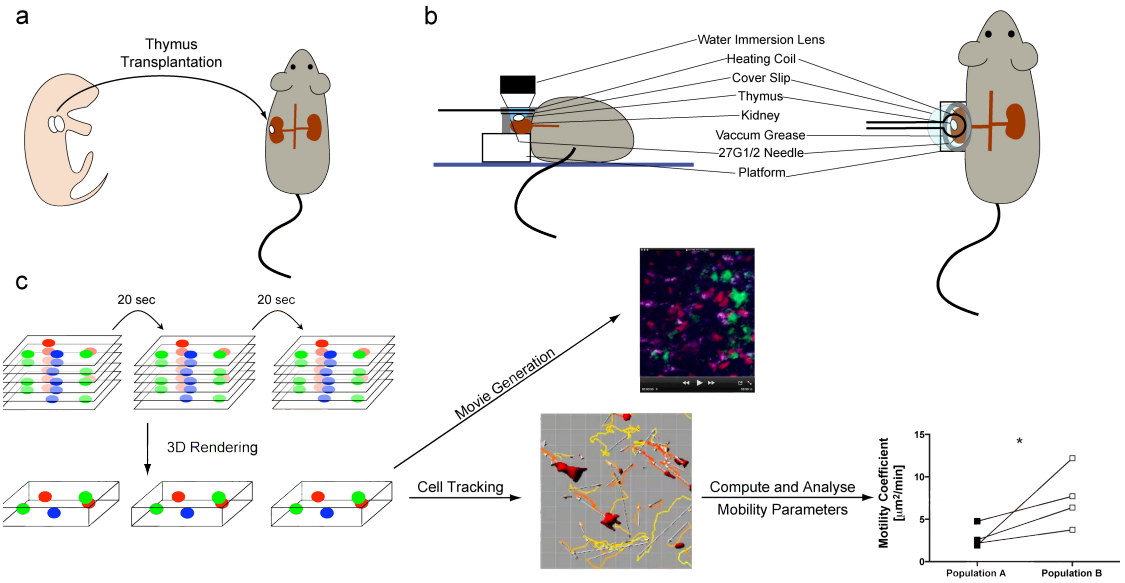

Fig. 14. Schematic presentation of the experimental set-up. (**a**) To perform MP IVM of transplanted thymi, timed pregnancies were set up and pregnant mice were sacrificed at gestation day E14.5-18.5. Thymi of the embryos were harvested and grafted immediately under the left kidney capsule of four-week old, male recipient mice. (**b**) Four weeks later, the transplanted animals were subjected to MP IVM. To do so, the left thymus-baring kidney of anesthetized mice was gently exposed, placed on a styrofoam platform and fixed to the platform with two 27G1/2 needles that were placed above and below the transplant, as distal as possible. In some experiments, the organ was additionally fixed to the platform by applying tissue glue. The exposed kidney/thymus was embedded in vacuum grease and PBS. A cover slip, that was attached to an x-y-z–positioner was placed on top of the thymus for further stabilization. Lastly, a heating coil was added and a temperature probe was inserted to keep the preparation at physiological temperatures. (**c**) For MP IVM, stacks of optical sections along the z-axis were acquired. Image acquisition of z-stacks was continuously repeated over a certain time period at a given time interval. Each z-stack was subsequently processed by image analysis software and rendered as a 3D volume. Movies were generated by playing individual 3D volumes at a 250–300x accelerated speed over real time. Using image analysis software, single cells were identified and their migratory path was tracked. Single cell tracks were then further analyzed and mobility parameters were extracted.

Taken together, we have demonstrated in aim 1 that transplanted embryonic thymus lobes faithfully mirror their endogenous counterpart in terms of cellular composition and architecture. Specifically, we have shown that the transplants are fully vascularized as early as four weeks after transplantation; they support T cell development and form cortical and medullary regions.

Medullas of transplanted thymi are located more superficially as compared to endogenous thoracic thymi. This is most likely due to the smaller overall size of the transplant (unpublished observation). We have shown that DCs localize to their respective anatomical location within the transplant and that their subset composition is essentially indistinguishable from thymic DCs of endogenous thymi. Furthermore, we have successfully designed a surgical stage that allowed us to expose and sufficiently immobilize transplanted thymi in order to perform time lapse MP IVM. MP IVM experiments of the following aims were based on the herein established system.

Aim 2: To analyze the motile behavior of thymic DCs and T cells

Subaim: 2.1 To differentiate between cortex and medulla in vivo

In order to observe the motile behavior of cells relative to immotile structural elements within the thymic cortex and medulla, it is indispensable to delineate them in vivo.

We found that thymic medullas could be specifically visualized in vivo by i.v. injection of 20 µg of the TRITC labeled lectin UEA-1, which specifically binds to mTECs, 18 hours before analysis by MPM (**Fig. 15a**). The binding of UEA-1 in vivo was specific as confirmed by immunofluorescence analysis. Briefly, cryosections of transplanted UEA-1 injected thymi were ex vivo stained with cytokeratin 8 mAb to delineate medulla and cortex and UEA-1 that was conjugated to a different fluorescent molecule to verify the specificity of the staining and analyzed by confocal microscopy (**Fig. 15b**). Using this technique to label medullas in vivo, we identified the localization of homed DCs in the thymus. We found that homed DCs colocalized with UEA-1^+ medullas and were enriched at the cortico-medullary junction while they were sparse in the cortex. The shape of the cells suggested that they had left the vasculature and were located within the thymic stroma (**Fig 15a**). This was in good agreement with previously published data[83].

In the presence of TCR tg thymocytes, cortex and medulla were identified by the relative enrichment of tg T cells in the medulla. TCR tg T cells express a pre-rearranged TCR and thus, RAG gene and TCR dependent steps of T cell development are accelerated in these animals, which leads to a significant enrichment of tg T cells in the medulla as compared to the cortex[189] (**Fig. 15c, d**).

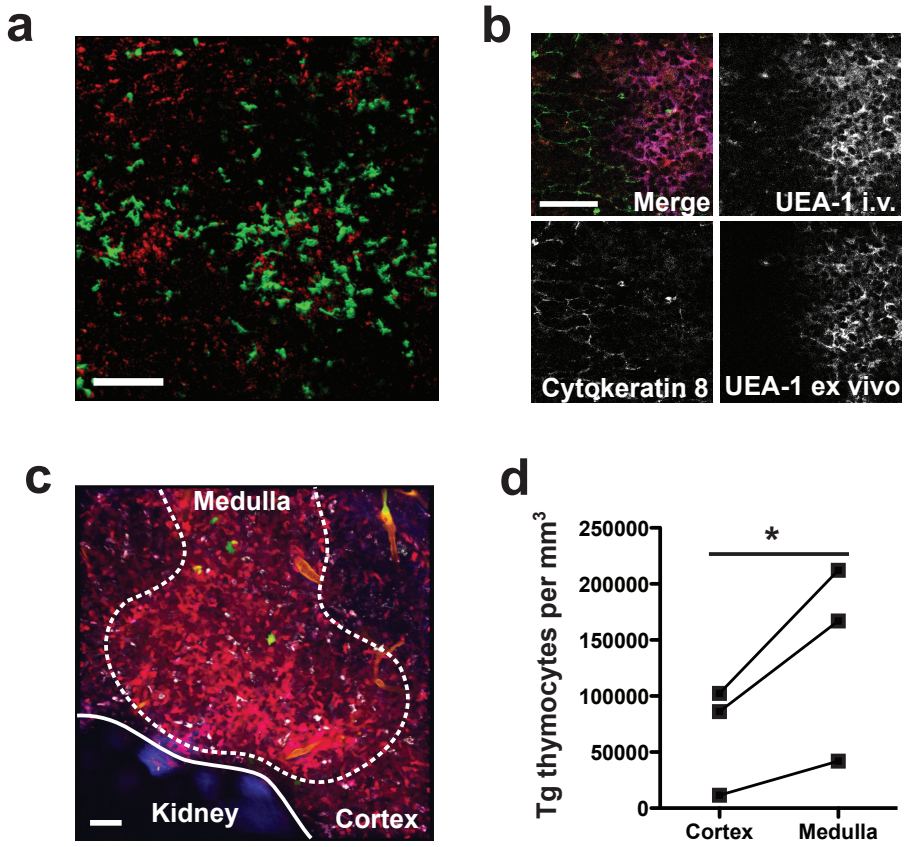

Fig. 15. In vivo differentiation of cortex and medulla. (**a**) Representative image from a MP IVM time-lapse recording of a transplanted thymus. 18 hours before imaging, UEA-1-TRITC and 2 × 10^6 splenic DCs from Actin-GFP donors were given i.v. Shown are medullas (red) and homed DCs (green). Scale bar is 100 µm (**b**) Representative confocal micrograph of a transplanted thymus. The transplanted animal was injected with 20 µg UEA-1-TRITC (red) i.v. and sacrificed 18 hours later. The thymus was harvested and cryosections were performed and stained with anti cytokeratin 8 mAb (green, cortex) and Alexa 647 labeled UEA-1 (blue, ex vivo, medulla). Scale bar is 50 µm. (**c**) Representative image from MP IVM recordings of transplanted thymi of animals that were sublethally irradiated and reconstitute with 10^7 BM cells from OT-I TCR tg × T-red donors. MP IVM was performed four weeks after BM transplantation. Denoted are cortex, medulla and kidney. Shown are TCR tg thymocytes (red); the vasculature was highlighted by the injection of high molecular weight FITC/TRITC-dextran (yellow); the kidney was identified by second harmonic signal (blue). Scale bar is 100 µm. (**d**) Evaluation of numbers of TCR tg thymocytes per mm^3 in cortex and medulla as shown in (**c**). Each symbol pair represents one independent experiment. Two-tailed, paired Student's *t*-test, $*P < 0.05$.

As thymocytes are highly proliferative, they are not suitable for ex vivo labeling before adoptive transfer and instead, require a genetically encoded label. Therefore, we generated BM chimeric animals by injecting tg BM from either T-red tg or DPE-GFP tg animals that were crossed on a TCR tg

background into sublethally irradiated, transplanted recipient mice. T-red and DPE-GFP animals express dsRed or GFP, respectively, under the CD4 promoter; hence, all T cells in these mice are fluorescently tagged and can be detected by MPM[190]. In this study, OT-I and P14 tg BM were used. OT-I tg T cells recognize the ovalbumin derived peptide SIINFEKL in the context of H-2K^{b} [191]; P14 tg T cells are specific for the LCMV glycoprotein derived peptide KAVYNFATC (gp33–41) in the context of H-2D^{b} [192]. The half-lives of SIINFEKL and gp33 on MHCI have been determined to be 31-44 hours (for SIINFEKL)[193] and 2.4 hours (for gp33)[194].

Cortex and medulla were differentiated as follows in the presence of fluorescently tagged TCR tg thymocytes: We delineated cortex and medulla after visual inspection of MPM images and determined the number of tg thymocytes per mm^3 using Imaris software. As TCR tg thymocytes prematurely express a fully functionally TCR, their RAG dependent development is accelerated and thus, TCR tg thymocytes specifically accumulate in the medulla[189]. In agreement with this, we found that there was a significant 2.5-fold ± 0.54 enrichment of TCR tg thymocytes in the medulla versus the cortex (*P < 0.05, **Fig. 15c, d**). Thus, the relative abundance of TCR tg thymocytes in the medulla can be used as a surrogate marker to differentiate between cortex and medulla in vivo.

Please note that we used the herein described methods to delineate cortex and medulla in vivo in all consecutive experiments.

Subaim 2.2: To analyze DC and thymocyte motility in cortex and medulla

Next, we sought to investigate the motile behavior of thymocytes and DCs that had homed to the thymus in cortex and medulla.

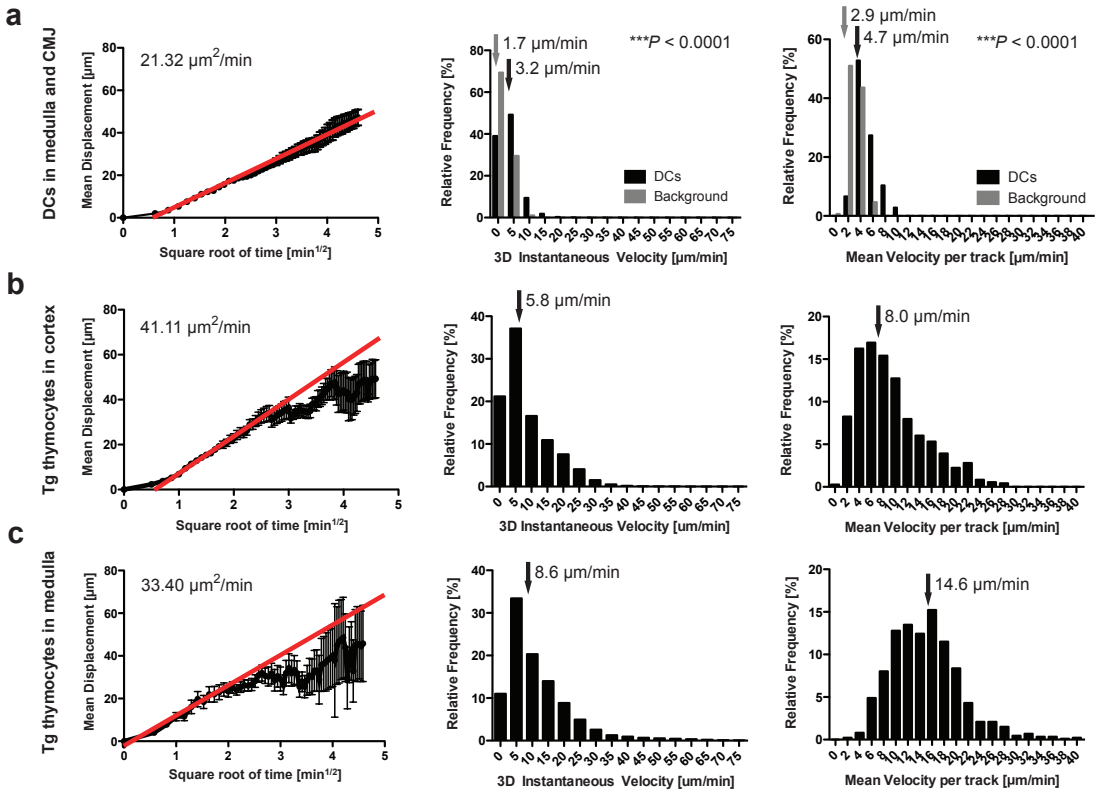

Fig. 16. Motility of thymic homed DCs two hours after transfer and thymocytes in cortex and medulla. Mean displacement plots (left panel), frequency histograms of 3DIV (middle panel) and mean velocity per track (right panel) of DCs in medulla and CMJ (**a**), cortical (**b**) and medullary OT-I TCR tg thymocytes (**c**). The straight line in the mean displacement plots (left panel, red) denotes the regression function of the initial linear segment of the curve. The motility coefficients M were calculated from the slope of the regression line and are depicted in the respective graphs. Color-coded arrows in the frequency histograms (middle and right panel) highlight the population's median. Gray bars (**a**, middle and right panel) indicate the 3DIV (middle panel) and mean velocity per track (right panel) of auto-fluorescent, immobile background structures. P values were calculated using Mann-Whitney U-Test, ***$P < 0.0001$

Cortex and medulla were identified by injection of fluorescently labeled UEA-1 or the relative accumulation of TCR tg thymocytes in the medulla, respectively (subaim 2.1). 18 hours after entering the thymus, homed DCs in medulla and cortico-medullar junction migrated randomly as determined by plotting the cells' mean displacement versus the square root of time (**Fig. 16a**, left panel, see also "Multi-photon microscopy" section). As compared to OT-I tg thymocytes in cortex and medulla, DCs move at a significantly lower 3D instantaneous velocity (3DIV, mean ± s.e.m. 4.0 ± 0.05 µm/min, median 3.2 µm/min, $P < 0.0001$) and mean velocity per track (mean ± s.e.m. 4.9 ± 0.16

μm/min, median 4.7 μm/min, $P < 0.0001$). The measured velocities did not result from insufficient immobilization of the thymus as determined by tracking of immobile auto-fluorescent structures in the same imaging volume (3DIV mean ± s.e.m. 2.1 ± 0.03 μm/min, median 1.7 μm/min, $P < 0.0001$; mean velocity per track mean ± s.e.m. 3.1 ± 0.08 μm/min, median 2.9 μm/min, $P < 0.0001$) (**Fig. 16a**, middle and right panel, **Table 4**). It is noteworthy that tracks of fast moving cells are prone to being split up into several smaller tracks, which results in their over-representation and accounts for the generally higher mean velocities per track as compared to 3DIV, which weights each cell's displacement between frames equally (see also "Multi-photon microscopy" section).

Table 4. Thymocyte and DCs motilities in the steady state

Cell type	3D instantaneous velocity [μm/min]		Mean velocity per track [μm/min]	
	mean ± s.e.m.	median	mean ± s.e.m.	median
Homed DCs	4.0 ± 0.05	3.2	4.9 ± 0.16	4.7
Cortical thymocytes	8.7 ± 0.03	5.8	9.2 ± 0.21	8.0
Medullary thymocytes	11.9 ± 0.07	8.6	15.0 ± 0.20	14.6

In contrast to DCs, OT-I transgenic thymocytes displayed higher velocities and migrated in a more confined pattern (**Fig. 16b, c**). Medullary TCR tg thymocytes (3DIV mean ± s.e.m. 11.9 ± 0.07 μm/min, median 8.6 μm/min, median velocity per track 15.0 ± 0.20 μm/min, median 14.6 μm/min) migrated with significantly higher 3DIV and mean velocities per track than cortical thymocytes (3DIV mean ± s.e.m. 8.7 ± 0.03 μm/min, median 5.8 μm/min, $P < 0.0001$; mean velocity per track 9.2 ± 0.21 μ m/min, $P < 0.0001$) in the absence of cognate Ag, which was in agreement with data obtained from in vitro systems[186] (**Fig. 16b, c**, middle panel, **Table 4**). Despite their higher velocity, medullary thymocytes scanned a smaller volume than cortical thymocytes, which was reflected by a lower motility coefficient (41.11 μm^2/min versus 33.40 μm^2/min) (**Fig. 16b, c**, left panel). This likely reflects the

sampling behavior of OT-I TCR tg thymocytes in the process of negative selection. We suggest that TCR tg thymocytes continuously scan APCs in the thymic medulla, which is reflected by relatively high velocities but confined migration patterns with low motility coefficients (**Fig. 16c**). Conversely, we hypothesize that thymocytes that encounter cognate Ag in the medulla engage in prolonged cognate interactions, which would result in lower velocities and even more confined migration patterns.

Subaim 2.3: To analyze the effect of cognate Ag on thymocyte behavior

In order to observe potential DC – thymocyte interactions in vivo, transplanted animals were sublethally irradiated and reconstituted with either OT-I × T-red TCR tg BM alone or a mixture of OT-I × DPE-GFP and P14 × T-red TCR tg BM. This protocol usually results in 10-15% TCR tg thymocytes. Three to four weeks after BM transplantation, 5×10^6 purified splenic DCs that were either labeled with CMAC or harvested from Actin-GFP donors were pulsed with 1 µM of the ovalbumin-derived peptide SIINFEKL and given i.v.. MP IVM was performed 18 hours later (**Fig. 17a**). The concentration used to pulse DCs was in the linear part of the loading curve and thus non-saturating (**Fig. 17b**). It is of note that at the time Ag pulsed DCs were given, TCR tg T cells can be detected in LNs, albeit at small numbers (<5%). Activation of peripheral T cells can lead to a cytokine storm that induces non-specific T cell apoptosis in the thymus[87]. If this was the case, administration of SIINFEKL pulsed DCs would not only affect specific OT-I TCR tg thymocytes but also non-specific P14 TCR tg thymocytes. However, this was not observed with this protocol due to the small number of peripheral specific T cells. Specific OT-I TCR tg but not non-specific P14 TCR tg thymocytes showed a remarkable change in motile behavior in the presence of SIINFEKL pulsed DCs. OT-I TCR tg thymocytes migrated significantly slower (3DIV mean ± s.e.m. 4.5 ± 0.07 µm/min, median 3.0 µm/min; mean velocity per track 9.0 ±

0.24 µm/min, median 7.2 µm/min) as compared to non-specific P14 TCR tg T cells in the same imaging volume (3DIV mean ± s.e.m. 11.0 ± 0.16 µm/min, median 9.0 µm/min, $P < 0.0001$; mean velocity per track 14.0 ± 0.35 µm/min, median 13.9 µ m/min, $P < 0.0001$) and OT-I TCR tg thymocytes in the absence of cognate Ag (**Fig. 17d, e** and **Fig. 16c**). We also noted that Ag specific T cells were more confined in their migration pattern and scanned a smaller volume as reflected by the mean displacement graph and the lower motility coefficient (motility coefficient of non-specific P14 thymocytes was 49.04 μm^2/min vs. 26.37 μm^2/min for Ag specific OT-I TCR tg T cells, **Fig. 17c**). This differential Ag-driven behavior would presumably allow the T cells to engage in prolonged interactions with Ag pulsed DCs. Indeed non-specific thymocytes only occasionally interacted with DCs and these interactions were short in nature (mean ± s.e.m. 3.7 ± 0.7 min, median 2.3 min). In contrast, Ag specific thymocytes formed much longer contacts (mean ± s.e.m. 18.7 ± 4.0 min, median 5.9 min, $P = 0.0049$). 18% of Ag specific thymocytes were interacting with Ag pulsed DCs throughout the entire imaging period of 60 minutes, and 24% for at least 30 minutes, which has been reported to be the minimal amount of time needed to form a mature immunological synapse between fully mature T cells and antigen presenting cells[195] (**Fig. 17f, g**). Notably, not all TCR tg specific thymocytes in the medulla engaged in prolonged contacts with peptide pulsed DCs. CLPs that have entered the thymus are de-synchronized during T cell development, which leads to a heterogeneous T cell population in the medulla. Because of this, it is not surprising that not all TCR tg thymocytes were interacting with Ag pulsed DCs as they were probably to be at different stages in their development.

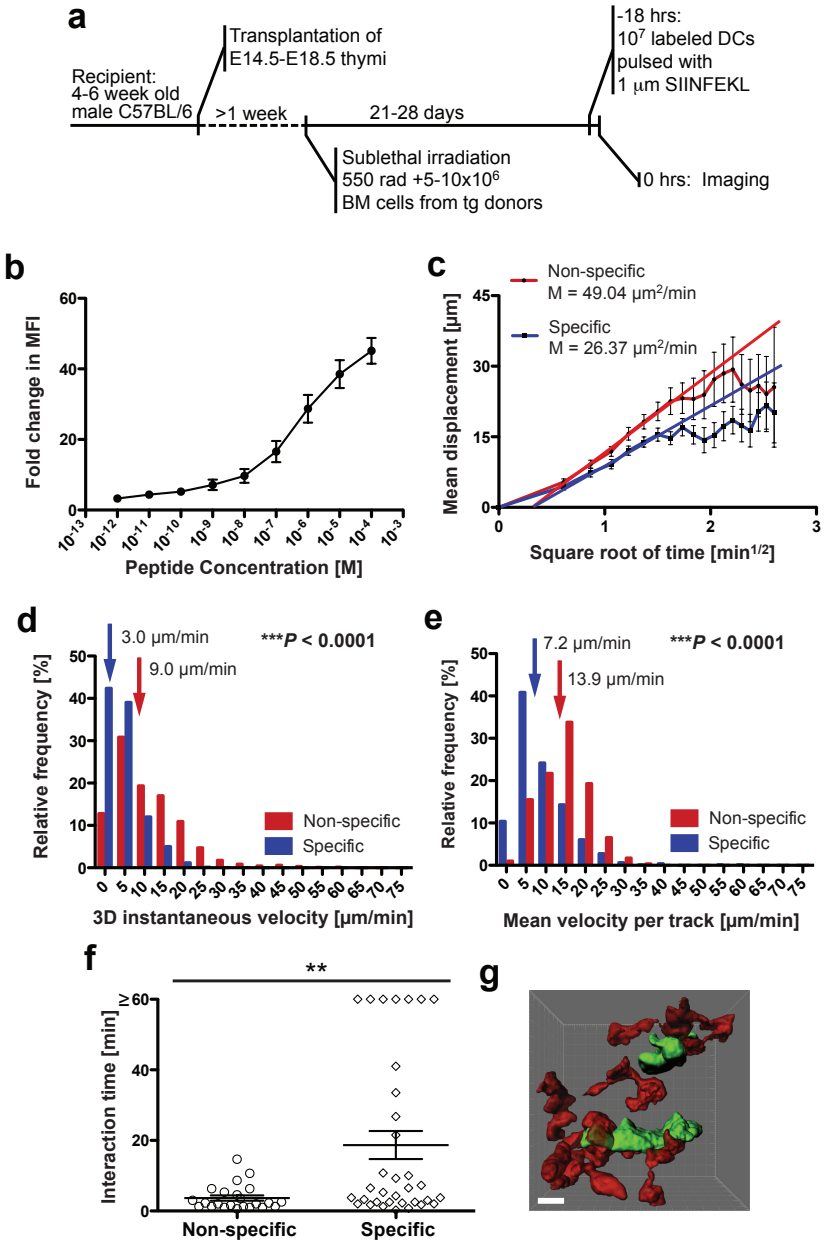

Fig. 17. Effects of cognate Ag on thymocyte behavior. (**a**) Schematic of the experimental protocol. Embryonic thymus lobes were transplanted under the kidney capsule of 4-6 week old recipient mice. Animals were sublethally irradiated and reconstitute with BM from TCR tg donor mice at least one week after transplantation. Four weeks later, splenic immature DCs that were pulsed with 1 μm SIINFEKL, were given i.v. and animals were subjected to MP IVM 18 hours later. (**b**) Loading curve of DCs that were pulsed with the indicated concentrations of SIINFEKL peptide and analyzed by flow cytometry. (**c**) Mean displacement plots of specific (blue) and non-specific thymocytes (red) with color-coded regression function of the initial linear segment of the curve. The motility coefficient of specific and non-specific thymocytes is depicted in the graph. (**d, e**) Frequency histograms of 3DIV (**d**) and mean velocity per track (**e**) of OT-I TCR tg specific (blue) or P14 TCR tg non-specific (red) thymocytes. Color-coded arrows indicate the population's median. (**f**) Absolute contact duration between T cells and DCs in the presence and absence of Ag. Mann-Whitney U-Test (**d-f**), $^{**}P = 0.0049$, $^{***}P < 0.0001$. (**g**) Representative, surface rendered MPM image. Shown are SIINFEKL pulsed DCs (green) and OT-I × T-red tg thymocytes (red), scale bar is 5 μm

Interestingly, the interactions times of OT-I tg thymocytes with Ag pulsed DCs (18.7 ± 4 minutes) greatly exceeded those that have been reported previously for OT-I thymocytes by Le Borgne et al[186] (1.9 minutes). However, one must keep in mind that the latter study utilized RIPm-OVA mice, which express membrane bound ovalbumin (mOVA) under the control of the rat insulin promoter (RIP), which is also active in mTECs but not DCs. Nevertheless, the interaction time was measured between thymocytes and DCs, which can gain access to ovalbumin derived peptides via mechanisms such as cross presentation[75]. Presumably, the Ag concentration on the DCs differs in these different systems and could account for the apparent discrepancies. Another possible explanation for the differences between the two data sets may lie in the expression of ovalbumin in mTECs in RIPm-OVA mice. It is possible that thymocytes preferentially interact with mTECs rather than DCs in this system, and hence the relevant interaction to evaluate would have been between mTECs and thymocytes. Indeed, the authors notice that OT-I T cells migrate in "confinement zones", as they seem to stay in the proximity of Ag bearing DCs[186]. Alternatively, this phenomenon can be explained by the interaction of specific T cells with Ag presenting mTECs. Thus, OT-I cells appear to migrate in a confined zone, while in fact, they may be interacting locally with unlabeled mTECs.

Taken together, we have shown that thymocytes are highly motile in vivo but change this behavior in the presence of cognate Ag. When Ag is presented by homed DCs, specific but not non-specific thymocytes engage in prolonged interactions with DCs. It is tempting to speculate that cognate prolonged interactions are not restricted to T cell – DC interactions but can also occur between thymocytes and other antigen presenting cells, such as mTECs. Indeed, indirect evidence for this has been provided by Le Borgne et al., however, further experiments that specifically evaluate these interactions will be required to draw any conclusions on this matter.

Aim 3: To analyze homed vs. thymus resident DCs

We have established in subaim 2.2 that homed DCs are motile and display a random walk behavior. It is possible that this migratory behavior helps them to present their acquired Ag to a maximal number of developing thymocytes. Thus, the function of homed DCs is not only limited to the delivery of peripheral Ag to the thymus, they also present the Ag and induce negative selection[83]. Indeed, MHC-II deficient but not sufficient homed DCs that have phagocytosed cognate Ag, failed to induce negative selection of specific thymocytes[83], which indicates that homed DCs present Ag rather than disseminating it to resident APCs for presentation purposes. We have also shown in vivo that homed Ag pulsed DCs engage in long-lived interactions with Ag specific thymocytes (subaim 2.3), providing further evidence that homed DCs play an important role in Ag presentation in the thymus.

In LNs, freshly homed DCs display a motile behavior which peaks at about 24 hours post transfer and then decreases with time[133]. Our aim was to address the motility of thymic DCs by comparing freshly homed thymic DCs to thymus resident DCs. We generated BM chimeric animals by lethally irradiating wt recipient mice and reconstituting them with BM from CD11c-YFP donor mice. CD11c-YFP animals express a fluorescent protein under the control of the CD11c promoter. The bulk of thymic DCs expresses YFP in these animals and can be easily identified by MPM[126]. BM chimeric animals were grafted with embryonic thymi and were rested for four weeks before intravenous injection of fluorescently labeled DCs. Two hours post DC transfer, the animals were subjected to MP IVM (**Fig. 18a**). At this time point, homed DCs could be readily detected in the thymus. Image analysis revealed that they moved with higher 3DIV and mean velocities per track as compared to endogenous, resident DCs (**Fig. 18b, Table 5**). Analysis of the migration patterns showed that homed DCs followed a more directional path, which was reflected by a higher meandering index (**Fig. 18c**). In agreement with this, they covered a greater volume, resulting in a higher motility coefficient as compared to thymus resident DCs (**Fig. 18d**). Homed and thymus resident

DCs also showed remarkable differences in shape. While homed DCs typically were more round and compactly shaped, resident DCs were spread out, with dendrites, and were often found in close association with capillaries (**Fig. 18e**).

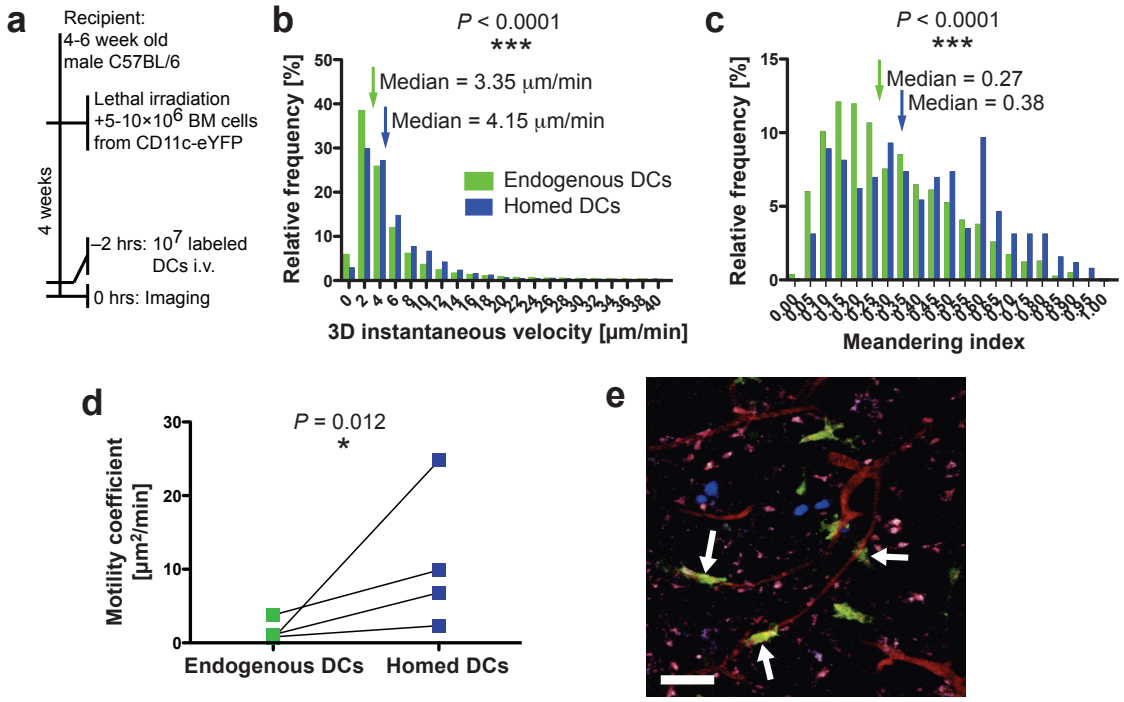

Fig. 18. Thymus resident DCs exhibit a lower motility than homed DCs. (**a**) Diagrammatic representation of experimental protocol. Thymus resident and homed thymic DCs were visualized in transplanted thymi by employing MP IVM. Briefly, transplanted recipient mice were lethally irradiated, reconstituted with CD11c-eYFP BM and rested for four weeks. Two hours before imaging, fluorescently labeled DCs were given i.v. (**b-d**) Shown are frequency distribution histograms of the 3DIV (**b**) and meandering index (**c**) of homed (blue) and resident DCs (green) as well as the motility coefficients (**d**). Color-coded arrows highlight the population's median (**b, c**). The meandering index is calculated by dividing each cell's absolute displacement by the length of the path. Data were pooled from four experiments (**b-d**). *P* values were calculated using Mann-Whitney U-Test (**b**) and two-tailed, unpaired Student's *t*-test (**c, d**) respectively. (**e**) Resident DCs are frequently found in close association with capillaries (arrows). Representative image shows blood vessels (red), resident DCs (green), homed DCs (blue) and auto-fluorescent structures (magenta). Scale bar = 50 μm.

Cumulatively this data indicate that two hours after adoptive transfer homed DCs are motile while resident DCs display a more sessile behavior. Interestingly, homed DCs move significantly slower 18 hours post adoptive

transfer as compared to two hours after i.v. injection as reflected by their mean and median 3DIVs ($P < 0.0001$, **Table 5, Fig. 19a**). At this time point the migration speed approximates the one of resident DCs. It is of note that these DCs also migrated statistically significantly slower than resident DCs ($P < 0.0001$, **Table 5, Fig. 19b**). Interestingly, this difference seems less pronounced when comparing the medians of the two populations (3DIV median for endogenous DCs 3.35 µm/min versus 3DIV median of 18 hours homed 3.2 µm/min) rather than the mean (**Table 5**). The median as compared to the mean is less affected by outliers of the data sets. Visual inspection of the frequency distribution histograms further supports the notion that the median is more representative of the population's behavior than the mean (**Fig. 19a, b**). The difference in the mean, and the less pronounced difference in the median is most likely caused by the comparison of DC populations in different mice. While the migratory behavior of resident and homed DCs two hours post transfer was addressed in the same imaging volume, data for DCs that have homed for 18 hours were derived from separate animals. Small differences, especially of slow moving cells, are likely caused by the preparation of different animals for MP IVM.

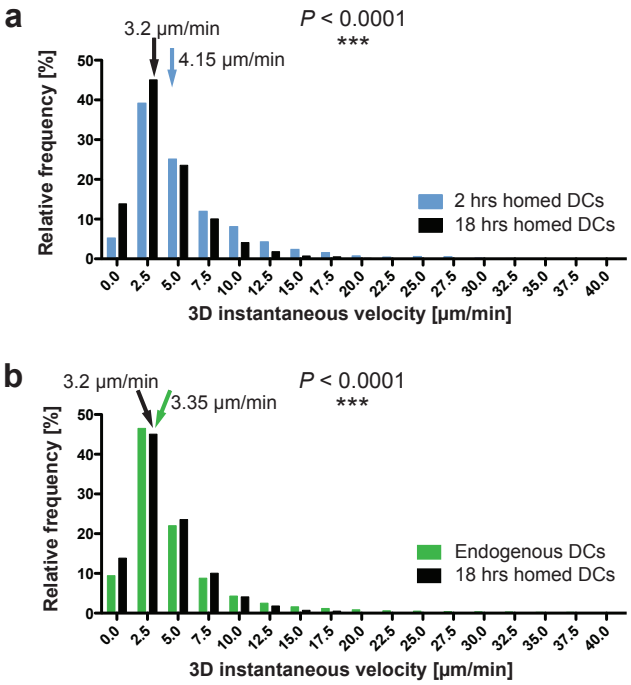

Fig. 19. Velocity of homed DCs decreases with time. Shown are frequency distribution histograms of the 3DIV of endogenous DCs versus homed DCs two hours (**a**) or 18 hours (**b**) post transfer. Color-coded arrows and numbers highlight the population's median. *P* values were calculated using Mann-Whiney U-Test, ***$P < 0.0001$

Table 5. Velocity of thymic DCs

Cell type	3D instantaneous velocity [µm/min]	
	mean ± s.e.m.	median
Endogenous DCs	5.07 ± 0.03	3.35
Homed DCs 2 hours	5.68 ± 0.07	4.15
Homed DCs 18 hours	4.0 ± 0.05	3.2

Thus, DCs move 18 hours post transfer significantly slower than two hours post transfer. Their migration speed approximates that of endogenous DCs at this time point. This is particularly interesting as the DCs subset composition at two and 18 hours post transfer differs significantly . At earlier time points, $CD8\alpha^{+}11b^{-}$ DCs are greatly overrepresented as compared to the endogenous DC pool. With time, the subset composition of homed DCs changes and at 18 hours post transfer, it grossly resembles the endogenous DC pool (**Fig. 13**). Hence, the difference in the subset composition could potentially account for the differences in speed. Therefore one has to assume that different DC subsets display different motile behaviors, which may be reflective of specific functional specializations. However, MP IVM analysis of different DC subsets is required to investigate these possibilities in depth.

Aim 4: To test whether thymus resident DCs acquire blood borne Ag

Subaim 4.1: To test whether thymic DCs can sample the blood

Thymic DCs play an important role in central tolerance induction by presenting self-peptides to thymocytes (see also section “T cell development” and “Thymic antigen presenting cells in positive and negative selection”). There are three known ways how thymic DCs can gain access to peptides for presentation during central tolerance: (1) They can generate peptides themselves by protein degradation, (2) acquire them from mTECs that expressed self-proteins by PGE, (3) or peripheral thymus-bound DCs can pick up self-proteins or commensal proteins in the periphery and transport it to the thymus as their cargo. As we observed that thymus resident DCs were often closely associated with capillaries (aim 3, **Fig. 18e** and **Fig. 20a-c**), we hypothesize that there could be a forth way for thymic DCs to gain access to self-proteins and / or commensal proteins that are not expressed in the thymus per se. We hypothesized that capillary-associated DCs could breach the endothelial layer and extend protrusions into the blood. This could be a previously unrecognized mechanism through which thymic DCs could to potentially pick up blood borne Ag and make it available for T cell selection.

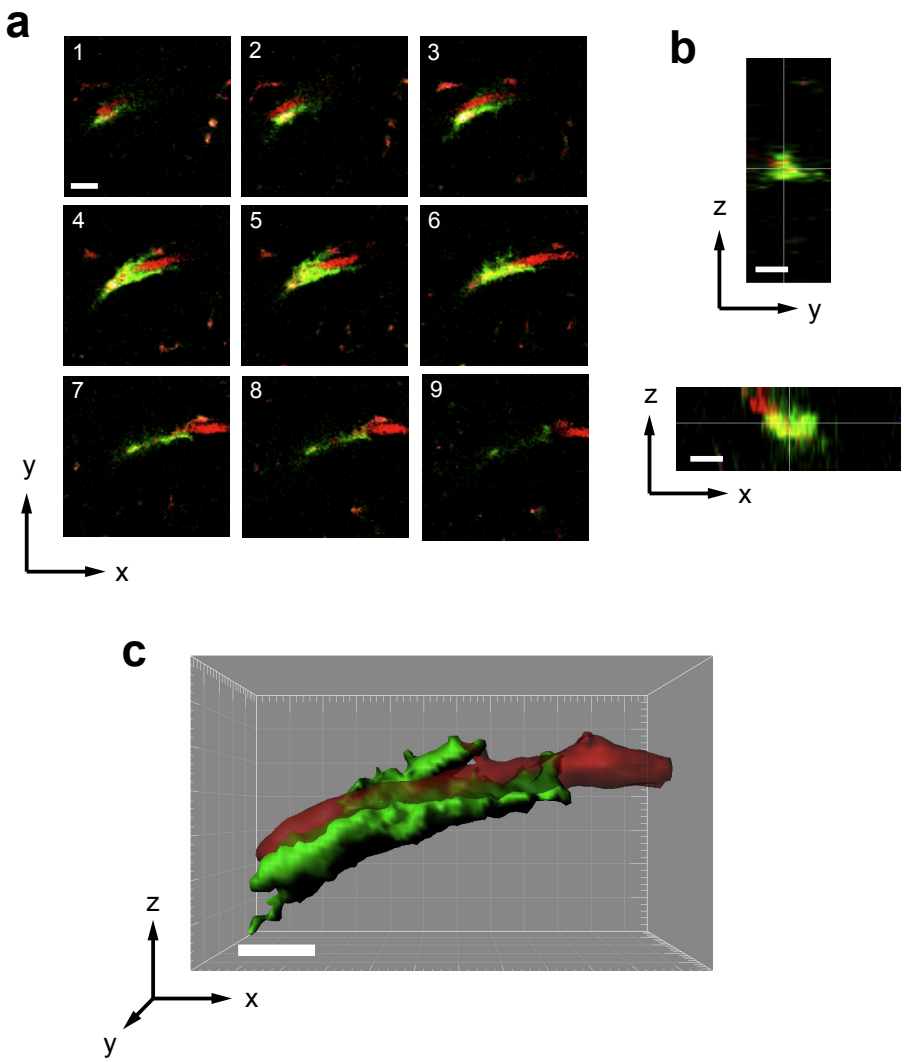

Fig. 20. Thymus resident DCs can be found in close association with capillaries. Representative immunofluorescence of a thymus that was grafted under the kidney capsule of a CD11c-YFP transgenic animal. Shown are a z-series (**a**, panel 1-9) and *zx*- and *zy*-side views (**b**) as well as a surface rendered illustration (**c**) of a representative DC (green) that is closely associated with a capillary (red). Step size is 2 µm; scale bars are 10 µm.

As DCs that breach the endothelial layer would be at least partially exposed to the blood, we designed an approach to specifically label these intravascular parts of DCs. To do so, we injected intravenously an anti CD11c mAb that was conjugated to phycoerythrin (PE). PE is relatively large fluorescent molecule (MW 240 kDa) and when conjugated to Abs it hinders them from passing through the endothelium[18,196]. Thus, intravenously injected PE-conjugated Abs can only stain structures that are within the vasculature. We hypothesize that DCs that extend protrusions into the blood as well as fully

intravascular DCs can be stained by i.v. injection of anti CD11c-PE mAbs, while DCs that are truly located within the thymic stroma cannot be labeled with this method (**Fig. 21a**). It is noteworthy that this method will not allow for differentiation between DCs that are in the process if immigrating / emigrating to / from the thymus and DCs that are strategically positioned in close association with blood vessels to potentially sample the blood for Ag (**Fig 21b**).

We named DCs that can breach the endothelial layer and are therefore located in both compartments, the thymic stroma and the vasculature, transendothelial (TE-) DCs.

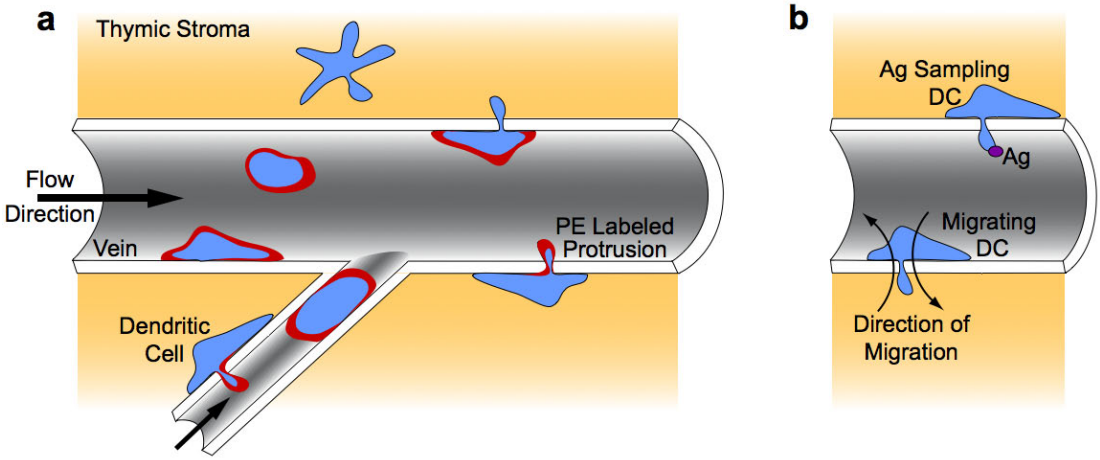

Fig. 21. Schematic of TE-DCs. (**a**) DCs that are exposed to the blood can be stained with an intravenously administered PE-labeled Ab. The staining intensity of the PE-label is likely to be proportional to the fraction of the DC that is located intravascularly. (**b**) Notably, TE-DCs may be a mixed population consisting of DCs that are in the process if immigrating/emigrating to/from the thymus and DCs that are sampling the blood potentially for antigenic material.

As hypothesized, intravenous injection of anti CD11c-PE but not isotype-PE control Ab specifically stained a small but highly significant fraction of thymic DCs (0.05 ± 0.007 vs. 1.18 ± 0.09, $P < 0.0001$, **Fig. 22a, b**). The thymi of four-week old male C57BL/6 mice consist of $210\times10^6 \pm 9.4\times10^6$ cells, of which 230,000 ± 12,000 are DCs and further, 1,800 ± 620 DCs can be labeled intravascularly (**Fig. 22c**) indicating that these cells are at least partially exposed to the blood flow. However, this approach does not allow for

differentiation between TE-DCs and entirely intravascular DCs (**Fig. 21a**). To address whether intravenous anti CD11c-PE-labeling identifies TE-DCs, thymic DCs from animals that were injected with anti CD11c-PE or isotype-PE control Ab were isolated, fixed on poly-L-lysine slides and competitively stained with an anti CD11c mAb of the same clone but conjugated to a different fluorescent molecule. We hypothesized that TE-DCs would be partially stained with the i.v. administered mAb and thus, epitopes that were not exposed to the blood would still be available for ex vivo staining, resulting in a polarized staining pattern. As a control, DCs from isotype control injected animals were co-stained ex vivo with two preparations of CD11c mAbs of the same clone, but conjugated to different labels. In this case, both mAbs should bind evenly to epitopes on the cells. Indeed, the obtained results were in agreement with this hypothesis (**Fig. 22d**).

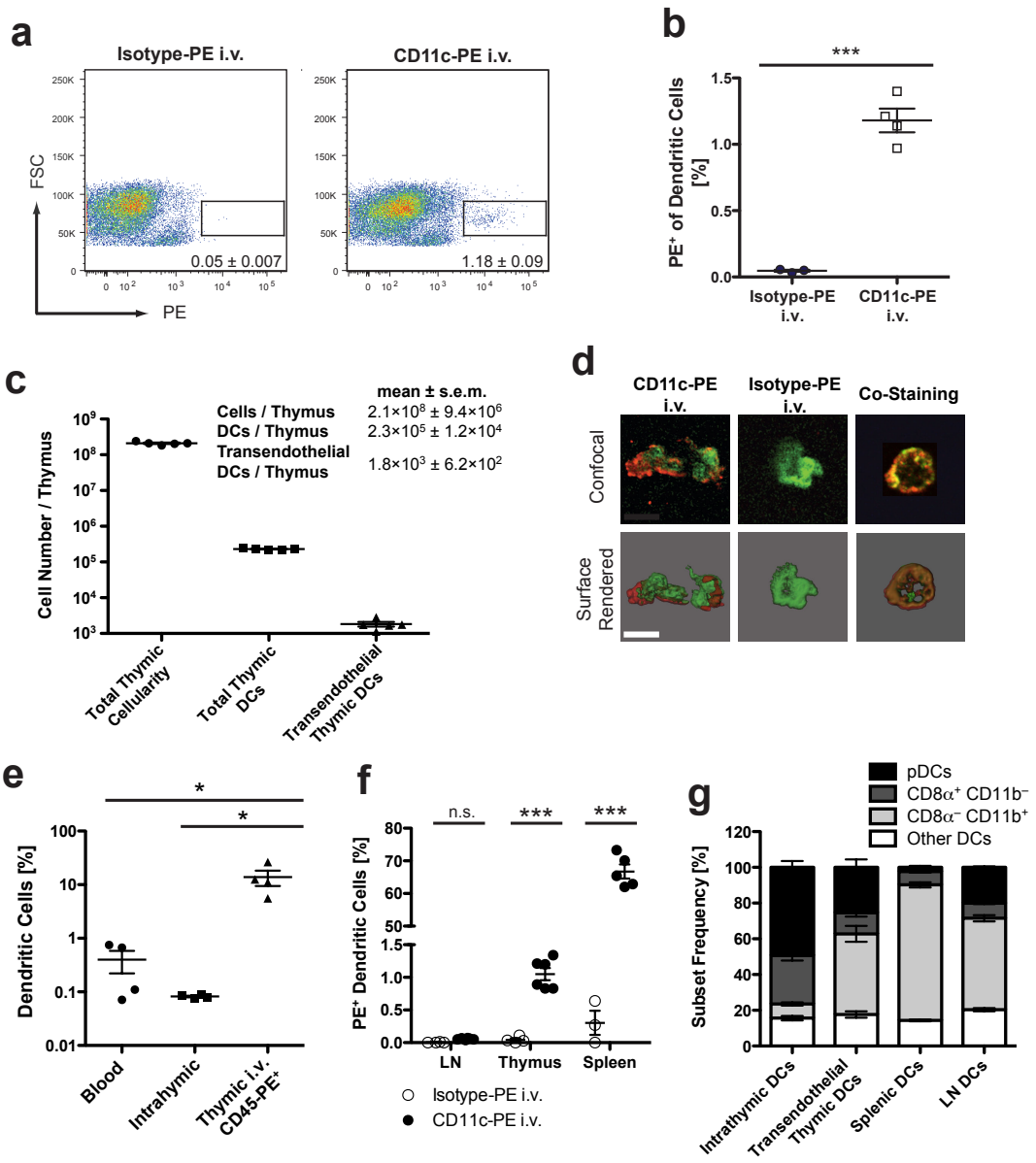
a
Isotype-PE i.v.
CD11c-PE i.v.
FSC
PE
0.05 ± 0.007
1.18 ± 0.09
b
***
PE+ of Dendritic Cells [%]
Isotype-PE i.v.
CD11c-PE i.v.
c
mean ± s.e.m.
Cells / Thymus 2.1×10^8 ± 9.4×10^6
DCs / Thymus 2.3×10^5 ± 1.2×10^4
Transendothelial DCs / Thymus 1.8×10^3 ± 6.2×10^2
Cell Number / Thymus
Total Thymic Cellularity
Total Thymic DCs
Transendothelial Thymic DCs
d
CD11c-PE i.v.
Isotype-PE i.v.
Co-Staining
Confocal
Surface Rendered
e
*
*
Dendritic Cells [%]
Blood
Intrahymic
Thymic i.v. CD45-PE+
f
n.s.
***
***
PE+ Dendritic Cells [%]
LN
Thymus
Spleen
Isotype-PE i.v.
CD11c-PE i.v.
g
pDCs
CD8α+ CD11b−
CD8α− CD11b+
Other DCs
Subset Frequency [%]
Intrathymic DCs
Transendothelial Thymic DCs
Splenic DCs
LN DCs

Fig. 22. Identification of transendothelial, bi-compartmental, thymic DCs. (**a, b**) Wild type animals were injected intravenously with anti CD11c-PE mAb or isotype-PE control mAb and sacrificed two minutes later, and single cell suspensions were stained ex vivo with a different clone of anti CD11c mAb. PE^+ thymic DCs were assessed by flow cytometry. (**a**) Representative FACS plots were gated on total CD11c positive cells. (**b**) Analysis of (**a**), the percentage of PE^+ cells was plotted. (**c**) Enumeration of thymic cellularity of four-week-old male mice. (**d**) Representative confocal images (upper panel) and surface rendered illustrations (lower panel) of DCs that were fixed on poly-L-lysine coated slides from mice that were injected with anti CD11c-PE mAb (left panel) or isotype-PE control mAb (middle and right panel). Slides were stained with anti CD11c-Alexa 488 alone (left and middle panel) or a combination of anti CD11c-Alexa 488 and anti CD11c-Alexa 647 (right panel). Shown are representative images of two independent experiments; scale bar is 10 µm. (**e**) Mice were injected with anti CD45-PE mAb, sacrificed two minutes after injection, and single cell suspensions of thymi and blood were prepared and ex vivo stained with anti CD45.2 and anti CD11c mAbs and analyzed by flow cytometry. Plotted are the percentage of DCs among total hematopoietic cells in blood and thymus as compared to the percentage of thymic DCs of PE^+ hematopoietic cells in thymus. (**f**) Percentage of PE^+ splenic, thymic and LN DCs of animals that were injected with anti CD11c-PE or isotype-PE control mAb. (**g**) Subset contribution of PE^+ and PE^- DCs in thymus and total DCs in LN and spleen of animals that were given anti CD11c-PE i.v. Representative data from two-three independent experiments, each symbol presents an individual animal, n = three-nine mice per group per experiment; *P* values were calculated using two-tailed, unpaired Student's *t*-test (**b**) or one-way ANOVA (**c, e-g**), ***$P < 0.0001$, **$P < 0.001$; shown are mean ± s.e.m.

It is possible that PE^+ DCs were not truly TE-DC but rather DCs that were located in the blood and were harvested with the organ. The following experiment was designed to address this possibility: C57Bl/6 mice were injected with anti CD45-PE mAb i.v. to label all vascular hematopoietic cells. The animals were sacrificed two minutes after Ab injection and blood and thymus were collected and ex vivo stained with anti CD45.2 mAb to identify all hematopoietic cells. The percentage of DCs among all hematopoietic cells in blood and thymus was then compared to the percentage of DCs among the intravascular CD45-PE^+ cells in thymus. Notably, $CD11c^+$ cells were significantly enriched in thymic, intravascular, hematopoietic population (13.9 ± 4.43 %) as compared to blood (0.4 ± 0.18 %, $P < 0.05$) and total thymic, hematopoietic cells (0.08 ± 0.003 %, $P < 0.05$). This finding strongly suggests that intravascular DCs do not originate from potential contaminating blood as the percentage of PE^+ DCs is significantly higher then the percentage of DCs in the blood or the whole thymus (**Fig. 22e**).

It is possible that thymic DCs were stained by free anti CD11c-PE Ab during the organ dissociation in the course of the DC preparation, even though the data obtained from the analysis of DCs that were fixed on poly-L-lysine slides suggested otherwise. Staining with free anti CD11c-PE Ab during the preparation would have resulted in a homogenous staining of the cell surface rather than the observed "patchy" staining (**Fig 22d**). However, to further evaluate this possibility, spleens, inguinal LNs and thymi of anti CD11c-PE injected animals were analyzed by FACS staining. We hypothesize that the bulk of splenic DCs but very few to no LN DCs would acquire the label. Indeed, 70% of splenic DCs but only a small and, compared to isotype control, non-significant percentage of LN DCs could be labeled intravenously (**Fig. 22f**).

Lastly, the subset composition of intravascularly stained thymic DCs differed greatly from the pool of total intrathymic DCs and resembled more closely the compositing of DC subsets that can be found inguinal LNs. As compared to intrathymic DCs, $CD11c^{+}CD8\alpha^{-}CD11b^{+}CD34^{int}CD103^{-}$ DCs were among intravascularly stained DCs, while pDCs and $CD11c^{+}CD8\alpha^{+}CD11b^{-}$ DCs were underrepresented (**Fig. 22g**). In the thymus and LNs, $CD8\alpha^{-}$ DCs express the chemokine receptor CX_3CR1. The difference in the subset composition of intrathymic versus bi-compartmental, TE-DCs provides another clue that the latter cell population is not stained by intravascular Ab that is released during the cell preparation. In this case one would expect a similar subset composition in both PE^{+} and PE^{-} DC populations.

Taken together, this data strongly suggests that a small percentage of thymic DCs have direct access to the blood. It is unlikely that they stem from contaminating blood or are an artifact caused by free Ab that was released during the cell preparation. These cells are likely to be bi-compartmental, transendothelial, as suggested by confocal microscopy, and are enriched in the $CD11c^{+}CD8\alpha^{-}CD11b^{+}CD103^{-}$ DC subset as compared to intrathymic DCs.

At this point, the importance of thymic TE-DCs remains unknown. We hypothesize that they extend protrusions into the bloodstream to acquire

circulating Ag and make it available for T cell selection. However, it is also possible that TE-DCs include cells that were in the process of migrating in or out of the thymus at the time the mAb was given (**Fig. 21b**). To address the latter possibility, we blocked DC homing by administration of a blocking mAb to α_4-integrins. Injection of the mAb one hour before i.v. administration of anti CD11c-PE did not affect the frequency of PE^+ DCs in the thymus, indicating that TE-DCs are not immigrating cells and that further, α_4-integrin is dispensable for acquiring an transendothelial phenotype (**Fig. 24a**).

We cannot rule out that TE-DCs are in the process of emigrating from the thymus into the blood. However, such a migration pattern has not been described to date and furthermore, we have never observed DC emigration from the thymus MP IVM either.

Future experiments will visualize the formation of transendothelial protrusions into the blood in vivo byMP IVM. We aim to address the hypothesis that intravascular labeling of TE-DCs can be directly visualized in vivo.

Subaim 4.2: To evaluate whether homed and thymus resident DCs can extend transendothelial protrusions

Image analysis of capillary-associated DCs revealed that they were almost exclusively thymus resident DCs rather than homed DCs (**Fig. 18e, 20a-c**). To confirm this observation, immature DCs were isolated, fluorescently labeled, given intravenously to C57Bl/6 recipients, followed 18 hours later by i.v. injection of anti CD11c-PE. In this setting, FACS analysis showed that transferred DCs were more abundantly stained with the intravascular Ab as compared to resident DCs (**Fig 23a, c**). However, the mean fluorescence intensity (MFI) of homed PE^+ DCs was significantly higher than the MFI of resident DCs (**Fig. 23b, c**). These findings raised suspicion as to whether homed PE^+ DCs were entirely intravascular rather than transendothelial (**Fig.**

22a). As shown previously, TE-DCs are only partially exposed to the blood. Thus, the injected Ab cannot physically access all available CD11c epitopes of the cell (**Fig. 21d**). Consequently, higher MFIs may indicate that cells were in fact fully intravascular. Indeed, MP IVM revealed that homed DCs are frequently "stuck" in capillaries in the thymus at two and 18 hours post transfer (unpublished observation). To experimentally address whether homed PE^{high} cells are fully intravascular, the following experiment was designed. CD57Bl/6 mice were injected with immature DCs 18 hours before administration of anti CD11c-PE mAb (clone N418). The animals were sacrificed; blood and thymi were collected and stained with anti CD11c mAb (clone HL3) to label all DCs and anti CD11c mAb (clone N418) as a competitive staining (**Fig. 23d**). The rational is that the intravenously administrated Ab binds to most, if not all, epitopes of blood borne DCs, and thus, only a few epitopes are available for staining by the in vitro administrated identical Ab clone. For intrathymic DCs, this scenario would be reversed. If homed PE^{high} cells are fully intravascular, then their staining pattern will be similar to that of blood derived DCs. If they are bi-compartmental, then the ratio of i.v. versus ex vivo administrated Ab would be more similar to that of resident thymic PE^{+} DCs. The results of this experiment suggested that adoptively transferred PE^{+} DCs are similar to blood borne DCs (**Fig. 23e**). Thus, they are most likely not transendothelial but instead are fully intravascular.

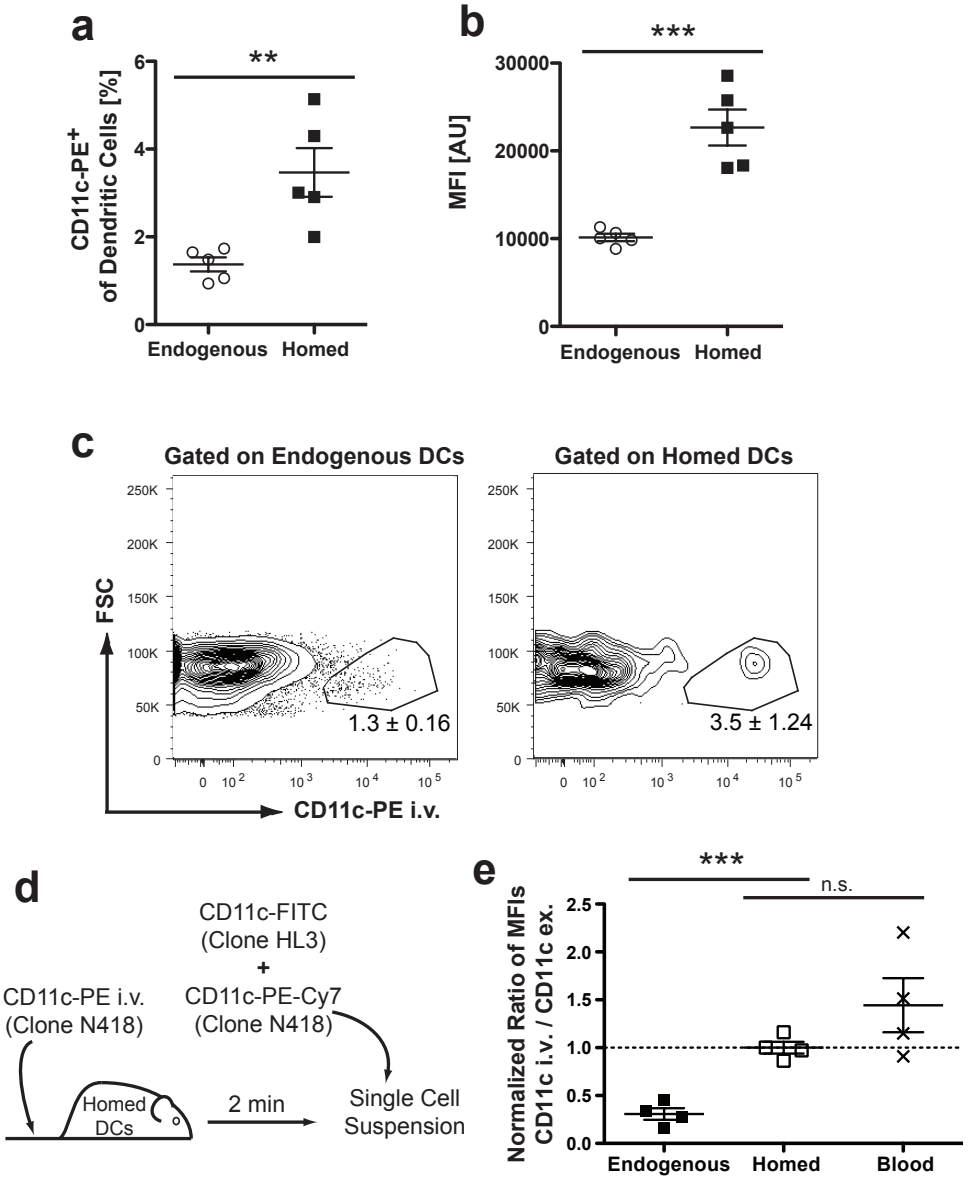

Fig. 23. Intravascular labeling of homed and endogenous thymic DCs. (**a, b**) Recipient mice were injected with fluorescently labeled DCs 18 hrs before intravenous injection of CD11c-PE and were sacrificed two minutes later. Single cell suspensions were analyzed by flow cytometry. Plotted are the percentage (**a**) and the MFI (**b**) of homed versus endogenous PE^+ DCs. (**c**) Representative FACS plots were gated on total $CD11c^+$ DCs. (**d**) To determine whether homed PE^{high} cells originate from blood contaminations, wild type animals were injected intravenously with anti CD11c-PE clone N418 and sacrificed two minutes later. Single cells suspension were prepared and stained with anti CD11c clone N418 (competitive staining) and CD11c clone HL3 (to identify all $CD11c^+$ cells). Single cell suspensions were analyzed by gating on total intravascularly labeled endogenously, homed and blood DCs, respectively. (**e**) The ratio of MFIs of in vivo and ex vivo Ab staining was calculated and normalized by the ratio of homed DCs. Shown are the ratios of the MFIs of intravenously administered Ab (CD11c i.v.) / ex vivo administered Ab (CD11c ex.) for endogenous thymic, homed thymic and blood borne DCs. Shown are representative data from two independent experiments, n = three-five mice per group per experiment; two-tailed, unpaired Student's *t*-test; ***P < 0.0001, **P < 0.01; shown are mean ± s.e.m.

Future experiments will aim to further our understanding of the bi-compartmental distribution of homed and thymus resident DCs, by performing immunofluorescence and MP IVM. This approach will allow us to address directly whether homed DCs contribute to the pool of transendothelial DCs and whether they exhibit a sampling phenotype or are simply caught during transendothelial migration.

Subaim 4.3: To assess the mechanism by which transendothelial DCs gain access to the blood stream

Next we asked by which mechanism DCs could extend transendothelial protrusions to gain access to the blood. It has been shown that circulating DCs home to the thymus by employing a multi-step adhesion cascade. Blockade of α_4 integrin abrogated homing of DCs into the thymus[83] (**Fig. 12c**) but did not alter the frequency of TE-DCs as evaluated by FACS analysis (**Fig. 24a**).

In order to assume a bi-compartmental phenotype, DCs have to penetrate through the endothelial barrier, including the underlying basement membrane. It is possible that the same molecules that are utilized for transendothelial migration also play a crucial role in this process. In particular, PECAM-1 and CD99 have been shown to promote transendothelial migration of monocytes[197]. As there are only limited reagents available to address the role of CD99 in adhesion and migration in mice we focused on the potential role of PECAM-1. PECAM-1 consists of six Ig-like extracellular domains that promote transendothelial migration[198,199] and thus, blocking of these domains with blocking mAb abrogates diapedesis. Howecer, pretreatment of mice with non-depleting anti PECAM-1 blocking mAb had no effect on the TE-DCs (**Fig. 24b**), suggesting that the formation of TE-DCs is PECAM-1 independent.

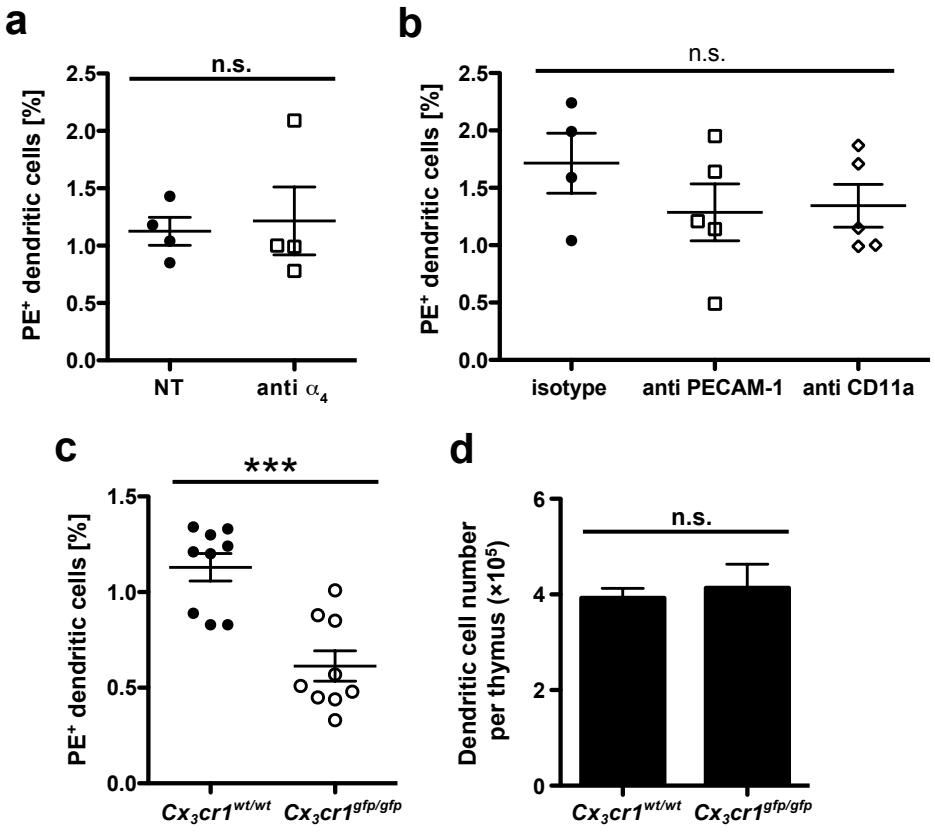

Fig. 24. Bi-compartmental localization of thymic DCs is dependent on CX_3CR1 but not α_4 integrin, PECAM-1 or α_L integrin. One hour before administration of anti CD11c-PE, animals were either injected with non-depleting anti α_4 (**a**), anti PECAM-1 (**b**) or anti α_L blocking mAb (**b**) or left untreated (NT, **a, b**). PE^+ DCs were assessed by flow cytometry. (**c**) Age and sex matched wild type and CX_3CR1 deficient animals were injected with anti CD11c-PE and analyzed for PE^+ thymic DCs by FACS. (**d**) Cell counts of DCs in whole thymus lobes of sex and age matched wild type and CX_3CR1 deficient mice. Data was pooled from two independent experiments, n = nine mice per group. P values were calculated using two-tailed, unpaired Student's *t*-test, n.s. non significant, ***$P < 0.0002$.

We have established here that TE-DCs are enriched in $CD11c^+CD8\alpha^-CD11b^+$ DCs (**Fig. 21g**). This subset also expressed the chemokine receptor CX_3CR1 which is also expressed on patrolling monocytes that "crawl" on resting endothelium[159]. Importantly, patrolling $CX_3CR1^{high}CCR2^-$ monocytes per se do not contribute to the pool of transendothelial DCs as they do not express CD11c[159] and thus cannot be labeled with anti CD11c-PE mAb. Crawling of monocytes on the endothelium is known to depend on LFA-1 ($\alpha_L ß_2$) and, to a lesser extent, on CX_3CR1[159]. To address the potential role of LFA-1 in the formation of TE-DCs, we injected an α_L integrin blocking mAb or isotype

control mAb and enumerated TE-DCs. Blockade of LFA-1 did not interfere with TE-DCs (**Fig. 24b**).

Given that CX_3CR1 contributes to the crawling behavior of monocytes and CX_3CR1^+ lamina propria DCs can directly sample the small intestine by protruding dendrites into the lumen[200], we tested the role of this chemokine receptor. Age and sex matched wild type or CX_3CR1 deficient mice (*Cx3cr1*$^{gfp/gfp}$)[106] were injected with PE labeled anti CD11c mAb or isotype control mAb. Flow cytometric analysis of thymic DCs showed that in the absence of CX_3CR1, significantly fewer cells acquired the intravascular label (**Fig. 24c**). This was not due to a developmental defect of DCs in CX_3CR1 deficient mice, as the number of DCs per thymus of wild type and deficient mice was virtually identical (**Fig. 24d**).

This data suggests that the appearance of TE-DCs is an active process that is at least partially regulated by the chemokine receptor CX_3CR1. How exactly CX_3CR1 promotes the formation of TE-DCs is not clear yet and future experiments will aim to further investigate the underlying mechanism.

Discussion

In vivo imaging of the thymus

The advent of time-lapse multi-photon intravital microscopy has enabled researchers to visualize cells deep within their native 3D environment in mice. Pioneer work in LN of mice has helped us to gain a better understanding of how immune responses are initiated and of the cross talk of lymphocytes with APCs[133,201]. To date, a multitude of organs, such as bone marrow, brain, lungs, skin and many more have been successfully subjected to MP IVM in mice[202-205]. However, the thymus has not been one of them.

Imaging of the thymus is particularly interesting due to its specialized function in T cell development and selection. Failure to develop a functional thymus, as seen in nude mice and in patients suffering from the DiGeorge Anomaly, is accompanied by a lack of T cells. The DiGeorge Anomaly describes a genetic encoded disorder that causes developmental defects in organs derived from the third and fourth pharyngeal pouches, such as the thymus and the heart. These individuals are severely immune depressed and their average life span does not exceed two years without treatment[206-209]. Similarly, mice that were thymectomized at birth, have reduced T cell numbers, are more susceptible to infections and die prematurely[210]. Thus, the thymus is an essential organ that supplies the body with polyclonal T cells that are important to fight bacterial, viral, fungal and parasitic insults. Despite its essential role in generating a protective T cell repertoire, only little is known about the dynamics of T cell development and antigen presentation within the thymus.

Only the thymi of medaka have been successfully visualized in live animals to date[211]. Medaka are translucent fish that develop ex utero. Because of this, they can be subjected to IVM without the requirement for surgically accessing

the thymus or induction of anesthesia. Experiments with medaka have provided new insights into the colonization of the thymus anlage, which occurs in medaka from anterior to posterior. Furthermore, thymocyte motility in the embryonic medaka thymus was greatly reduced as compared to T cells in adult thymi[211].

The mammalian thymus has not been subjected to IVM because of the different anatomical and optical features of mammals as compared to medaka. In mammals the thoracic thymus is located in the ribcage and in direct contact with lungs and heart, which makes it inaccessible for (MP) IVM. Even under the hypothetical assumption that it would be possible to access the thoracic thymus without interfering with respiration, the immobilization of the organ would pose a significant obstacle. As the thymus rests on the heart it moves with the heartbeat. Technically, there are imaging devices available that allow for synchronization of the heartbeat with the cycle time. However, as the thymus also directly contacts both lungs, synchronization would have to be achieved with the heartbeat and respiration. In order to provide consistent respiration, the lungs would have to be mechanically ventilated. Even if it were possible to access and sufficiently immobilize the thoracic thymus, it would still be difficult to visualize cells that are located in the medulla because the thymus is a relatively opaque tissue. The maximal penetration depth by MPM is about 200 µm and the medullas of thoracic thymi in almost 80% of six to twelve week-old mice are located deeper within the organ. One alternative approach to image the thoracic thymus is by subjecting ectopic, cervical thymi to MP IVM. Cervical thymi consist of a single lobe, they are smaller in size, and medullary regions are located more superficially[35]. They are not located within the ribcage; instead, they are spread out in the deep cervical region. They are often found in similar anatomical regions as the deep cervical lymph nodes, although their number and exact location vary and not each mouse has one[35]. Cervical thymi are often mistaken for deep cervical LNs as they are similar in size and appearance. Because of their location deep within the cervical neck region, it is challenging to sufficiently expose them for MP IVM without causing substantial damage to the surrounding tissue. Though cervical thymi have

been shown to support T cell development, their function still remains somewhat enigmatic[35]. Further experiments, such as transplantation into athymic nude mice will be necessary to demonstrate whether or not they are equally effective in supporting T cell development as compared to thoracic thymus lobes.

It is of note that explanted. mammalian thymus tissue has been successfully subjected to MPM. Bousso et al used reaggregated thymic organ cultures and fetal thymic organ cultures in combination with MPM to visualize encounters between thymocytes and stromal cells[183]. Though this ex vivo system provides all cell types present in a native thymus, the thymic architecture is disrupted. It can be concluded that intact cortical and medullary regions are indispensable for central tolerance[184]. Additionally, this system cannot provide important factors such as a constant blood flow or innervation that contribute to / may influence dynamics within the thymus.

Other studies took advantage of so called acute thymic slice preparation to visualize thymocyte – stromal cell interaction during positive selection[185,186]. This approach enables to follow developing T cells through cortex and medulla. However, the disadvantage of this set up is that the preparation of the thymus requires a broad range of different temperatures ranging from 4°-37°C that may influence cellular behavior. Also, factors like blood flow or innervation cannot be provided in this in vitro system.

We have demonstrated here for the first time that it is possible to image the thymus of mice in vivo. Because of the constraints of the location of the thoracic thymus, we took advantage of a transplantation model by which individual thoracic thymus lobes of embryonic donor mice were transplanted under the kidney capsule of young recipient mice. We have shown that transplanted thymi closely mirror their endogenous counterparts in terms of compartmentalization into cortex and medulla, vascularization, T cell development, DC subset composition and DC homing. Importantly, we found that medullas were located more superficially in transplanted thymi than endogenous thymi, which was most likely due to the overall reduced size of the transplant. This reduction in size can likely be attributed to the location of

the transplant. While the kidney provides a nourishing environment with ample opportunities for revascularization, there is a space restriction due to the capsule. Thus, it seems likely that the grafted, revascularized thymus lobe provides all features necessary to unfold to its full potential but is prevented by the spatial limitation dictated by the limited space between kidney and its capsule.

In order to successfully subject transplanted thymus lobes to MP IVM microscopy, the organ has to be completely immobilized. Owing to the acquisition process, even subtle movements will introduce motion artifacts that are nearly impossible to correct for post acquisition with current imaging software. In order to generate a 4D movie, a predetermined imaging volume is recorded by acquiring a series of optical section along the *z*-axis at a given time interval over a given period of time. Generally, we acquire 8-12 optical sections that are vertically spaced no more than 3 µm apart at a time interval of 15 or 20 seconds for 241 or 181 cycles, respectively. This results in a one-hour acquisition. Thus, a 3D snapshot is made every 15 (or 20) seconds. We have no information about the events between each acquisition (cycle). In a well-immobilized organ, it is fairly straightforward to reassemble most cell tracks based on the information that has been gathered. However, motion artifacts introduce a new level of complexity. Slight, consistent motion artifacts such drifting within the *xy*-plane can be corrected using image processing software. Drifts along the *z*-axis, as well as inconsistent or rapid drifts are difficult to correct for and thus can render the collected movies uninterpretable. In other words, it is of highest priority to sufficiently immobilize the organ for MP IVM. One option to reduce drifts would be to expose and separate the kidney as much as possible from the torso of the animal. Unfortunately, this is problematic, as it would constrict the blood flow to and especially from the kidney, causing hypoxia of the tissue which ultimately influences cell motility and causes stasis. We found that the most efficient way for immobilization was to glue the organ to its platform with tissue glue and to additionally place a small needle above and below the transplant, distally to the thymus to pin the kidney down. Pinning down the kidney is likely to obstruct the local microcirculation; however, the

microcirculation to the transplant remains unaffected as long as the distance between the needles and the transplant is sufficient.

Lastly, to visualize cellular behavior within the thymus, it is crucial that the cells of interest are fluorescently tagged. However, developing thymocytes are highly proliferative cells and as a result, ex vivo labeling of thymocytes with fluorescent cell trackers such as CFSE followed by adoptive transfer is not feasible. Cell trackers are diluted when a cell divides. Labeled thymocytes that are highly proliferative would rapidly dilute out the label to a degree where it is below the detection limit of the microscope. Another problem with adoptively transferred thymocytes is their poor ability to home to the thymus from the blood. While adoptively transferred HSPC, LSK, CLP and CLP-2 can give rise to T cells in the thymus, only CLP-2 cells are equipped with the necessary machinery to do so[41,212-214], and more committed thymocyte precursors have lost their ability to enter the thymus from the blood and instead express trafficking molecules that are geared for interstitial migration within the organ[40]. DN3 cells and their progeny that have down regulated the surface expression of CD44 retain poor capacity to home to the thymus when given intravenously[40,41,215]. We therefore worked with genetically tagged thymocytes that express either GFP or dsRed under the CD4 promoter to circumvent these shortcomings. All T cells express the fluorescent protein in these mice.

Using the herein described approaches we were able to describe the dynamic behavior of thymocytes and DCs and their interactions with each other in thymi of living mice.

Thymocyte behavior

We have shown here that TCR tg thymocytes migrate at higher velocities in the medulla as compared to the cortex in the absence of cognate Ag. Medullary thymocytes also scan a smaller volume and appear to migrate in a more confined fashion. These results are in agreement with data derived from explanted thymi[186].

Why do medullary thymocytes move faster than cortical thymocytes, yet are more confined in their migration? The answer is likely to be found in the different selection processes that take place in cortex and medulla, respectively. TCR tg thymocytes prematurely express a fully rearranged TCR[189], eliminating the need for β-selection. Positive selection generates a self-restricted T cell pool by selecting for TCR specificities that can interact with self-peptide presented on MHC molecules[40]. It is known that positive selection is greatly abbreviated in time, and TCR tg T cells will receive a positively selecting signal faster, as the TCR of TCR tg mice has already been selected for passing positive selection (cloned from a peripheral T cell). Consequently, this scenario would eliminate the need to scan the cortex thoroughly for sAg, as they possess the ability to scan a greater volume (higher motility coefficient). For that reason, TCR tg thymocytes have been used to study positively selected T cells while wt thymocytes served as negative controls due to the high percentage of cells that get deleted during this process[48]. It has been shown that positively selected thymocytes migrate more directly as compared to pre-selection thymocytes[48]. After passing positive selection, TCR tg thymocytes enter the medulla where they test their TCR in the course of negative selection[40]. This time the scenario is markedly different, as wt animals do not express cognate ligands for the tg TCR and thus cannot shorten the quest of tg thymocytes. We suggest that higher velocities and low motility coefficients, which indicate that these cells patrol through a smaller volume, are reflective of the scanning behavior of TCR tg thymocytes in medulla versus cortex. Specifically, high velocities may enable

tg thymocytes to interact with a maximal number of cells and the confined migration could be indicative of preferential scanning of APCs in the vicinity.

Ag-specific thymocytes dramatically change their migratory behavior in the presence of cognate Ag. We have shown here in vivo that specific OT-I TCR tg thymocytes reduce their speed by a third and further restrict the volume that they scan upon adoptive transfer of peptide pulsed DCs. This altered behavior was not observed in control cells that were present in the same imaging volume, excluding any bystander effects. A similar change in OT-I cell motility has been described in an ex vivo study that utilized the RIP-mOVA system[186]. In RIP-mOVA mice, mTECs express ovalbumin due to the transcriptional regulator Aire and it has been shown that thymic DCs can gain access to the protein and present it to developing T cells[75]. Therefore, our approach differs from the RIP-mOVA system in the APC that is presenting the cognate Ag and, presumably, in the Ag dose that is being presented. Despite these differences, there is a surprising consistency among OT-I T cell motility in the presence and absence of Ag between these studies. The measured mean velocities per track, which tend to be an over-estimate of the actual velocity of the cells, are almost identical[186].

We have shown in our study for the first time that long-lasting cognate interactions are formed during negative selection in vivo. 18% of Ag specific thymocytes interacted with DCs for the entire imaging period of 60 minutes and 24% for at least 30 minutes. Thus, we have shown for the first time that these interactions can last long enough to form an immunological synapse, which has been shown to take 30 minutes to form in peripheral tissues[195]. It is noteworthy that immunological synapses during positive and negative selection differ in their architecture and stability as compared to immunological synapses that are established during T cell activation in peripheral tissues. Also synapses in positive versus negative selection differ, while only short-lived multifocal synapses are built during positive selection, negative selection includes the formation of more stable synapses that can last up to seven hours in vitro[216,217].

The interaction times measured in our study greatly exceeded those that had been measured in the ex vivo RIP-mOVA model between OT-I TCR tg thymocytes and DCs[186]. This difference is most likely caused by the different source of the antigen. In RIP-mOVA mice, mTECs express the cognate protein and DCs gain access to it by Ag transfer[75], thus, it is likely that specific thymocytes preferentially interact with mTECs rather than DCs in RIP-mOVA mice. Indeed, it was shown in that OT-I T cells migrated in confinement zones in RIP-mOVA mice, meaning that OT-I TCR tg thymocytes stayed in the vicinity of DCs but didn't interact with them[186]. These confinement zones could reflect the interaction of specific T cells with Ag expressing mTECs, which were not visualized in this study. Assuming that OT-I T cells preferentially interact with mTECs, one could speculate that the relatively short interaction times in the presence of cognate Ag are non-specific interactions rather than Ag-driven ones. The interaction time of OT-I T cells in the presence or absence of Ag (mean interaction time 1.2 min versus 1.9 min) differed by only a third[186], while we observed a much greater difference for mean interaction times for cognate and non-cognate T cell – DC interactions (18.7 min versus 3.7 min). It is of note that by adoptively transferring Ag pulsed DCs, we specifically targeted the Ag to these DCs. Furthermore the amount of Ag that is presented by pulsed transferred DCs is likely to differ from the amount presented by DCs in RIP-mOVA mice, which have to gain access to it from mTECs via Ag transfer[75]. It is possible that the interaction times that were measured between OT-I TCR tg thymocytes with and DCs in RIP-mOVA mice were non-specific as OT-I T cell motility was reduced by a third in RIP-mOVA mice as compared to wt mice but the measured interaction times were increased by a third[186]. The inversed correlation between thymocyte speed and interaction time could indicate that the observed DC – T cell interactions are indeed non-specific and consequently the increase of interaction time could be explained by the reduction of migration speed of the thymocytes.

We also found in our study that not all Ag specific thymocytes engaged in prolonged interactions, which was expected, as thymocytes are a heterogeneous population with regard to their developmental stage.

Thymocytes in the medulla and CMJ mainly consist of DP, semi-mature and mature SP thymocytes. SP semi-mature but not mature SP cells are still susceptible to negative selection[57]. Thus, the developmental stage of the thymocytes influences their susceptibility to negative selection and could explain the fact that not all tg thymocytes engage in prolonged interactions.

Thymic DCs

Thymic DCs are a heterogeneous population. They can either be subdivided according to the expression of surface markers or their place of origin. Approximately 10% of all thymic DCs have not developed in situ but homed to the organ from the periphery by employing a multi-step adhesion cascade[80,83,84,118,119]. While all splenic DC subsets from Flt3L injected animals have a similar capacity to home to the thymus from the blood, pDCs and $CD8\alpha^{+}11b^{-}$ (but not $CD8\alpha^{-}11b^{+}$) cDCs are preferentially retained or have a higher survival rate in the organ. The DC subset contribution of homed DCs closely resembles the endogenous subset distribution at 18 hours post DC transfer. In line with this, it has been shown that thymic pDCs and $CD8\alpha^{-}$ DCs can enter the thymus from the periphery while $CD8\alpha^{+}11b^{-}$ DCs are predominantly thymus resident. About 30% of resident $CD8\alpha^{+}11b^{-}$ cDCs and pDCs in the thymus carry IgH rearrangement in the TCRα locus, indicating that they have developed intrathymically from DN cells[81]. This suggests that thymic pDCs can develop in situ as well as entering the thymus from the periphery. It is currently unknown whether thymic DCs can leave the organ in the steady-state. We have shown in adoptive transfer experiments that all DC subsets home to the thymus equally well, but are retained differentially. Adoptive transfer experiments rely on the injection of non-physiologically high numbers of DCs, thus, it is not clear whether thymic DCs can emigrate under the steady state as well. This is a particularly interesting point as thymic pDCs can arise intra- and extrathymically. It is possible that thymus-borne pDCs leave the organ, circulate through the blood and re-enter the thymus.

Homed DCs display a motile behavior upon entering the thymus. As it was shown that they can carry Ag as their cargo and induce central tolerance against it[83,84], it is conceivable that this behavior serves to optimize the display of the delivered Ag within the thymus. In contrast, thymus resident DCs are more sessile and have a more dendritic, spread-out shape. We found that they were often in tight contact with small blood vessels, which was not observed for homed DCs. It is of note that two hours post transfer, homed

DCs were frequently found “stuck” in the lumen of thymic blood vessels. We speculate that resident DCs can breach the endothelial layer and access the blood given their association with vascular structures. Indeed, we found that thymic DCs can be stained intravascularly, demonstrating that they are exposed to the blood. The staining intensity and pattern was consistent with a transendothelial positioning rather than fully intravascular localization. We named these cells TE-DCs. They are defined by their location within the thymic stroma but are at least partially exposed to the lumen of a blood vessel. We also provided evidence that thymus resident but not homed DCs are specialized in adopting a transendothelial phenotype.

This previously under-appreciated positioning of some thymus resident DC poses an interesting question: why do thymic DCs breach the endothelial layer to access the blood? The most intriguing scenario is that they do so to sample the blood for self-peptides and proteins in order to make them available for T cell selection. Assuming that this is the case, homed and resident DCs differ not only by their place of origin but may also have different specializations. While homed DCs can deliver Ag from peripheral tissues to the thymus, a subset of resident DCs is strategically positioned to access the blood from the thymus to sample for circulating antigenic material. Therefore both subsets would play an important role in making peripheral Ag available for T cell selection; however, they do so by employing different mechanisms. Sampling blood-borne Ag for presentation could be crucial for inducing tolerance to abundant serum proteins that are too large to diffuse into the thymus and are not expressed in the thymus per se.

Another possible explanation for the appearance of transendothelial DCs is that these cells may be caught in the process of migrating to and from the thymus. Homed DCs employ a multi-step adhesion cascade and blockade of α_4 integrins abrogated DC homing to the thymus but did not interfere with the emergence of transendothelial DCs. While it is not known whether α_4 integrins also play a role in the possible emigration of thymic DCs, this experiment at least excludes the possibility that TE-DCs are in the process of homing to the thymus.

The role of CX_3CR1 in transendothelial DCs

This apparent sampling behavior of TE-DCs led us to investigate the possible mechanisms for extending these transendothelial protrusions. As these protrusions must breach the endothelial layer, likely candidates are molecules that have an established role in transendothelial migration. We therefore investigated the role of PECAM-1 but found that blockade of the extracellular Ig like domains that are indispensable for diapedesis[198,199] did not affect the formation of TE-DCs. It has been shown that CX_3CR1^+ DCs in the lamina propria can sample the lumen of the gut and that this process is dependent on the expression of CX_3CR1[200]. In thymus and LN, the expression of CX_3CR1 coincides with $CD8\alpha^-11b^+$ DC subset. This subset is the main constituent of transendothelial DCs and expression of CX_3CR1 is required for the appearance of these cells. CX_3CR1 deficient animals did not show any defects concerning DC number or location as compared to wt animals. The ligand for CX_3CR1, fractalkine, is expressed by resting endothelium and can either be secreted or expressed as a transmembrane molecule[90]. Resident $CD11b^+11c^-Ly6C^-CX_3CR1^+$ monocytes have been shown to display a crawling behavior and to patrol the vasculature. This process was largely mediated through binding to LFA-1 ($\alpha_L ß_2$)[159]. It is noteworthy that transendothelial DCs are distinct from patrolling monocytes as judged by the differential expression of CD11c and CD11b[159]. Likewise, blockade of LFA-1 also had no effect on the formation of TE-DCs.

How can CX_3CR1 mediate the formation of transendothelial protrusions? In the lamina propria, CX_3CR1 dependent protrusions are extended into the lumen by adherence to epithelial cells that express fractalkine[159]. This chemokine can be expressed on resting endothelium, but the presence of fractalkine in the thymus or thymic microvessels has not been addressed yet. It is of note that thymic DCs failed to migrate in response to fractalkine in a chemotaxis assay[82]. Interestingly, a second chemokine has been identified recently as a ligand for CX_3CR1 – eotaxin-3 (CCL26)[218]. Eotaxin-3 is

expressed by vascular endothelial cells, and has been shown to promote transendothelial migration of eosinophils[219,220]. To this end it has not been addressed whether eotaxin-3 is expressed in the thymus. It is possible that CX_3CR1 – eotaxin-3 interactions promote the formation of transendothelial protrusions.

Concluding remarks

The thymus is a particularly interesting organ as it provides the necessary environment for T cell development and selection. There is substantial evidence that positive selection relies on the presentation of self-peptide that has been generated in the thymus. In contrast, antigenic material for tolerance induction during negative selection is either expressed in the thymus per se or derived from the peripheral tissues. In order to present peripheral Ag in the thymus, it has to gain access to the organ. This can either be achieved by delivery of Ag by thymus-bound DCs, or by uptake of circulating Ag from the blood by thymic APCs. We have demonstrated here for the first time in vivo that delivery of cognate Ag to the thymus dramatically affects the motile behavior of specific, but not non-specific thymocytes. Homed, thymic DCs engaged in long-lived, Ag-dependent interactions with thymocytes. We have further shown that thymus resident DCs could gain access to the blood. We hypothesize that this process is geared toward gaining access to circulating antigenic material and to make it available for T cell selection. Thus, it appears that DCs play an important role in T cell selection not only by Ag presentation, but also by “fetching” it from the periphery.

Materials and methods

Mice

C57BL/6 mice were from Charles River Laboratories and were used at 4–12 weeks of age. OT-I and P14 mice, which carry a transgenic TCR specific for ovalbumin amino acids 257–264 (SIINFEKL) in H-2Kb and LCMV gp33–41 (KAVYNFATC) in H-2Db, respectively, were from Taconic Farms. DPE-GFP and T-Red mice were generated previously[190] and crossed to OT-I[191] and P14[192] mice, respectively. Transgenic mice (C57BL/6 background) expressing enhanced green fluorescent protein (eGFP) under the β -actin promoter were generated as described[221]. *Cx$_3$xr1$^{gfp/gfp}$* mice were generated previously[106] and purchased from the Jackson Laboratory. All experiments were in accordance with National Institutes of Health guidelines and were approved by the Committees on Animal Care and Use of both Harvard Medical School and the Immune Disease Institute.

Reagents

Fluorochrome-conjugated mAbs to mouse B220 (RA3-6B2), CD4 (GK1.5), CD8α (53-6.7), CD11b (M1/70), CD11c (HL3 and N418), CD25 (PC61), CD31 (390 an MEC13.3), PDCA-1 (927 and 129C1) and Kb-SIINFEKL (25-D1.16), purified neutralizing mAbs to mouse P-selectin (RB40.34), CD31 (390 and MEC13.3) and VCAM-1 (MK2.7) were purchased from BD Biosciences, BioLegend, eBioscience and Bio X cell. Chimeric, non-depleting, anti α_4 (CRL19.11) was provided by R. Palframan (Celltech, London, UK). TRITC labeled and unlabeled Ulex Europaeus agglutinin I (UEA-1) was purchased from Vector Laboratories; unlabeled UEA-1 was conjugated to Alexa Fluor® 647 or Alexa Fluor® 488 according to the manufacture's manual (Invitrogen). Anti Cytokeratin 8 mAb secreting hybridoma (TROMA-1) was obtained from

the Developmental Studies Hybridoma Bank at the University of Iowa and PTX was from Calbiochem.

BM chimeras

1-5 × 10^7 CD4 and CD8 depleted BM cells from tibia and femur from donor animals were injected into the lateral tail vein of sublethally (550 rad) or lethally (myeloablative, 950 rad) irradiated C57BL/6 mice. For mixed BM chimeras, OT-I TCR tg and P14 TCR tg BM was mixed at equal ratios and injected in irradiated C57BL/6 recipient mice (550 rad).

DC isolation

C57BL/6 mice were injected subcutaneously with 2 × 10^6 to 5 × 10^6 B16 melanoma cells secreting Flt3 ligand as described[222]. After 10–14 d, mice were killed and splenic DCs were purified by digestion in 50 µg/ml Liberase TM (Roche) for 20 min at 37ºC followed by density-gradient centrifugation over NycoPrep (Axis-Shield) according to the vendor's manual. These preparations routinely contained 75–85% $CD11c^+$ DCs. When indicated, DC maturation was induced by culture for 24 h in complete medium in the presence of 1 µg/ml of lipopolysaccharide (E. coli 0.26:B6; Sigma-Aldrich). Mature DC cultures typically resulted in enrichment in $CD11c^+$ cells (90–95%) and in the up-regulation of classical maturation markers (CD86 and MHC class II) for all $CD11c^+$ cells.

Thymus transplantation

Individual thymus lobes from E14.5 – 18.5 embryos were transplanted under the kidney capsule of anesthetized recipient mice. At the day of imaging, transplanted thymi were gently exposed and immobilized on a Styrofoam platform with two 27G1/2 needles. The exposed thymus was submerged in sterile saline and covered with a glass cover slip. A thermocouple was placed

next to the thymus to monitor local temperature, which was maintained at 37–39ºC.

In vivo labeling of thymic medullas

Thymic medullas were labeled in vivo injection of 20 µg TRITC labeled UEA-1 either intravenously or under the transplant bearing kidney capsule, distally to the graft, 18 hours before evaluation by MPM.

Alternatively, medullas were identified by the relative accumulation of TCR tg × T-Red or TCR tg × DPE-GFP thymocytes. Using Volocity or Imaris software, the number of TCR tg thymocytes per mm^3 was calculated for cortex and medulla. Medullas were characterized by a 2.5fold enrichment of TCR tg thymocytes as compared to cortex.

Multi-photon microscopy

MPM was performed on a Prairie system at an excitation wavelength of 850 nm, from a tunable MaiTai Ti:sapphire laser (Spectra-Physics). For three and for four-dimensional offline analysis of thymic architecture and cell migration, stacks of 9-11 optical x–y sections with 3 µm z spacing were acquired every 15 s or 20 s, respectively, with physical zooming to ×1–2 through a 20×/0.95 numerical aperture water-immersion objective lens (Olympus). Emitted fluorescence and second-harmonic signals were detected through 455/70nm, 450/80nm, 590/50 nm and 665/65 nm bandpass filters with non-descanned detectors to generate four-color images. Sequences of image stacks were transformed into volume-rendered three-dimensional volumes. T series were converted into movies using Volocity (Perkin Elmer) and Imaris (Bitplane) software. Motility parameters such as three-dimensional instantaneous velocities, mean velocities per track, mean displacement plots, meandering indices and motility coefficients were determined by semi-automated cell tracking with Imaris and Volocity Software and computational analysis by MatLab (Mathworks), Excel (Microsoft Office) or Prism (GraphPad).

Peptide loading of DCs

10^7 immature DCs per ml were pulsed with 1 µM SINFEKL peptide for 45 minutes at 37ºC in PBS supplemented with 2% FCS. DCs were washed twice before i.v. injections.

For the generation of loading curves, immature DCs were incubated with the indicated concentration of SIINFEKL peptide for two hours, washed, and stained with anti CD11c and anti Kb-SIINFEKL mAbs for 15 minutes. DC loading efficiency was evaluated by flow cytometry.

Interaction analysis

Interactions between T cells and DCs were defined as physical contacts lasting more than one min and were obtained by frame-to-frame inspection of 4D recordings.

Immunofluorescence

For cryosections, thymi were harvested, fixed in phosphate-buffered L-lysine with 1% paraformaldehyde/periodate (PLP), dehydrated in 30% sucrose in PBS, snap-frozen in TBS tissue-freezing liquid (Triangle Biomedical Sciences) and stored at –80ºC. Sections of 30 µm thickness were mounted on Superfrost Plus slides (Fisherbrand) and stained with fluorescent antibodies in a humidified chamber after Fc-receptor blockade with 1 µg/ml antibody 2.4G2 (Bio X cell). Samples were mounted in FluorSave reagent solution (EMD-Calbiochem) and stored at 4ºC until analysis.

For immunofluorescence analysis of DCs, $MHCII^+$ cells isolated by MACS purification and incubated on poly-L-lysine coated slides for 15 minutes at room temperature, non-adherent cells were removed by washing and slides were fixed by incubation with PLP for one hour at 4ºC. Slides were stained as described.

Images were collected with a Bio-Rad confocal microscopy system using an Olympus BX50WI microscope and 10×/0.4 numerical aperture or 60×/1.2 numerical aperture water-immersion objective lenses. Images were analyzed with LaserSharp2000 software (Bio-Rad Cell Science), Volocity (Perkin Elmer) and Imaris (Bitplane).

Homing assays

Immature or mature DCs were labeled for 15 min at 37ºC with 30 µM CFSE (carboxyfluorescein succinimidyl ester) or 3 µM DDAO-SE (7-hydroxy-9H-(1,3-dichloro-9,9-dimethylacridin-2-one) succinimidyl ester; all from Molecular Probes) at a concentration of 10^7 cells / ml. Dead cells and excess label were removed by centrifugation, and 1 to 5 × 10^7 labeled DCs were then injected in the tail veins of recipient mice. In some experiments, DCs were pretreated with 50 µg/ml of blocking mAb for one hour at 37ºC and washed before simultaneous injected with control populations; for inhibition of endothelial adhesion molecules, 100 µg mAb was injected along with the labeled DCs. Mice were killed at indicated time points and single-cell suspensions were generated from spleens and thymi and cell samples were incubated with anti-CD11c and analyzed on a FACS Canto (BD Biosciences). The total number of homed DCs was calculated by multiplication of the fraction of $CFSE^+$ (or DDAO-SE^+) $CD11c^+$ events by the total cellularity of the target organ.

Intravascular labeling of leukocytes

Leukocytes were labeled intravascularly by i.v. injection of PE conjugated monoclonal Ab to CD45 or CD11c. Animals were sacrificed two minutes post injection by CO_2 asphyxiation.

Statistical analysis

Data are presented as mean ± s.e.m. for normally distributed data sets. Statistical significance was assessed by two-tailed, unpaired Student's *t*-test for comparison of two groups or by one-way analysis of variance (ANOVA) followed by the Student Newman Keuls post-test for more than two groups. Differences with *P* values of less than 0.05 were considered significant. Non-normally distributed data were presented as medians and compared with the Mann–Whitney U-test (two groups) or the Kruskal–Wallis test followed by Dunn's test to compare multiple samples.

Abbreviations

3D	three dimensional
3DIV	three dimensional instantaneous velocity
4D	four dimensional
Ab	antibody
Ag	antigen
ANOVA	analysis of variance
APC	antigen presenting cell
APECED	autoimmune polyendocrinopthy-candidiases-ectodermaldystrophy
AU	arbitrary unit
BCR	B cell receptor
BM	bone marrow
CDA	cystidine deaminase
cDCs	conventional dendritic cell
CFSE	carboxyfluorescein succinimidyl ester
Cld	claudin
CLP	common lymphoid progenitor
CMJ	cortico-medullary junction
cTEC	cortical thymic epithelial cell
Cnx	connexin
DC	dendritic cell
Dll	delta like ligand
DN	double negative
DP	double positive
DZ	denritische Zelle
FACS	fluorescence activated cell sorting
FITC	fluorescein isothiocyanate
Foxn1	forkhead box N1
FSC	forward scatter
PECAM-1	platelet-endothelial cell adhesion molecule-1
GFP	green fluorescent protein

GPCR	G protein coupled receptor
HSA	heat stable antigen (CD24)
HSC	hematopoietic stem cell
HSPC	hematopoietic stem and progenitor cell
i.v.	intravenous
Ii	invariant chain
IVM	intravital videomicroscopy
kDa	kilo dalton
KLF2	Kruppel like factor 2
LC	langerhans cell
LN	lymph node
LRR	leucine rich repeat
LSK	lineage$^-$ Sca-1$^+$ c-Kit$^+$ cells
MFI	mean fluorescence intensity
MHC	major histocompatibility complex molecule
MHC-I	major histocompatibility complex molecule class I
MHC-II	major histocompatibility complex molecule class II
mOVA	membrane bound ovalbumin
MΦ	macrophage
MP	multi photon
MP IVM	multi photon intravital videomicroscopy
MPM	multi photon microscopy
mTEC	medullary thymic epithelial cell
MW	molecular weight
NC	neural crest
NK	natural killer
n.s.	non significant
NT	not treated
OVA	ovalbumin
PA-GFP	photoactivatable green fluorescent protein
pDC	plasmacytoid dendritic cell
PE	phycoerythrin
PGE	promiscuous gene expression

PLT	primary lymphoid organ
PSGL-1	P-selectin glycoprotein ligand 1
PTX	*Bordetella pertussis* toxin
PVS	perivascular space
RIP	rat insulin promoter
RTOC	reaggregated thymic organ culture
S1P	sphingosine-1-phosphate
S1P1	sphingosine-1-phosphate receptor
sAg	self antigen, Selbstantigen
s.e.m.	standard error of the mean
SCA	subcapsular area
SLO	secondary lymphoid organ
SP	single positive
SSC	side scatter
TCR	T cell receptor
TE	transendothelial
TD	thoracic duct
tg	transgenic
Treg	regulatory T cell
TRITC	tetramethylrhodamine isothiocyanate
UEA-1	*Ulex Europeaus* agglutinin 1
VCAM-1	vascular cell adhesion molecule 1
VLA4	very late antigen 4
VLR	variable lymphocyte receptor
wt	wild type
YFP	yellow fluorescent protein

References

1 O'Leary, J. G., Goodarzi, M., Drayton, D. L. & von Andrian, U. H. T cell- and B cell-independent adaptive immunity mediated by natural killer cells. *Nat. Immunol.* **7**, 507-516 (2006).

2 Paust, S., Senman, B. & von Andrian, U. H. Adaptive immune responses mediated by natural killer cells. *Immunol. Rev.* **235**, 286-296 (2010).

3 Janeway, C. A., Jr. & Medzhitov, R. Innate immune recognition. *Annu. Rev. Immunol.* **20**, 197-216 (2002).

4 Beutler, B. Innate immunity: an overview. *Mol. Immunol.* **40**, 845-859 (2004).

5 Flajnik, M. F. & Kasahara, M. Comparative genomics of the MHC: glimpses into the evolution of the adaptive immune system. *Immunity* **15**, 351-362 (2001).

6 Litman, G. W., Anderson, M. K. & Rast, J. P. Evolution of antigen binding receptors. *Annu. Rev. Immunol.* **17**, 109-147 (1999).

7 Cooper, M. D. & Alder, M. N. The evolution of adaptive immune systems. *Cell* **124**, 815-822 (2006).

8 Alder, M. N. *et al.* Diversity and function of adaptive immune receptors in a jawless vertebrate. *Science* **310**, 1970-1973 (2005).

9 Pancer, Z. *et al.* Somatic diversification of variable lymphocyte receptors in the agnathan sea lamprey. *Nature* **430**, 174-180 (2004).

10 Schatz, D. G. & Ji, Y. Recombination centres and the orchestration of V(D)J recombination. *Nat. Rev. Immunol.* **11**, 251-263 (2011).

11 Nagawa, F. *et al.* Antigen-receptor genes of the agnathan lamprey are assembled by a process involving copy choice. *Nat. Immunol.* **8**, 206-213 (2007).

12 Guo, P. *et al.* Dual nature of the adaptive immune system in lampreys. *Nature* **459**, 796-801 (2009).

13 Rogozin, I. B. *et al.* Evolution and diversification of lamprey antigen receptors: evidence for involvement of an AID-APOBEC family cytosine deaminase. *Nat. Immunol.* **8**, 647-656 (2007).

14 Bajoghli, B. *et al.* Evolution of genetic networks underlying the emergence of thymopoiesis in vertebrates. *Cell* **138**, 186-197 (2009).

15 Bajoghli, B. *et al.* A thymus candidate in lampreys. *Nature* **470**, 90-94 (2011).

16 Nehls, M. *et al.* Two genetically separable steps in the differentiation of thymic epithelium. *Science* **272**, 886-889 (1996).

17 Felten, D. L., Felten, S. Y., Carlson, S. L., Olschowka, J. A. & Livnat, S. Noradrenergic and peptidergic innervation of lymphoid tissue. *J. Immunol.* **135**, 755s-765s (1985).

18 Zachariah, M. A. & Cyster, J. G. Neural crest-derived pericytes promote egress of mature thymocytes at the corticomedullary junction. *Science* **328**, 1129-1135 (2011).

19 Blackburn, C. C. & Manley, N. R. Developing a new paradigm for thymus organogenesis. *Nat. Rev. Immunol.* **4**, 278-289 (2004).

20 Bleul, C. C. *et al.* Formation of a functional thymus initiated by a postnatal epithelial progenitor cell. *Nature* **441**, 992-996 (2006).

21 Rossi, S. W., Jenkinson, W. E., Anderson, G. & Jenkinson, E. J. Clonal analysis reveals a common progenitor for thymic cortical and medullary epithelium. *Nature* **441**, 988-991 (2006).

22 Hamazaki, Y. *et al.* Medullary thymic epithelial cells expressing Aire represent a unique lineage derived from cells expressing claudin. *Nat. Immunol.* **8**, 304-311 (2007).

23 Gordon, J., Bennett, A. R., Blackburn, C. C. & Manley, N. R. Gcm2 and Foxn1 mark early parathyroid- and thymus-specific domains in the developing third pharyngeal pouch. *Mech. Dev.* **103**, 141-143 (2001).

24 Corbeaux, T. *et al.* Thymopoiesis in mice depends on a Foxn1-positive thymic epithelial cell lineage. *Proc. Natl. Acad. Sci. U. S. A.* **107**, 16613-16618.

25 Kuratani, S. & Bockman, D. E. Impaired development of the thymic primordium after neural crest ablation. *Anat. Rec.* **228**, 185-190 (1990).

26 Foster, K. *et al.* Contribution of neural crest-derived cells in the embryonic and adult thymus. *J. Immunol.* **180**, 3183-3189 (2008).

27 Bockman, D. E. & Kirby, M. L. Dependence of thymus development on derivatives of the neural crest. *Science* **223**, 498-500 (1984).

28 Anderson, G., Jenkinson, E. J., Moore, N. C. & Owen, J. J. MHC class II-positive epithelium and mesenchyme cells are both required for T-cell development in the thymus. *Nature* **362**, 70-73 (1993).

29 Owen, J. J. & Ritter, M. A. Tissue interaction in the development of thymus lymphocytes. *J. Exp. Med.* **129**, 431-442 (1969).

30 Hikosaka, Y. *et al.* The cytokine RANKL produced by positively selected thymocytes fosters medullary thymic epithelial cells that express autoimmune regulator. *Immunity* **29**, 438-450 (2008).

31 Hollander, G. A. *et al.* Developmental control point in induction of thymic cortex regulated by a subpopulation of prothymocytes. *Nature* **373**, 350-353 (1995).

32 Rodewald, H. R., Paul, S., Haller, C., Bluethmann, H. & Blum, C. Thymus medulla consisting of epithelial islets each derived from a single progenitor. *Nature* **414**, 763-768 (2001).

33 Rodewald, H. R. Thymus organogenesis. *Annu. Rev. Immunol.* **26**, 355-388 (2008).

34 Gray, D., Abramson, J., Benoist, C. & Mathis, D. Proliferative arrest and rapid turnover of thymic epithelial cells expressing Aire. *J. Exp. Med.* **204**, 2521-2528 (2007).

35 Terszowski, G. *et al.* Evidence for a functional second thymus in mice. *Science* **312**, 284-287 (2006).

36 Millman, B., Pransky, S., Castillo, J., 3rd, Zipfel, T. E. & Wood, W. E. Cervical thymic anomalies. *Int. J. Pediatr. Otorhinolaryngol.* **47**, 29-39 (1999).

37 Steinmann, G. G., Klaus, B. & Muller-Hermelink, H. K. The involution of the ageing human thymic epithelium is independent of puberty. A morphometric study. *Scand. J. Immunol.* **22**, 563-575 (1985).

38 Lynch, H. E. *et al.* Thymic involution and immune reconstitution. *Trends Immunol.* **30**, 366-373 (2009).

39 Vicente, R., Adjali, O., Jacquet, C., Zimmermann, V. S. & Taylor, N. Intrathymic transplantation of bone marrow-derived progenitors provides long-term thymopoiesis. *Blood* **115**, 1913-1920 (2010).

40 Petrie, H. T. & Zuniga-Pflucker, J. C. Zoned out: functional mapping of stromal signaling microenvironments in the thymus. *Annu. Rev. Immunol.* **25**, 649-679 (2007).

41 Scimone, M. L., Aifantis, I., Apostolou, I., von Boehmer, H. & von Andrian, U. H. A multistep adhesion cascade for lymphoid progenitor cell homing to the thymus. *Proc. Natl. Acad. Sci. U. S. A.* **103**, 7006-7011 (2006).

42 Wu, L. *et al.* CD4 expressed on earliest T-lineage precursor cells in the adult murine thymus. *Nature* **349**, 71-74 (1991).

43 Feyerabend, T. *et al.* Deletion of Notch1 Converts Pro-T Cells to Dendritic Cells and Promotes Thymic B Cells by Cell-Extrinsic and Cell-Intrinsic Mechanisms. *Immunity* **30**, 67-79 (2009).

44 Saint-Ruf, C. *et al.* Analysis and expression of a cloned pre-T cell receptor gene. *Science* **266**, 1208-1212 (1994).

45 Pang, S. S. *et al.* The structural basis for autonomous dimerization of the pre-T-cell antigen receptor. *Nature* **467**, 844-848 (2010).

46 Yamasaki, S. *et al.* Mechanistic basis of pre-T cell receptor-mediated autonomous signaling critical for thymocyte development. *Nat. Immunol.* **7**, 67-75 (2006).

47 von Boehmer, H. Unique features of the pre-T-cell receptor alpha-chain: not just a surrogate. *Nat. Rev. Immunol.* **5**, 571-577 (2005).

48 Witt, C. M., Raychaudhuri, S., Schaefer, B., Chakraborty, A. K. & Robey, E. A. Directed migration of positively selected thymocytes visualized in real time. *PLoS Biol.* **3**, e160 (2005).

49 Singer, A., Adoro, S. & Park, J. H. Lineage fate and intense debate: myths, models and mechanisms of CD4- versus CD8-lineage choice. *Nat. Rev. Immunol.* **8**, 788-801 (2008).

50 He, X. *et al.* CD4-CD8 lineage commitment is regulated by a silencer element at the ThPOK transcription-factor locus. *Immunity* **28**, 346-358 (2008).

51 Brugnera, E. *et al.* Coreceptor reversal in the thymus: signaled CD4+8+ thymocytes initially terminate CD8 transcription even when differentiating into CD8+ T cells. *Immunity* **13**, 59-71 (2000).

52 Park, J. Signaling by intrathymic cytokines, not T cell antigen receptors, specifies CD8 lineage choice and promotes the differentiation of cytotoxic-lineage T cells. . *Nat. Immunol.* **11**, 257-264 (2010).

53 Ueno, T. *et al.* CCR7 signals are essential for cortex-medulla migration of developing thymocytes. *J. Exp. Med.* **200**, 493-505 (2004).

54 McCaughtry, T. M., Baldwin, T. A., Wilken, M. S. & Hogquist, K. A. Clonal deletion of thymocytes can occur in the cortex with no involvement of the medulla. *J. Exp. Med.* **205**, 2575-2584 (2008).

55 Kurobe, H. *et al.* CCR7-dependent cortex-to-medulla migration of positively selected thymocytes is essential for establishing central tolerance. *Immunity* **24**, 165-177 (2006).

56 Kyewski, B. & Klein, L. A central role for central tolerance. *Annu. Rev. Immunol.* **24**, 571-606 (2006).

57 Kishimoto, H. & Sprent, J. Negative selection in the thymus includes semimature T cells. *J. Exp. Med.* **185**, 263-271 (1997).

58 Carlson, C. M. *et al.* Kruppel-like factor 2 regulates thymocyte and T-cell migration. *Nature* **442**, 299-302 (2006).

59 Chu, Y. W. *et al.* Exogenous IL-7 increases recent thymic emigrants in peripheral lymphoid tissue without enhanced thymic function. *Blood* **104**, 1110-1119 (2004).

60 Weinreich, M. A., Jameson, S. C. & Hogquist, K. A. Postselection thymocyte maturation and emigration are independent of IL-7 and ERK5. *J. Immunol.* **186**, 1343-1347 (2011).

61 McCaughtry, T. M., Wilken, M. S. & Hogquist, K. A. Thymic emigration revisited. *J. Exp. Med.* **204**, 2513-2520 (2007).

62 Mazzucchelli, R. I. *et al.* Visualization and identification of IL-7 producing cells in reporter mice. *PLoS One* **4**, e7637 (2009).

63 Marrack, P. & Kappler, J. The T cell receptor. *Science* **238**, 1073-1079 (1987).

64 Nitta, T. *et al.* Thymoproteasome shapes immunocompetent repertoire of CD8+ T cells. *Immunity* **32**, 29-40 (2010).

65 Murata, S. *et al.* Regulation of CD8+ T cell development by thymus-specific proteasomes. *Science* **316**, 1349-1353 (2007).

66 Nakagawa, T. *et al.* Cathepsin L: critical role in Ii degradation and CD4 T cell selection in the thymus. *Science* **280**, 450-453 (1998).

67 Nedjic, J., Aichinger, M., Emmerich, J., Mizushima, N. & Klein, L. Autophagy in thymic epithelium shapes the T-cell repertoire and is essential for tolerance. *Nature* **455**, 396-400 (2008).

68 Klein, L., Hinterberger, M., Wirnsberger, G. & Kyewski, B. Antigen presentation in the thymus for positive selection and central tolerance induction. *Nat. Rev. Immunol.* **9**, 833-844 (2009).

69 Anderson, M. S. *et al.* Projection of an immunological self shadow within the thymus by the aire protein. *Science* **298**, 1395-1401 (2002).

70 Derbinski, J., Schulte, A., Kyewski, B. & Klein, L. Promiscuous gene expression in medullary thymic epithelial cells mirrors the peripheral self. *Nat. Immunol.* **2**, 1032-1039 (2001).

71 Mathis, D. & Benoist, C. Aire. *Annu. Rev. Immunol.* **27**, 287-312 (2009).

72 Aschenbrenner, K. *et al.* Selection of Foxp3+ regulatory T cells specific for self antigen expressed and presented by Aire+ medullary thymic epithelial cells. *Nat. Immunol.* **8**, 351-358 (2007).

73 Wirnsberger, G., Mair, F. & Klein, L. Regulatory T cell differentiation of thymocytes does not require a dedicated antigen-presenting cell but is under T cell-intrinsic developmental control. *Proc. Natl. Acad. Sci. U. S. A.* **106**, 10278-10283 (2009).

74 Millet, V., Naquet, P. & Guinamard, R. R. Intercellular MHC transfer between thymic epithelial and dendritic cells. *Eur. J. Immunol.* **38**, 1257-1263 (2008).

75 Gallegos, A. M. & Bevan, M. J. Central tolerance to tissue-specific antigens mediated by direct and indirect antigen presentation. *J. Exp. Med.* **200**, 1039-1049 (2004).

76 Neijssen, J. *et al.* Cross-presentation by intercellular peptide transfer through gap junctions. *Nature* **434**, 83-88 (2005).

77 Pang, B. *et al.* Direct antigen presentation and gap junction mediated cross-presentation during apoptosis. *J. Immunol.* **183**, 1083-1090 (2009).

78 Hinterberger, M. *et al.* Autonomous role of medullary thymic epithelial cells in central CD4(+) T cell tolerance. *Nat. Immunol.* **11**, 512-519 (2010).

79 Gao, E. K., Lo, D. & Sprent, J. Strong T cell tolerance in parent----F1 bone marrow chimeras prepared with supralethal irradiation. Evidence for clonal deletion and anergy. *J Exp Med* **171**, 1101-1121 (1990).

80 Li, J., Park, J., Foss, D. & Goldschneider, I. Thymus-homing peripheral dendritic cells constitute two of the three major subsets of dendritic cells in the steady-state thymus. *J. Exp. Med.* **206**, 607-622 (2009).

81 Corcoran, L. *et al.* The lymphoid past of mouse plasmacytoid cells and thymic dendritic cells. *J. Immunol.* **170**, 4926-4932 (2003).

82 Lei, Y. *et al.* Aire-dependent production of XCL1 mediates medullary accumulation of thymic dendritic cells and contributes to regulatory T cell development. *J. Exp. Med.* **208**, 383-394 (2011).

83 Bonasio, R. *et al.* Clonal deletion of thymocytes by circulating dendritic cells homing to the thymus. *Nat. Immunol.* **7**, 1092-1100 (2006).

84 Proietto, A. I., van Dommelen, S. & Wu, L. The impact of circulating dendritic cells on the development and differentiation of thymocytes. *Immunol. Cell. Biol.* **87**, 39-45 (2009).

85 Liu, K. *et al.* Origin of dendritic cells in peripheral lymphoid organs of mice. *Nat. Immunol.* **8**, 578-583 (2007).

86 Raviola, E. & Karnovsky, M. J. Evidence for a blood-thymus barrier using electron-opaque tracers. *J. Exp. Med.* **136**, 466-498 (1972).

87 Martin, S. & Bevan, M. J. Antigen-specific and nonspecific deletion of immature cortical thymocytes caused by antigen injection. *Eur. J. Immunol.* **27**, 2726-2736 (1997).

88 Baba, T., Nakamoto, Y. & Mukaida, N. Crucial contribution of thymic Sirp alpha+ conventional dendritic cells to central tolerance against blood-borne antigens in a CCR2-dependent manner. *J. Immunol.* **183**, 3053-3063 (2009).

89 Atibalentja, D. F., Byersdorfer, C. A. & Unanue, E. R. Thymus-blood protein interactions are highly effective in negative selection and regulatory T cell induction. *J. Immunol.* **183**, 7909-7918 (2009).

90 Alvarez, D., Vollmann, E. H. & von Andrian, U. H. Mechanisms and consequences of dendritic cell migration. *Immunity* **29**, 325-342 (2008).

91 Steinman, R. M. & Banchereau, J. Taking dendritic cells into medicine. *Nature* **449**, 419-426 (2007).

92 Shortman, K. & Naik, S. H. Steady-state and inflammatory dendritic-cell development. *Nat. Rev. Immunol.* **7**, 19-30 (2007).

93 Fogg, D. K. *et al.* A clonogenic bone marrow progenitor specific for macrophages and dendritic cells. *Science* **311**, 83-87 (2006).

94 Naik, S. H. *et al.* Development of plasmacytoid and conventional dendritic cell subtypes from single precursor cells derived in vitro and in vivo. *Nat. Immunol.* **8**, 1217-1226 (2007).

95 Onai, N. *et al.* Identification of clonogenic common Flt3+M-CSFR+ plasmacytoid and conventional dendritic cell progenitors in mouse bone marrow. *Nat. Immunol.* **8**, 1207-1216 (2007).

96 Massberg, S. *et al.* Immunosurveillance by hematopoietic progenitor cells trafficking through blood, lymph, and peripheral tissues. *Cell* **131**, 994-1008 (2007).

97 Wu, L. & Shortman, K. Heterogeneity of thymic dendritic cells. *Semin Immunol* **17**, 304-312 (2005).

98 Wright, D. E., Bowman, E. P., Wagers, A. J., Butcher, E. C. & Weissman, I. L. Hematopoietic stem cells are uniquely selective in their migratory response to chemokines. *J. Exp. Med.* **195**, 1145-1154 (2002).

99 Geissmann, F., Jung, S. & Littman, D. R. Blood monocytes consist of two principal subsets with distinct migratory properties. *Immunity* **19**, 71-82 (2003).

100 Ley, K., Laudanna, C., Cybulsky, M. I. & Nourshargh, S. Getting to the site of inflammation: the leukocyte adhesion cascade updated. *Nat. Rev. Immunol.* **7**, 678-689 (2007).

101 Bursch, L. S. *et al.* Identification of a novel population of Langerin+ dendritic cells. *J. Exp. Med.* **204**, 3147-3156 (2007).

102 Stutte, S., Jux, B., Esser, C. & Forster, I. CD24a expression levels discriminate Langerhans cells from dermal dendritic cells in murine skin and lymph nodes. *J. Invest. Dermatol.* **128**, 1470-1475 (2008).

103 Poulin, L. F. *et al.* The dermis contains langerin+ dendritic cells that develop and function independently of epidermal Langerhans cells. *J. Exp. Med.* **204**, 3119-3131 (2007).

104 Ginhoux, F. *et al.* Blood-derived dermal langerin+ dendritic cells survey the skin in the steady state. *J. Exp. Med.* **204**, 3133-3146 (2007).

105 Cavanagh, L. L. *et al.* Activation of bone marrow-resident memory T cells by circulating, antigen-bearing dendritic cells. *Nat. Immunol.* **6**, 1029-1037 (2005).

106 Jung, S. *et al.* Analysis of fractalkine receptor CX(3)CR1 function by targeted deletion and green fluorescent protein reporter gene insertion. *Mol. Cell. Biol.* **20**, 4106-4114 (2000).

107 Vremec, D., Pooley, J., Hochrein, H., Wu, L. & Shortman, K. CD4 and CD8 expression by dendritic cell subtypes in mouse thymus and spleen. *J. Immunol.* **164**, 2978-2986 (2000).

108 Cella, M. *et al.* Plasmacytoid monocytes migrate to inflamed lymph nodes and produce large amounts of type I interferon. *Nat. Med.* **5**, 919-923 (1999).

109 Diacovo, T. G., Blasius, A. L., Mak, T. W., Cella, M. & Colonna, M. Adhesive mechanisms governing interferon-producing cell recruitment into lymph nodes. *J. Exp. Med.* **202**, 687-696 (2005).

110 Penna, G., Sozzani, S. & Adorini, L. Cutting edge: selective usage of chemokine receptors by plasmacytoid dendritic cells. *J. Immunol.* **167**, 1862-1866. (2001).

111 Vermi, W. *et al.* Role of ChemR23 in directing the migration of myeloid and plasmacytoid dendritic cells to lymphoid organs and inflamed skin. *J. Exp. Med.* **201**, 509-515 (2005).

112 Zabel, B. A., Silverio, A. M. & Butcher, E. C. Chemokine-like receptor 1 expression and chemerin-directed chemotaxis distinguish plasmacytoid from myeloid dendritic cells in human blood. *J. Immunol.* **174**, 244-251 (2005).

113 Hammad, H. & Lambrecht, B. N. Lung dendritic cell migration. *Adv. Immunol.* **93**, 265-278 (2007).

114 Iwasaki, A. Mucosal dendritic cells. *Annu. Rev. Immunol.* **25**, 381-418 (2007).

115 Banchereau, J. *et al.* Immunobiology of dendritic cells. *Annu. Rev. Immunol.* **18**, 767-811 (2000).

116 Mullins, D. W. *et al.* Route of immunization with peptide-pulsed dendritic cells controls the distribution of memory and effector T cells in lymphoid tissues and determines the pattern of regional tumor control. *J. Exp. Med.* **198**, 1023-1034 (2003).

117 Proietto, A. I. *et al.* Dendritic cells in the thymus contribute to T-regulatory cell induction. *Proc. Natl. Acad. Sci. U. S. A.* **105**, 19869-19874 (2008).

118 Duncan, S. R., Capetanakis, N. G., Lawson, B. R. & Theofilopoulos, A. N. Thymic dendritic cells traffic to thymi of allogeneic recipients and prolong graft survival. *J. Clin. Invest.* **109**, 755-764 (2002).

119 Donskoy, E. & Goldschneider, I. Two developmentally distinct populations of dendritic cells inhabit the adult mouse thymus: demonstration by differential importation of hematogenous precursors under steady state conditions. *J. Immunol.* **170**, 3514-3521 (2003).

120 Robert, C. *et al.* Interaction of dendritic cells with skin endothelium: A new perspective on immunosurveillance. *J. Exp. Med.* **189**, 627-636 (1999).

121 Ingulli, E., Mondino, A., Khoruts, A. & Jenkins, M. K. In vivo detection of dendritic cell antigen presentation to CD4(+) T cells. *J. Exp. Med.* **185**, 2133-2141 (1997).

122 Geijtenbeek, T. B. *et al.* DC-SIGN-ICAM-2 interaction mediates dendritic cell trafficking. *Nat. Immunol.* **1**, 353-357 (2000).

123 Lin, C. L., Suri, R. M., Rahdon, R. A., Austyn, J. M. & Roake, J. A. Dendritic cell chemotaxis and transendothelial migration are induced by distinct chemokines and are regulated on maturation. *Eur. J. Immunol.* **28**, 4114-4122 (1998).

124 Bonasio, R. & von Andrian, U. H. Generation, migration and function of circulating dendritic cells. *Curr. Opin. Immunol.* **18**, 503-511 (2006).

125 Kissenpfennig, A. *et al.* Dynamics and function of Langerhans cells in vivo: dermal dendritic cells colonize lymph node areas distinct from slower migrating Langerhans cells. *Immunity* **22**, 643-654 (2005).

126 Lindquist, R. L. *et al.* Visualizing dendritic cell networks in vivo. *Nat. Immunol.* **5**, 1243-1250 (2004).

127 Tomura, M. *et al.* Monitoring cellular movement in vivo with photoconvertible fluorescence protein "Kaede" transgenic mice. *Proc. Natl. Acad. Sci. U. S. A.* **105**, 10871-10876 (2008).

128 Patterson, G. H. & Lippincott-Schwartz, J. A photoactivatable GFP for selective photolabeling of proteins and cells. *Science* **297**, 1873-1877 (2002).

129 Victora, G. D. *et al.* Germinal center dynamics revealed by multiphoton microscopy with a photoactivatable fluorescent reporter. *Cell* **143**, 592-605 (2010).

130 Smith, A. L. & Fazekas de St Groth, B. Antigen-pulsed CD8alpha+ dendritic cells generate an immune response after subcutaneous injection without homing to the draining lymph node. *J. Exp. Med.* **189**, 593-598 (1999).

131 Miller, M. J., Hejazi, A. S., Wei, S. H., Cahalan, M. D. & Parker, I. T cell repertoire scanning is promoted by dynamic dendritic cell behavior and random T cell motility in the lymph node. *Proc. Natl. Acad. Sci. U. S. A.* **101**, 998-1003 (2004).

132 Bousso, P. & Robey, E. Dynamics of CD8(+) T cell priming by dendritic cells in intact lymph nodes. *Nat. Immunol.* **4**, 579-585 (2003).

133 Mempel, T. R., Henrickson, S. E. & Von Andrian, U. H. T-cell priming by dendritic cells in lymph nodes occurs in three distinct phases. *Nature* **427**, 154-159 (2004).

134 Halin, C., Rodrigo Mora, J., Sumen, C. & von Andrian, U. H. In vivo imaging of lymphocyte trafficking. *Annu. Rev. Cell. Dev. Biol.* **21**, 581-603 (2005).

135 Cahalan, M. D., Parker, I., Wei, S. H. & Miller, M. J. Two-photon tissue imaging: seeing the immune system in a fresh light. *Nat. Rev. Immunol.* **2**, 872-880 (2002).

136 Baumjohann, D. & Lutz, M. B. Non-invasive imaging of dendritic cell migration in vivo. *Immunobiology* **211**, 587-597 (2006).

137 Elbe, A. *et al.* Maturational steps of bone marrow-derived dendritic murine epidermal cells. Phenotypic and functional studies on Langerhans cells and Thy-1+ dendritic epidermal cells in the perinatal period. *J. Immunol.* **143**, 2431-2438 (1989).

138 Sozzani, S. *et al.* Migration of dendritic cells in response to formyl peptides, C5a, and a distinct set of chemokines. *J. Immunol.* **155**, 3292-3295 (1995).

139 Sozzani, S. *et al.* Receptor expression and responsiveness of human dendritic cells to a defined set of CC and CXC chemokines. *J. Immunol.* **159**, 1993 (1997).

140 Merad, M. *et al.* Langerhans cells renew in the skin throughout life under steady-state conditions. *Nat. Immunol.* **3**, 1135-1141 (2002).

141 Yamagami, S. *et al.* CCR5 chemokine receptor mediates recruitment of MHC class II-positive Langerhans cells in the mouse corneal epithelium. *Invest. Ophthalmol. Vis. Sci.* **46**, 1201-1207 (2005).

142 Stumbles, P. A. *et al.* Regulation of dendritic cell recruitment into resting and inflamed airway epithelium: use of alternative chemokine receptors as a function of inducing stimulus. *J. Immunol.* **167**, 228-234. (2001).

143 Merad, M. *et al.* Depletion of host Langerhans cells before transplantation of donor alloreactive T cells prevents skin graft-versus-host disease. *Nat. Med.* **10**, 510-517 (2004).

144 Sallusto, F. *et al.* Rapid and coordinated switch in chemokine receptor expression during dendritic cell maturation. *Eur. J. Immunol.* **28**, 2760-2769 (1998).

145 Sozzani, S. *et al.* Cutting edge: Differential regulation of chemokine receptors during dendritic cell maturation: A model for their trafficking properties *J. Immunol.* **161**, 1083-1086 (1998).

146 Dieu, M. C. *et al.* Selective recruitment of immature and mature dendritic cells by distinct chemokines expressed in different anatomic sites. *J. Exp. Med.* **188**, 373-386 (1998).

147 Martin-Fontecha, A. *et al.* Regulation of dendritic cell migration to the draining lymph node: impact on T lymphocyte traffic and priming. *J. Exp. Med.* **198**, 615-621 (2003).

148 Saeki, H., Moore, A. M., Brown, M. J. & Hwang, S. T. Cutting edge: secondary lymphoid-tissue chemokine (SLC) and CC chemokine receptor 7 (CCR7) participate in the emigration pathway of mature dendritic cells from the skin to regional lymph nodes. *J. Immunol.* **162**, 2472-2475. (1999).

149 Vassileva, G. *et al.* The reduced expression of 6Ckine in the plt mouse results from the deletion of one of two 6Ckine genes. *J. Exp. Med.* **190**, 1183-1188 (1999).

150 von Andrian, U. H. & Mackay, C. R. T-cell function and migration. Two sides of the same coin. *N. Engl. J. Med.* **343**, 1020-1034 (2000).

151 Vestweber, D. & Blanks, J. E. Mechanisms that regulate the function of the selectins and their ligands. *Physiol. Rev.* **79**, 181-213 (1999).

152 Rot, A. & von Andrian, U. H. Chemokines in innate and adaptive host defense: basic chemokinese grammar for immune cells. *Annu. Rev. Immunol.* **22**, 891-928 (2004).

153 Alon, R., Rossiter, H., Wang, X., Springer, T. A. & Kupper, T. S. Distinct cell surface ligands mediate T lymphocyte attachment and rolling on P- and E-selectin under physiological flow. *J. Cell Biol.* **127**, 1485-1495 (1994).

154 Imhof, B. A. & Aurrand-Lions, M. Adhesion mechanisms regulating the migration of monocytes. *Nat. Rev. Immunol.* **4**, 432-444 (2004).

155 Laird, D. J., von Andrian, U. H. & Wagers, A. J. Stem cell trafficking in tissue development, growth, and disease. *Cell* **132**, 612-630 (2008).

156 Springer, T. A. Traffic signals for lymphocyte recirculation and leukocyte emigration: the multistep paradigm. *Cell* **76**, 301-314 (1994).

157 Gordon, S. & Taylor, P. R. Monocyte and macrophage heterogeneity. *Nat. Rev. Immunol.* **5**, 953-964 (2005).

158 Palframan, R. T. *et al.* Inflammatory chemokine transport and presentation in HEV: A remote control mechanism for monocyte recruitment to lymph nodes in inflamed tissues. *J. Exp. Med.* **194**, 1361-1374. (2001).

159 Auffray, C. *et al.* Monitoring of blood vessels and tissues by a population of monocytes with patrolling behavior. *Science* **317**, 666-670 (2007).

160 Palucka, K., Banchereau, J. & Mellman, I. Designing vaccines based on biology of human dendritic cell subsets. *Immunity* **33**, 464-478 (2010).

161 de Vries, I. J. *et al.* Magnetic resonance tracking of dendritic cells in melanoma patients for monitoring of cellular therapy. *Nat. Biotechnol.* **23**, 1407-1413 (2005).

162 Morse, M. A. *et al.* Migration of human dendritic cells after injection in patients with metastatic malignancies. *Cancer Res.* **59**, 56-58. (1999).

163 Lim, Y. C. *et al.* Important contributions of P-selectin glycoprotein ligand-1-mediated secondary capture to human monocyte adhesion to P-selectin, E-selectin, and TNF-alpha-activated endothelium under flow in vitro. *J. Immunol.* **161**, 2501-2508. (1998).

164 Pendl, G. G. *et al.* Immature mouse dendritic cells enter inflamed tissue, a process that requires E- and P-selectin, but not P-selectin glycoprotein ligand 1. *Blood* **99**, 946-956. (2002).

165 Wethmar, K. *et al.* Migration of immature mouse DC across resting endothelium is mediated by ICAM-2 but independent of beta2-integrins and murine DC-SIGN homologues. *Eur. J. Immunol.* **36**, 2781-2794 (2006).

166 Dieu-Nosjean, M. C. *et al.* Macrophage inflammatory protein 3alpha is expressed at inflamed epithelial surfaces and is the most potent chemokine known in attracting Langerhans cell precursors. *J. Exp. Med.* **192**, 705-718 (2000).

167 Ginhoux, F. *et al.* Langerhans cells arise from monocytes in vivo. *Nat. Immunol.* **7**, 265-273 (2006).

168 Varol, C. *et al.* Monocytes give rise to mucosal, but not splenic, conventional dendritic cells. *J. Exp. Med.* **204**, 171-180 (2007).

169 Landsman, L., Varol, C. & Jung, S. Distinct differentiation potential of blood monocyte subsets in the lung. *J. Immunol.* **178**, 2000-2007 (2007).

170 Tacke, F. *et al.* Monocyte subsets differentially employ CCR2, CCR5, and CX3CR1 to accumulate within atherosclerotic plaques. *J. Clin. Invest.* **117**, 185-194 (2007).

171 Serbina, N. V. & Pamer, E. G. Monocyte emigration from bone marrow during bacterial infection requires signals mediated by chemokine receptor CCR2. *Nat. Immunol.* **7**, 311-317 (2006).

172 Farkas, L., Beiske, K., Lund-Johansen, F., Brandtzaeg, P. & Jahnsen, F. L. Plasmacytoid dendritic cells (natural interferon- alpha/beta-producing cells) accumulate in cutaneous lupus erythematosus lesions. *Am. J. Pathol.* **159**, 237-243. (2001).

173 Nestle, F. O. *et al.* Plasmacytoid predendritic cells initiate psoriasis through interferon-alpha production. *J. Exp. Med.* **202**, 135-143 (2005).

174 Jahnsen, F. L. *et al.* Experimentally induced recruitment of plasmacytoid (CD123high) dendritic cells in human nasal allergy. *J. Immunol.* **165**, 4062-4068. (2000).

175 Wendland, M. *et al.* CCR9 is a homing receptor for plasmacytoid dendritic cells to the small intestine. *Proc. Natl. Acad. Sci. U. S. A.* **104**, 6347-6352 (2007).

176 Di Rosa, F. & Pabst, R. The bone marrow: a nest for migratory memory T cells. *Trends Immunol.* **26**, 360-366 (2005).

177 Kamath, A. T. *et al.* The development, maturation, and turnover rate of mouse spleen dendritic cell populations. *J. Immunol.* **165**, 6762-6770. (2000).

178 Denk, W., Strickler, J. H. & Webb, W. W. Two-photon laser scanning fluorescence microscopy. *Science* **248**, 73-76 (1990).

179 Sumen, C., Mempel, T. R., Mazo, I. B. & Von Andrian, U. H. Intravital microscopy; visualizing immunity in context. *Immunity* **21**, 315-329 (2004).

180 Balagopalan, L., Sherman, E., Barr, V. A. & Samelson, L. E. Imaging techniques for assaying lymphocyte activation in action. *Nat. Rev. Immunol.* **11**, 21-33 (2011).

181 Beltman, J. B., Maree, A. F. & de Boer, R. J. Analysing immune cell migration. *Nat. Rev. Immunol.* **9**, 789-798 (2009).

182 Klug, D. B. *et al.* Interdependence of cortical thymic epithelial cell differentiation and T-lineage commitment. *Proc Natl Acad Sci U S A* **95**, 11822-11827 (1998).

183 Bousso, P., Bhakta, N. R., Lewis, R. S. & Robey, E. Dynamics of thymocyte-stromal cell interactions visualized by two-photon microscopy. *Science* **296**, 1876-1880 (2002).

184 Akiyama, T. *et al.* Dependence of self-tolerance on TRAF6-directed development of thymic stroma. *Science* **308**, 248-251 (2005).

185 Bhakta, N. R., Oh, D. Y. & Lewis, R. S. Calcium oscillations regulate thymocyte motility during positive selection in the three-dimensional thymic environment. *Nat. Immunol.* **6**, 143-151 (2005).

186 Le Borgne, M. *et al.* The impact of negative selection on thymocyte migration in the medulla. *Nat. Immunol.* **10**, 823-830 (2009).

187 Bulloch, K., Cullen, M. R., Schwartz, R. H. & Longo, D. L. Development of innervation within syngeneic thymus tissue transplanted under the kidney capsule of the nude mouse: a light and ultrastructural microscope study. *J. Neurosci. Res.* **18**, 16-27 (1987).

188 Loor, F. & Kindred, B. Differentiation of T-cell precursors in nude mice demonstrated by immunofluorescence of T-cell membrane markers. *J. Exp. Med.* **138**, 1044-1055 (1973).

189 Hogquist, K. A., Baldwin, T. A. & Jameson, S. C. Central tolerance: learning self-control in the thymus. *Nat. Rev. Immunol.* **5**, 772-782 (2005).

190 Mempel, T. R. *et al.* Regulatory T cells reversibly suppress cytotoxic T cell function independent of effector differentiation. *Immunity* **25**, 129-141 (2006).

191 Hogquist, K. A. *et al.* T cell receptor antagonist peptides induce positive selection. *Cell* **76**, 17-27 (1994).

192 Pircher, H., Burki, K., Lang, R., Hengartner, H. & Zinkernagel, R. M. Tolerance induction in double specific T-cell receptor transgenic mice varies with antigen. *Nature* **342**, 559-561 (1989).

193 Kukutsch, N. A., Rossner, S., Austyn, J. M., Schuler, G. & Lutz, M. B. Formation and kinetics of MHC class I-ovalbumin peptide complexes

on immature and mature murine dendritic cells. *J. Invest. Dermatol.* **115**, 449-453 (2000).

194 Henrickson, S. E. *et al.* T cell sensing of antigen dose governs interactive behavior with dendritic cells and sets a threshold for T cell activation. *Nat. Immunol.* **9**, 282-291 (2008).

195 Grakoui, A. *et al.* The immunological synapse: a molecular machine controlling T cell activation. *Science* **285**, 221-227 (1999).

196 Pereira, J. P., An, J., Xu, Y., Huang, Y. & Cyster, J. G. Cannabinoid receptor 2 mediates the retention of immature B cells in bone marrow sinusoids. *Nat. Immunol.* **10**, 403-411 (2009).

197 Petri, B. & Bixel, M. G. Molecular events during leukocyte diapedesis. *FEBS J.* **273**, 4399-4407 (2006).

198 Newman, P. J. *et al.* PECAM-1 (CD31) cloning and relation to adhesion molecules of the immunoglobulin gene superfamily. *Science* **247**, 1219-1222 (1990).

199 Vaporciyan, A. A. *et al.* Involvement of platelet-endothelial cell adhesion molecule-1 in neutrophil recruitment in vivo. *Science* **262**, 1580-1582 (1993).

200 Niess, J. H. *et al.* CX3CR1-mediated dendritic cell access to the intestinal lumen and bacterial clearance. *Science* **307**, 254-258 (2005).

201 Miller, M. J., Wei, S. H., Parker, I. & Cahalan, M. D. Two-photon imaging of lymphocyte motility and antigen response in intact lymph node. *Science* **296**, 1869-1873 (2002).

202 Mazo, I. B. *et al.* Bone marrow is a major reservoir and site of recruitment for central memory CD8+ T cells. *Immunity* **22**, 259-270 (2005).

203 Svoboda, K., Denk, W., Kleinfeld, D. & Tank, D. W. In vivo dendritic calcium dynamics in neocortical pyramidal neurons. *Nature* **385**, 161-165 (1997).

204 Looney, M. R. *et al.* Stabilized imaging of immune surveillance in the mouse lung. *Nat Methods* **8**, 91-96 (2011).

205 Ng, L. G. *et al.* Migratory dermal dendritic cells act as rapid sensors of protozoan parasites. *PLoS Pathog.* **4**, e1000222 (2008).

206 Conley, M. E., Beckwith, J. B., Mancer, J. F. & Tenckhoff, L. The spectrum of the DiGeorge syndrome. *J. Pediatr.* **94**, 883-890 (1979).

207 Barrett, D. J. *et al.* Clinical and immunologic spectrum of the DiGeorge syndrome. *J. Clin. Lab. Immunol.* **6**, 1-6 (1981).

208 Thomas, R. A., Landing, B. H. & Wells, T. R. Embryologic and other developmental considerations of thirty-eight possible variants of the DiGeorge anomaly. *Am. J. Med. Genet. Suppl.* **3**, 43-66 (1987).

209 Muller, W. *et al.* The DiGeorge syndrome. I. Clinical evaluation and course of partial and complete forms of the syndrome. *Eur. J. Pediatr.* **147**, 496-502 (1988).

210 Miller, J. F. Analysis of the thymus influence in leukaemogenesis. *Nature* **191**, 248-249 (1961).

211 Li, J., Iwanami, N., Hoa, V. Q., Furutani-Seiki, M. & Takahama, Y. Noninvasive intravital imaging of thymocyte dynamics in medaka. *J. Immunol.* **179**, 1605-1615, doi:179/3/1605 [pii] (2007).

212 Perry, S. S. *et al.* L-selectin defines a bone marrow analog to the thymic early T-lineage progenitor. *Blood* **103**, 2990-2996 (2004).

213 Kondo, M., Weissman, I. L. & Akashi, K. Identification of clonogenic common lymphoid progenitors in mouse bone marrow. *Cell* **91**, 661-672 (1997).

214 Martin, C. H. *et al.* Efficient thymic immigration of B220+ lymphoid-restricted bone marrow cells with T precursor potential. *Nat. Immunol.* **4**, 866-873 (2003).

215 Wu, L., Kincade, P. W. & Shortman, K. The CD44 expressed on the earliest intrathymic precursor population functions as a thymus homing molecule but does not bind to hyaluronate. *Immunol. Lett.* **38**, 69-75 (1993).

216 Richie, L. I. *et al.* Imaging synapse formation during thymocyte selection: inability of CD3zeta to form a stable central accumulation during negative selection. *Immunity* **16**, 595-606 (2002).

217 Hailman, E., Burack, W. R., Shaw, A. S., Dustin, M. L. & Allen, P. M. Immature CD4(+)CD8(+) thymocytes form a multifocal immunological synapse with sustained tyrosine phosphorylation. *Immunity* **16**, 839-848 (2002).

218 Nakayama, T. *et al.* Eotaxin-3/CC chemokine ligand 26 is a functional ligand for CX3CR1. *J. Immunol.* **185**, 6472-6479, (2010).

219 Cuvelier, S. L. & Patel, K. D. Shear-dependent eosinophil transmigration on interleukin 4-stimulated endothelial cells: a role for endothelium-associated eotaxin-3. *J. Exp. Med.* **194**, 1699-1709 (2001).

220 Ogilvie, P., Paoletti, S., Clark-Lewis, I. & Uguccioni, M. Eotaxin-3 is a natural antagonist for CCR2 and exerts a repulsive effect on human monocytes. *Blood* **102**, 789-794 (2003).

221 Wright, D. E. *et al.* Cyclophosphamide/granulocyte colony-stimulating factor causes selective mobilization of bone marrow hematopoietic stem cells into the blood after M phase of the cell cycle. *Blood* **97**, 2278-2285 (2001).

222 Mora, J. R. *et al.* Selective imprinting of gut-homing T cells by Peyer's patch dendritic cells. *Nature* **424**, 88-93 (2003).

Curriculum vitae

ELISABETH VOLLMANN, MSc.

Address: 60 Magazine Street
Cambridge
02139, MA
Phone no. (work): (617)-432-6832
Phone no. (home): (617)-910-7726
e-mail: vollmann@idi.harvard.edu
Place of birth: Graz, Austria
Nationality: Austria
Current visa status: J-1

Employment History

2006 –	Research scholar, Immune Disease Institute (former Center for Blood Research), Boston, 02115, MA, USA, PI: Dr. Ulrich von Andrian
2006 –	Graduate student, University of Vienna, Vienna, Austria and the Immune Disease Institute, Boston, MA 02115, USA Thesis title: Visualization of thymocyte – dendritic cell interactions during negative selection
2005 – 2006	Technical assistant, Institute of Molecular Pathology, Vienna, Austria, PI: Dr. Ludger Klein Topic: Establishment of central tolerance
2004 – 2005	Diploma thesis, Institute of Molecular Pathology, Vienna, Austria, PI: Dr. Ludger Klein Thesis title: A mouse model to study the role of medullary thymic epithelial cells in central tolerance
Summer 2004	Internship, Institute of Molecular Pathology, Vienna, Austria, PI: Dr. Hartmut Beug Topic: The role of endoglin in tumour progression
Summer 2003	Internship, Veterinarian University, Department of Virology, Vienna, Austria, PI: Dr. Matthias Renner Topic: Generation of a retroviral gene therapy
Summer 2002	Internship, Company Biochemie, Department of Toxicology, Vienna, Austria PI: Dr. Elisabeth Gammer Topic: Evaluation of candidate antibiotics in vitro and in vivo

Education

2007	BD certified in handling, operating and troubleshooting of BD FACS Canto machines
2006 –	Graduate student, University of Vienna, Vienna, Austria
2006	Diploma (Master of Science)
2004 – 2005	Diploma thesis about central tolerance, Institute of Molecular Pathology, Vienna, Austria, PI: Dr. Ludger Klein
2000 – 2005	Undergraduate studies of biology, Karl-Franzens University, Graz, Austria

Awards and Honours

2010	Poster prize at the Immune Disease Retreat, Cape Cod
2008	Conference assistant at the Keystone Symposium "Leukocyte Trafficking"
2007 – 2010	Recipient of a DOC-fFORTE fellowship by the Austrian Academy of Sciences

Publications

Alvarez D., Vollmann E.H., von Andrian U.H., 2008, Mechanisms and consequences of dendritic cell migration. Immunity, 29(3):325-42.

Aschenbrenner K., D'Cruz L., Vollmann E.H., Hinterberger M., Emmerich J., Swee L.K., Klein L., 2007. Thymic selection of Foxp3^{+} regulatory T cells specific for self-antigen expressed and presented by medullary epithelial cells. Nature Immunology, 8(4):351-8.

Rangachari M., Eriksson U., Vollmann E.H., Penninger J.M., 2005. A novel model for pathogenesis of autoimmune heart failure: the role of dendritic cells. International Congress Series, 1285, 192-201, Book Chapter.

Acknowledgments

First of all, I want to thank everyone in the von Andrian lab. I had a wonderful time and learned a lot. I want to specifically mention Silke, Jenn and Guiying, who made me feel welcome right from the get-go. I absolutely have to single out Ashley, the best bay-mate ever, who miraculously does not seem to get too fed up with me or tired of proof reading and correcting the same mistakes over and over again (further, further, further, however, further,…). Special thanks also to David and Scott – you guys are contagiously passionate about science – and Meghan, Elena, Mike, Jung and Susi for brightening my days. It is f***ing awesome working and hanging out with you.

Uli, where should I start? Do you remember "the" seminar that you gave at the IMP in Vienna in 2005, after which I cornered you? Back then in the days when I was still a Master's student. I still remember June 22nd 2005 – the day you invited me to interview with your lab. I was dancing through my lab in Vienna. Joining your lab was/is a great opportunity for me. I learned a ludicrous amount of stuff, starting with the highs and the lows of imaging, how to successfully apply for grants and to prepare manuscripts, and that counting red and green blobs by hand is as silly as it sounds ;o). Seriously, I am really grateful for everything you've done for me. Thank you!

A very special "thank you" goes to Josef. You took it upon yourself to mentor me despite having an entire ocean and six hours time difference separating mentor and mentee. I feel very honored and excited that I had you with me on this journey!

There is also one particular person who helped me tremendously with his incredible sense of duty. Kenji, without you I would probably have written my thesis on a typewriter.

I have met many wonderful scientists on my way. Thanks a lot for Angela, Nina and Gaelle – it wouldn't even have been half as fun without you.

I want to further extend my thanks to my former co-pilots Jelena, Martin, Jan and Ludger. You are totally rocking and I can't believe that we managed to stay in touch! Martin, I promise, I'm gonna send these shirts soon.

But most importantly, I want to thank my family – my mom, my dad and Bertl. Nothing would have been possible without you. Vielen Dank für eure Unterstützung!! =)

Lastly, I thank you! You actually read this to the very end.